

Jussi Hemmo

Electrical Power Systems for Finnish Nanosatellites

School of Electrical Engineering

Thesis submitted for examination for the degree of Master of Science in Technology.
Espoo 15.11.2013

Thesis supervisor:

Prof. Raimo Sepponen

Thesis instructor:

Prof. Jorma Kyyrä



Aalto University
School of Engineering

Author: Jussi Hemmo
Title: Electrical Power Systems for Finnish Nanosatellites
Date: 15.11.2013
Language: English
Number of pages: 8 + 87

Department of Electronics

Professorship: Applied Electronics

Code: S-66

Supervisor: Prof. Raimo Sepponen

Instructor: Prof. Jorma Kyrrä

Nanosatellites are lightweight, small and use low power compared to conventional satellites. University satellites are often based on CubeSat standard. 1U CubeSat is a cube shaped nanosatellite with dimensions of 10 cm x 10 cm x 10 cm and maximum mass of 1.33 kilograms. CubeSats are traditionally built from COTS-components (Commercial Off-the-Shelf) with low resources. Typically nanosatellites have limited mission time and short development and testing time.

Electrical Power System (EPS) is responsible in producing and storing energy needed for subsystems and payloads in a spacecraft. It consists of primary and secondary power sources and EPS-board controlling the distribution of the energy to subsystems and payloads. EPS provides telemetry data about currents, voltages, battery status etc. to OBC (On-Board Computer).

This thesis discusses the requirements for Aalto-1 and Aalto-2 electrical power systems. Also preliminary design of an EPS for Aalto-2 nanosatellite is presented.

Keywords: Nanosatellite, Electrical Power System, EPS, Aalto-1, Aalto-2, CubeSat, Step-down, Step-up, Boost, DC-DC converter, Solar Cell

Tekijä: Jussi Hemmo
Työn nimi: Suomalaisen nanosatelliittien tehonsyöttöjärjestelmät
Päivämäärä: 15.11.2013
Kieli: Englanti
Sivumäärä: 8 + 87

Elektronikan laitos

Professuuri: Sovellettu elektronikka

Koodi: S-66

Valvoja: Prof. Raimo Sepponen

Ohjaaja: Prof. Jorma Kyrrä

Nanosatelliitit ovat pieniä ja kevyitä satelliitteja, jotka käyttävät vähän tehoa verrattuna perinteisiin satelliitteihin. Yliopistosatelliittien suunnittelussa käytetään usein ns. CubeSat standardia. Siinä määritellään, että 1U CubeSat on kuution muotoinen nanosatelliitti, jonka mitat ovat 10 cm x 10 cm x 10 cm ja sallittu massa maksimissaan 1.33 kilogrammaa. Nanosatelliitit on yleensä rakennettu ns. COTS-komponenteista (Commercial off-the-shelf), vähäisillä resursseilla verrattuna perinteisiin satelliittiprojekteihin. Tyypillisesti CubeSat-tyypisten nanosatelliittien kehittämiseen ja testaamiseen käytetty aika on lyhyt.

Satelliitin tehonsyöttöjärjestelmä (EPS, Electrical Power System) tuottaa ja varastoi alijärjestelmien ja hyötykuormien tarvitseman energian. Se koostuu yleensä aurinkopaneeleista, akuista ja tehonjakelujärjestelmästä, joka huolehtii tehon jakamisesta järjestelmille. Tehonsyöttöjärjestelmä tuottaa myös telemetria-dataa virroista, jännitteistä, akun kunnosta ym. satelliitin tietokoneelle.

Tämän työn tarkoituksesta on määritää vaatimukset Aalto-1 ja Aalto-2 nanosatelliittien tehonsyöttöjärjestelmille ja kehittää Aalto-2 nanosatelliitin tehonsyöttöjärjestelmän prototyypin.

Avainsanat: Nanosatelliitti, Tehonsyöttöjärjestelmä, Aalto-1, Aalto-2, CubeSat, aurinkokenno, DC-DC konvertteri

Preface

This thesis determines requirements for Aalto-1 and Aalto-2 nanosatellites and a prototype for the Aalto-2 electrical power system is developed. The work took place at the School of Electrical Engineering, Aalto University.

I thank and acknowledge Aalto-1 & Aalto-2 project coordinator Dr. Jaan Praks for giving me a chance to participate in such an interesting project. I also thank my family for supporting me throughout my studies, Matti Vaaja for soldering help and interesting conversations during the project and Jussi Kuutti for early proofreading and all kind of help during the work. I thank my beloved Katri for her support during the thesis work and I dedicate this thesis to her.

I am grateful to my thesis supervisor professor Raimo Sepponen for corrections and my instructor professor Jorma Kyrrä for his valuable expertise about power electronics and helping in structuring the thesis.

Esboo 15.11.2013

Jussi Hemmo

Table of Contents

Abstract in English.....	i
Abstract in Finnish.....	ii
Preface.....	iii
Table of Contents.....	iv
List of acronyms	vi
1 Introduction.....	1
1.1 CubeSat concept.....	2
1.2 Aalto-1.....	2
1.3 Aalto-2.....	3
1.4 Aim and structure of the thesis.....	3
2 Effects of the space environment.....	4
2.1 Thermal environment.....	4
2.2 Shock and vibration.....	5
2.3 Radiation.....	5
2.4 Component selection.....	8
2.4.1 Reliability consideration.....	9
3 Power system architectures.....	11
3.1 DC-DC converters.....	13
3.1.1 Linear voltage converters.....	13
3.1.2 Inductive DC-DC converters.....	14
3.1.2.1 Step-down converters.....	15
3.1.2.2 Step-up converters.....	16
3.1.2.3 Buck-boost converters.....	16
3.1.2.4 Charge pumps.....	17
3.2 Protection circuits.....	17
4 Solar cells.....	18
4.1 Solar cell theory.....	18
4.2 Maximum power point tracking.....	20
4.3 MPPT algorithms.....	23
4.3.1 Perturb-and-observe.....	23
4.3.2 Incremental conductance.....	24
4.3.3 Parasitic capacitance.....	25
4.3.4 Constant voltage and constant current.....	26
4.3.5 Comparison of different methods.....	27
5 Solar cell selection and solar panel design	28
5.1 Selecting suitable solar cells for Aalto-1.....	28
5.2 Bonding of the solar cells.....	30
5.2.1 Methods used for connecting cells to strings.....	30
5.2.2 Methods used for solar cell bonding to substrate.....	31
5.2.3 The method used for Aalto-1.....	31
5.3 Solar panels for Aalto-2.....	33
6 Electrical power system requirements.....	34
6.1 Requirements for Aalto-1.....	35
6.2 Requirements for Aalto-2.....	35
6.2.1 Top level requirements.....	36
6.2.2 Functional requirements.....	36
6.2.3 Telemetry and telecommand.....	36
6.3 Power and mass budget of the Aalto-2 EPS.....	37
6.3.1 Total power production of the solar panels.....	37

6.3.2 Power consumption of the subsystems and payloads.....	38
6.3.3 Size and mass budget.....	39
6.4 Pinout and CubeSat Kit connector.....	42
7 Aalto-1 EPS architecture.....	43
8 Aalto-2 preliminary EPS architecture.....	45
8.1 Microcontroller.....	45
8.2 Selection of DC-DC converters.....	47
8.3 Maximum power point tracking.....	49
8.4 Protection circuits.....	51
8.5 Telemetry.....	52
8.6 Remove before flight and separation switch interfaces.....	52
8.7 Battery selection and design.....	52
8.8 Component selection (passive).....	54
9 Functional testing of the Aalto-2 EPS prototype.....	55
9.1 General about testing.....	55
9.2 Test results.....	56
9.2.1 DC-DC Converters.....	56
9.2.2 Maximum power point tracking and battery charging capabilities.....	60
9.2.3 Over-current protection.....	62
9.2.4 Burn-in testing.....	63
10 Summary and future work.....	64
10.1 Summary.....	64
10.2 Future work.....	65
References.....	66
Appendix A.....	71
Appendix B.....	73
Appendix C.....	77
Appendix D.....	82

List of acronyms

1U, 2U, 3U	1-Unit, 2-Unit and 3-Unit CubeSat sizes, respectively
1s2p	Battery configuration - one cell in series and 2 cells in parallel
2s2p	Battery configuration - 2 parallel strings with two cells in series per string
ADS	Antenna Deployment System
ADCS	Attitude Determination and Control System
AM0	Air Mass Zero. Describes the solar irradiance in space, outside the Earth's atmosphere
BCR	Battery Charge Regulator
BOL	Beginning of Life
CDR	Critical Design Review
CDS	CubeSat Design Specification
COTS	Commercial Off-the-Shelf
CVCM	Collected Volatile Condensable Material
DC-DC	Direct Current to Direct Current
DET	Direct Energy Transfer
DOD	Depth of Discharge
DPA	Distributed Power System
EM	Engineering Model
EPB	Electrostatic Plasma Brake
EPS	Electrical Power System
ESA	The European Space Agency
FM	Flight Model
FMECA	Failure Mode, Effects and Criticality Analysis
GPS	Global Positioning System
I ² C	Inter-Integrated Circuit bus
IBA	Intermediate Bus Architecture
IC	Integrated-Circuit
ICD	Interface Control Document
LEO	Low Earth Orbit
MEC	Mechanical Structure of the Satellite
NASA	The National Aeronautics and Space Administration
OBC	On-Board Computer
P-POD	Poly-PicoSatellite Orbital Deployer
PCB	Printed Circuit Board

PCM	Power Conditioning Module
PFM	Proto Flight Model
POD	PicoSatellite Orbital Deployer
POL	Point-of-Load
QM	Qualification Model
SCA	Solar Cell Assembly
SOC	State of Charge
SPENVIS	Space Environment, Effects, and Education System
SPST	Single Pole, Single Throw
STK	Systems Tool Kit
TBC	To Be Confirmed
TBD	To Be Determined
TID	Total Ionizing dose
TML	Total Mass Loss
TT&C	Telemetry, Tracking and Command
RADMON	Radiation Monitor
UHF	Ultra High Frequency

1 Introduction

Satellites are used for numerous purposes to make lives of mankind safer and more convenient. Most common types are communications, weather, Earth observation, navigation and research satellites. Satellites consists of different subsystems and payloads, which are in most cases electrical devices. Environmental conditions in space are more severe than on Earth, mostly due to low residual pressure and radiation. Extremely low pressure causes outgassing of the materials, and reduce the heat transfer. Radiation causes errors on logic devices and degrades the performance of electronic components. Eventually components fail as the total radiation dose has grown large enough. Therefore, special care is needed when designing electrical devices to be used in space. One of the most essential subsystems on spacecraft is the power system.

A spacecraft power system generally consists of primary power sources, secondary power sources and power control and a distribution system. Solar arrays are used as a primary power source in most spacecrafts, where long lifetime is required. Solar energy is a reliable power source as incoming solar radiation (insolation) does not vary significantly when the satellite is on top of Earth's atmosphere. Batteries are typically used as secondary power source to store and deliver the energy generated by solar arrays. Energy storage is necessary for the operation during orbital eclipse periods and situations where more peak power is needed than solar arrays can produce.

The power system is responsible for distributing the power to subsystems and payloads of the satellite. In most configurations electrical power system (EPS) also supplies telemetry about voltages, currents and temperatures to help estimating power production and usage. Simplified model of a typical EPS is presented in Figure 1.1.

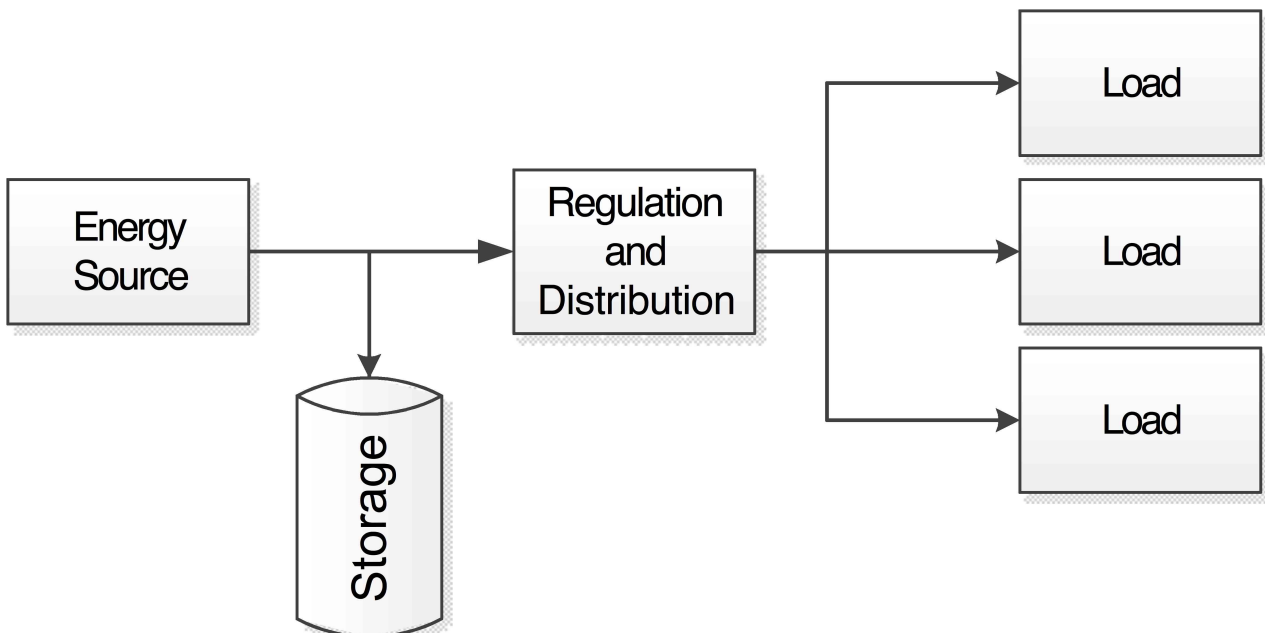


Figure 1.1: Block diagram of a typical electrical power system

1.1 CubeSat concept

The CubeSat Project began in 1999 as a collaborative effort by California Polytechnic University and Stanford University. The project provides standards for designing picosatellites to reduce development time and cost. CubeSat Design Specifications (CDS) were developed to provide access to space for small payloads. (CDS, 2009) Miniaturization of the electronics enables the possibility to manufacture smaller payloads and subsystems for the satellites.

The CubeSat specification defines One-unit (1U) CubeSat to be a small $100 \pm 0.1 \text{ mm} \times 100 \pm 0.1 \text{ mm} \times 113.5 \pm 0.1 \text{ mm}$ cube shaped satellite with maximum mass of 1.33 kg. CubeSats are scalable by 1U increments and for example maximum dimensions of three-unit (3U) CubeSat are $100 \pm 0.1 \text{ mm} \times 100 \pm 0.1 \text{ mm} \times 340.5 \pm 0.3 \text{ mm}$ with a maximum mass of 4.0 kg. CubeSats are small, light-weight and affordable compared to conventional satellites. This makes it easier for universities, high schools or private companies to design and manufacture their own satellites and gain more hands-on experience about different problems in spacecraft design. (CDS, 2009) The specification needs to be followed when using Poly-PicoSatellite Orbital Deployer (P-POD) developed and built by California Polytechnic State University. Mass or dimensional constraints can be exceeded with extra cost by using some other available deployer e.g. ISIS-POD manufactured by Innovative Solution in Space. When the deployment system is standardized, it is easier for a satellite developer to follow given specifications to get access to space.

1.2 Aalto-1

The first Finnish CubeSat project Aalto-1 was initiated in 2010 by the Department of Radio Sciences and Engineering of Aalto University School of Electrical Engineering. Aalto-1 is a 3U CubeSat with 3-axis stabilization. Dimensions of Aalto-1 are 100.0 mm x 100.0 mm x 340.5 mm and weight is targeted to be below the 4.0 kg limit for a 3U CubeSat. Since 2010 over 50 students from different departments of Aalto University have been participating in designing and building the Aalto-1 satellite. As of this writing, the launch of the Aalto-1 has been scheduled for 2014. (Näsilä et al., 2012)

The project has partners around the space industry in Finland and payloads are provided by Finnish institutions and universities. Technical Research Centre of Finland develops miniature Aalto-1 spectral imager (AaSI) for remote sensing purposes. AaSI is intended primarily to be technology demonstration to verify if such a miniaturized spectral imager based on Fabry-Perot interferometer is able to work in space environment. If the operation is successful, it will be used for the Aalto-1 remote-sensing campaign. University of Helsinki and University of Turku designs and delivers miniaturized particle telescope RADMON to provide information about proton and electron radiation environment on Low Earth Orbit (LEO). Finnish Meteorological Institute designs and manufactures electrostatic plasma brake (EPB), which is used as a de-orbiting device. It is based to e-sail concept which is developed to enable possibility for faster and cheaper interplanetary travel. (Kestilä et al. 2013)

One of the primary mission goals beside the scientific mission is to educate students and have real hands on experience of project working. Therefore, the Aalto-1 project offers special assignment, bachelor thesis and diploma thesis topics and arranges courses on various CubeSat topics.

1.3 Aalto-2

Aalto University is participating in a EU funded QB50 project with 2U CubeSat Aalto-2. The QB50 network will consist of 50 2U and 3U CubeSats. All the CubeSats have standardized sensors for in situ measurements of lower thermosphere. QB50 orbit is a sun-synchronous circular orbit with an altitude of 350 – 400 km (TBC before CDR) \pm 7 km, an inclination of $98.6 \pm 0.08^\circ$ and eccentricity of ± 0.04 (Singarayar et al. 2013). The launch for QB50 satellites is planned to be in mid 2015.

QB50 project allows participants to have their own payloads in addition to QB50 provided instrumentation. Aalto-2 shall therefore have one or more payloads (TBD) in addition to the mandatory instruments. The subsystems developed for Aalto-1 are used also as Aalto-2 subsystems whenever possible to reduce workload. Subsystems developed in-house for Aalto-1 are satellite structure, On-Board Computer (OBC), Antenna Deployment System (ADS), GPS, S-Band and UHF-radios. The mechanical structure for Aalto-2 has to be re-designed as Aalto-1 is a 3U satellite. In addition, attitude determination and control system (ADCS) and EPS are developed and manufactured in-house for Aalto-2. At the time of writing this thesis, Aalto-2 project has advanced to the detailed design phase.

1.4 Aim and structure of the thesis

The aim of this thesis is to determine requirements for Aalto-1 and Aalto-2 electrical power systems and develop a working prototype of the EPS for Aalto-2 nanosatellite. This thesis is structured as follows. Chapter 2 describes the environmental effects in space environment. These environmental conditions have to be taken in account when designing electronic system targeted for use in space. Chapter 3 discusses architectures used in traditional power systems and theory about DC-DC converters. Chapter 4 is dedicated to solar cell theory and maximum power point algorithms used to extract maximum available power of the cells. Chapter 5 is focused on the selection of suitable solar cells for nanosatellites and methods to connect the cells to form solar panels. Requirements for Aalto-1 and Aalto-2 nanosatellites are determined in Chapter 6. After clearing out the requirements, architectures of Aalto-1 and Aalto-2 are described in Chapters 7 and 8 respectively. Results and conclusions of the functional testing of the Aalto-2 prototype are presented in Chapter 9. Chapter 10 contains the summary and conclusions. Also suggestions how to proceed with the design are given.

2 Effects of the space environment

There are several environmental effects to be considered when operating an electrical device in space environment. LEO (Low Earth Orbit) is considered to be a vacuum, which affects the satellite in numerous ways. The vacuum causes deformations to materials and material outgassing referring to vaporization of material's surface atoms. Outgassing leads to deposition of material, which might be hazardous for optically or electrically sensitive surfaces (Fortescue et al., 2011).

Because of the possibility of outgassing, used materials should be chosen carefully. NASA (The National Aeronautics and Space Administration) and ESA (The European Space Agency) publishes a list of suitable materials with low outgassing values (NASA, 2012; ESA). Other environmental effects which has to be taken into account when designing spacecrafts are described briefly in the next chapters.

2.1 Thermal environment

Thermal environment in space is different compared to Earth as thermal energy cannot travel by convection due to the low residual pressure. Therefore, heat transfers only by conducting and radiating. This fact has to be considered when choosing components for the satellite.

A satellite on orbit has several heat sources:

- Direct solar flux; relative to the distance to Sun
- Albedo reflected radiation
- Infrared radiation reflected from Earth
- Heat generated by satellite's internal electronics

The temperature of the satellite is highly dependent of the chosen orbit and the temperature varies cyclically on it. When the satellite is on eclipse, only the Earth's infrared radiation and heat generated by the electronics are present, and the satellite cools down. Respectively, when the satellite is subject to direct solar flux, the temperature on the surface and inside the satellite rises. (Jacques, 2009)

Electrical components have certain temperature ranges in which they are designed to operate. High temperatures decrease the component lifetime and the majority of failures in electronic equipment are caused by thermal issues (Amy et al, 2009). Temperature gradients are of high scale when the satellite enters or exits the eclipse. That rapid change of temperature causes thermal shocks to components, especially to solar cells on the satellites' surface.

Batteries are very vulnerable to low temperatures and capacity losses occur when they are subject to them. Used battery chemistry determines the temperature characteristics. Batteries often require active heating to keep the temperature over a certain point. Heating is used in most CubeSats using batteries, but otherwise active thermal control is not generally used in nanosatellites because of the strict power and weight budgets. Also availability of electronic components with wide temperature operation ranges reduce the need of active thermal control.

2.2 Shock and vibration

A large portion of vibration originates from the launch vehicle's engines during the launch. Another large source of vibrations are aerodynamic effects caused by vehicle penetration through the lower region of the Earth's atmosphere. During the launch vibrations are of large scale and acceleration might be even 15 g depending on launch vehicle. Generally low mass payload vehicles such as missiles exhibit a high peak acceleration. (Fortescue et al., 2011) Such vehicles are often used as CubeSat launchers. When the satellite is on orbit, vibrational forces are moderately low and acceleration is smaller than on Earth.

Shock and vibration cause stress to the Printed circuit board (PCB) substrate and solder joints between the PCB and component packages (Amy et al, 2009). Risk of vibration induced damage is relatively low when soldering is done in a reliable way and inspected carefully. However the possibility of damage has to be taken into account when designing EPS-board because the vibration might break electrical contacts between the PCB and components. Damage is more likely if heavy components are used, as moment of inertia is dependent on mass.

Solar cells are fragile and vibration and shock effects should be taken into account when the bonding methods to the satellite are considered. Passive methods such as stiffening ribs or additional support can be used to damp the vibration on PCBs. Also some bonding materials have high dampening properties to reduce the vibration or shock effects. (Amy et al, 2009)

2.3 Radiation

The near-Earth space environment includes the radiation field, which can be extremely harmful for the electronic systems of the spacecraft. In the near-Earth environment there are several types of ionizing radiation present affecting spacecrafts such as protons and electrons trapped inside the Van Allen belts, cosmic ray protons and heavy ions, protons and heavy ions from solar flares. (Fortescue et al., 2011; LaBel et al., 1996)

The absorbed dose, also known as the total ionizing dose (TID) is used when measuring the rate of survivability of electronic components in a radiation environment. TID describes the energy deposited in a material by ionizing radiation per unit mass (J/kg). SI unit for absorbed dose is *gray* (Gy), but in the electronics industry *rad* (radiation absorbed dose) is widely used for the absorbed dose ($1 \text{ Gy} = 100 \text{ rads}$). Especially non-radiation-hardened SiO_2 films, silicon MOS devices and bipolar transistors are vulnerable to ionizing radiation. The basic phenomenon which causes degradation in radiation environment is that incident particles impinge the material causing displacement of atoms, which changes the electrical properties of the material. This leads to degradation of the component and eventually to component failure.

Single heavy particles produce a dense track of electron-hole pairs. This may lead to transient upsets on logic devices often referred to as single event effects (SEE) including single event upsets (SEU) and single event latch-ups (SEL). Silicon MOS, bipolar circuits and GaAs circuits are susceptible for single event upsets. SEUs do not damage the component permanently, but they may cause soft errors. SELs on the other hand cause permanent failure, often by short circuiting the component. Power MOS devices, silicon bipolar transistors and integrated circuits are vulnerable to SELs. Particle radiation is primarily caused by protons and electrons which are trapped in the Van Allen belts or ejected due the solar events. These particles may have energies up to several hundred million electron volts and the more energy the particles have, the deeper they can penetrate into the substance. (LaBel et al., 1996, Messenger et al., 2001)

Radiation also has effects on passive components by changing their characteristics. A common effect of radiation to tantalum capacitors are radiation-induced conductivity and variation in stored charge. Metallic thin-film resistors are quite tolerant to radiation. Table 1 describes primary and secondary damage mechanisms that radiation cause to the semiconductor devices and other components. (Srour & McGarry, 1988)

Table 1: Primary and secondary mechanisms causing permanent or temporary failures in the Space Radiation Environment for different devices, circuits, and components (Srour & McGarry, 1988)

Devices, Circuits, and Components	Damage Mechanisms								Temporary	
					Permanent					
	Lifetime Degradation	Carrier Removal	Trapping	Mobility Degradation	Charge Buildup and Interface Trap Effects	Single-Particle Latchup	Permanent Single-Particle Effects	Absorption		
Silicon bipolar transistors and integrated circuits	P	S			S ^a	P			P	
Silicon MOS transistors and integrated circuits				S	P	P	P ^b		P	
JFETs		P	P	S	S					
p-n junction diodes	P	P	P		S					
LEDs and laser diodes	P			P		P				
Charge-coupled devices	P						S ^c			
Photodetectors	P					P				
Microwave devices and circuits	P	P		S						
GaAs transistors and integrated circuits		P		S		S ^d			P	
Capacitors						P				
Diffused resistors		P		S						
Optical components (fibers, windows, mirrors)								P		

P = Primary; S = Secondary.

^aCharge buildup can be a primary failure mechanism in some types of bipolar integrated circuits [76].

^bPermanent single-particle effects occur in MNOS memories [104], [105] and in power MOS devices [106].

^cSingle proton interactions can cause relatively large increases in dark current density in CCDs [9].

^dFurther study of the effects of charge buildup in passivation layers in GaAs integrated circuits is required to evaluate the importance of this potential failure mechanism [96].

The radiation environment has to be known when considering radiation protection for the satellite to ensure that components survive on the chosen orbit through the mission. Therefore, the European Space Agency has developed a free tool called SPENVIS (Space Environment, Effects, and Education System) which can be used to estimate radiation in specific orbits. Information can be used together with the component manufacturer data sheets, which often state how much radiation the component can tolerate.

The most effective way to avoid problems caused by radiation is to shield the satellite in such a way that the radiation cannot harm sensitive electronics. This is often difficult in the CubeSat applications because of the strict weight and size limitations. When adequate shielding is not possible, radiation-tolerant or radiation-hardened components may be used to strengthen the electrical systems against radiation.

High energy particle radiation affects also solar cells degrading them and lowering their efficiency. The rate of degradation depends on the energy of the incident particle and the type of the cell as different materials react differently to radiation. Radiation effects depend on doping of the cells, thickness of the active region and the chosen orbit. (Fortescue et al., 2011) Figure 2.1 gives an estimate of displacement damage equivalent fluence caused by 1 MeV electrons and protons on different orbit heights and inclinations. The figure shows that the damage is fairly small in lower orbits (< 900 km), where CubeSats are commonly launched.

Using a coverglass as a shield on top of the cell decreases the degradation by slowing down the particles before they impinge the active region of the cell. Thickness of the coverglass affects the degradation speed and by using a thicker coverglass the end-of-life (EOL) performance of the solar cells can be increased significantly. (Messenger et al., 2001) The SPENVIS is also capable to estimate damage equivalent fluences for Si, GaAs, and multi-junction solar cells for various orbits. Manufacturers of space-graded cells usually deliver specifications for estimating degradation of cell efficiency in relation to the total ionizing radiation dose.

Also ultraviolet radiation causes optical and electrical changes to materials. This affects especially the properties of the solar cell coverglass and adhesive used for coverglass bonding. Exposure to UV-light darkens the coverglass causing efficiency deterioration of the cells. (Fortescue et al., 2011)

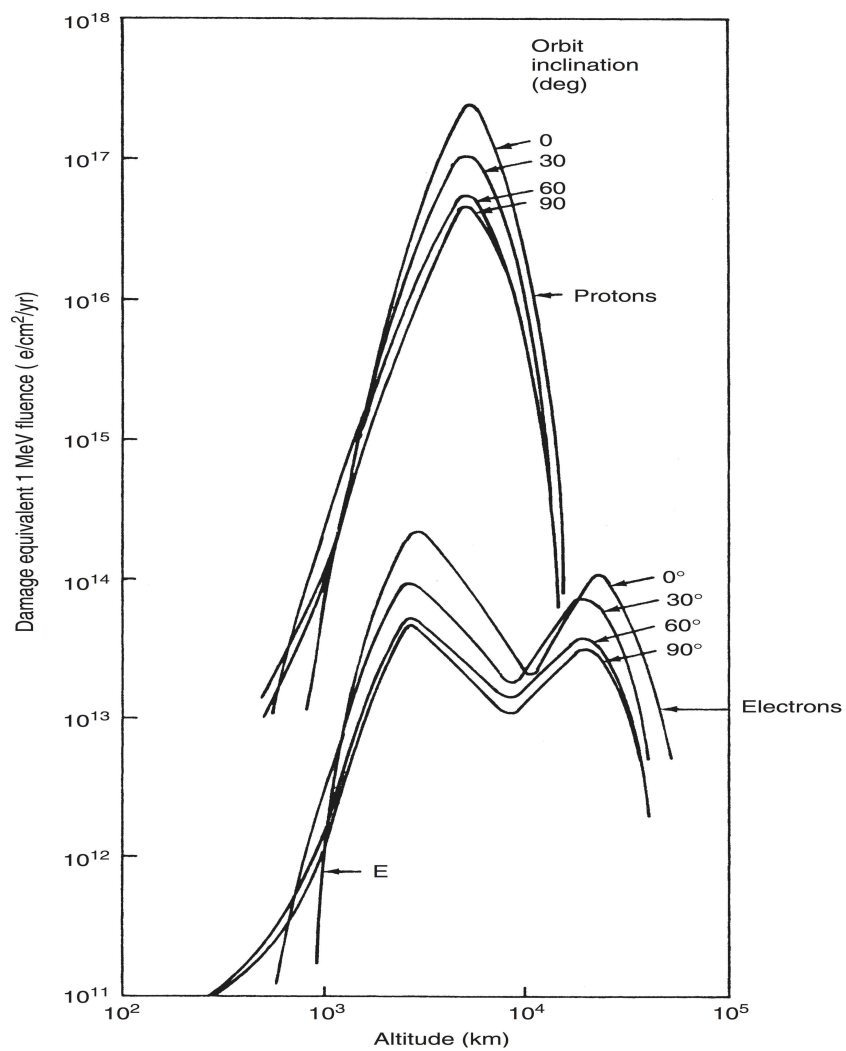


Figure 2.1: Damage equivalent 1 MeV fluence caused by electrons and protons due to trapped particles, to silicon cells protected by 150 µm fused silica covers and infinitely thick rear shielding (Rauschenbach, H. S. 1980)

2.4 Component selection

Traditionally leaded metal or ceramic packages have been used in space applications because they are hermetically sealed and offer some protection against radiation. However plastic encapsulated microcircuits (PEMS) are gaining acceptance in several fields including space applications due to the advantages they offer. Nonetheless some of the properties of PEMS have to be taken into account when using them as components in space electronics (Bjorndahl & McMullen, 1999):

- How well encapsulation protects the circuit against moisture absorption
- Protection against radiation induced damage
- Handling PEMS components during storage and assembly

One of the biggest problems in using plastic encapsulated components in space is the “Popcorn effect”, which was first presented by Fukuzawa et al. in 1985 in their study “Moisture resistance degradation of plastic LSI's by reflow soldering”. When high temperature moisture is present in a package, it might vaporize due to the thermal cycles in the vacuum and cause stress to the package. This might crack the package or cause delamination between the mold compound and the lead frame or die. The “Popcorn effect” can be reduced by baking the component before attaching it to the PCB. Proper handling during storage and assembly is also necessary. If the storage conditions are not adequate, components might absorb moisture. Problems with moisture absorption have reduced in recent years as manufacturers have noticed the problem and plastic encapsulants have evolved. (Bjorndahl & McMullen, 1999; Chen & Li, 2011) Another problem in using plastic packaging is that some types of plastics are subject to material outgassing and therefore ceramic casing should be used when applicable.

In space applications, individual components have to be tested if there is no proof of flight-heritage. This is necessary as some components cannot tolerate the space environment, e.g. aluminium electrolytic capacitors electrolyte evaporates in vacuum. For CMOS devices, radiation-hardened components are highly recommended. Low quiescent power ICs should be used to save energy. Also military rated components are suggested, but at least industrial rated should be used. Usually in traditional space projects radiation-tolerant or radiation-hardened components are used, but they are not generally used in CubeSat projects because of their high price. The European Space Components Information Exchange System (ESCIERS) provides a component database about components used in space. The database is used to choose components for Aalto-2 flight model when applicable to ensure component reliability in space environment. (ESCIERS, 2012)

Traditionally manual inspection of the solder joints has been developed as a standard in applications demanding high reliability. Therefore packages which do not allow visual inspection such as BGA packages are not suggested to be used in space applications and are avoided also in the Aalto-2 EPS design. Also some of the packaging options are not suitable because the lack of equipment for soldering. Using such components makes prototyping hard.

Pre-launch environment has to be taken in consideration for flight parts. Usually designing, manufacturing and integrating all parts on the final CubeSat is a lengthy process which may take several months or even years. For this reason all flight parts should be stored in suitable premises. Some of the parts might degrade if stored too long. Used components shall go through a derating process. The derating is used to lower the mechanical, thermal and electrical stresses for the components. Simple table presenting NASA's recommended derating values for different part types is shown in Table 2. (NASA-PD-ED-1201)

Table 2: Recommended derating levels for different part types

PART TYPE	RECOMMENDED DERATING LEVEL
Capacitors	Max. of 60% of rated voltage
Resistors	Max. of 60% of rated power
Semiconductor Devices	Max. of 50% of rated power
	Max. of 75% of rated voltage
	Max. junction temperature of 110°C
Microcircuits	Max. supply voltage of 80% of rated voltage
	Max. of 75% of rated power
	Max. junction temperature of 100°C
Inductive Devices	Max. of 50% of rated voltage
	Max. of 60% of rated temperature
Relays and Connectors	Max. of 50% of rated current

2.4.1 Reliability consideration

Solar arrays and electrical power distribution systems, including batteries cause most of the insurance claims according the study performed by Brandhorst & Rodiek. Large number of the insurance claims of larger satellites in LEO and GEO orbits results from problems in solar panel deployment systems. Most of the anomalies occur in infant mortality period, which often originates of bad design or manufacturing defects in panels or individual cells. (Brandhorst Jr. & Rodiek, 2008)

As CubeSats are inexpensive and launch costs are small compared to conventional satellites, risk tolerance does not have to be at the same level as in conventional satellites. This leads to possibility to have less redundancy on board as financial losses are not that massive. The possibility to take larger risks also allows the use of modern technology in CubeSats. In traditional satellites components have to be tested thoroughly, which costs a lot of time and money. There are some guidelines to follow to make sure that design is reliable:

1. Keeping the design simple, as additional functions and components increases probability of failure

When designing a power supply, simplicity is a good design rule. Trade-offs between reliability and system features have to be made. DC/DC converters are one of the most failure prone parts in power supplies. When only a single converter supplies power to the subsystems, all payloads and subsystems connected lose power in the DC/DC converter failure situation. It is a good idea to limit different delivered voltage levels to minimum to keep converter amount as small as possible. It is important to dimension the converter suitable for the different load conditions to lower the stress and keep the converter in normal operation temperatures. This is even more important in space application, as convective heat transfer is not present in space. An easy assembly of the device also increases the reliability.

2. Correct design

All the chosen components should have more electrical and mechanical strength than they have to handle during the launch phase and in different operation modes. Derating the components using values stated in Table 2 is a good way to ensure sufficient electrical strength. Mechanical stress may be reduced by using light weight components and a reliable bonding method to the substrate.

3. Adequate testing

Environmental testing in similar conditions where the design is used is needed to ensure that the product can survive for the defined mission time. In many cases it is wise to test components suitability for use in space in an early phase of the design process as changes in later phases are more expensive in terms of time and money. Testing shall be done for several units to achieve reliable results.

4. Failure analysis

FMECA (Failure mode, effects and criticality analysis) is a risk analysis method, which gives designer valuable information on where a single point failure might happen and where the design needs improvement.

There are also multiple ways to increase reliability:

- Redundancy; One way to increase reliability is to add hardware redundancy to avoid single point failures. Adding independent power paths for charging batteries and several DC/DC step converters in parallel. Then single failure in battery charge regulators (BCR) or DC/DC converters will not cause (fatal) failure and loss of the satellite. Several battery-packs in parallel are worth considering.
- Using at least industry rated components.
- Use of reliable packaging, inspection of solder joints. Using traditional space approach when solder joints can be inspected without any special tools.

3 Power system architectures

There are three main types of power supply architectures: centralized, distributed and systems using intermediate bus. The centralized power system provides various voltages to loads through multiple outputs from one centralized location. The biggest advantage in using such architecture is to have all power processing technology in a single box. On the other hand, having the voltages delivered from one position using low voltages and high current causes copper losses and low efficiency when variable sized loads are connected. Centralized power system architecture is presented in Figure 3.1. (Chakraborty, 2006)

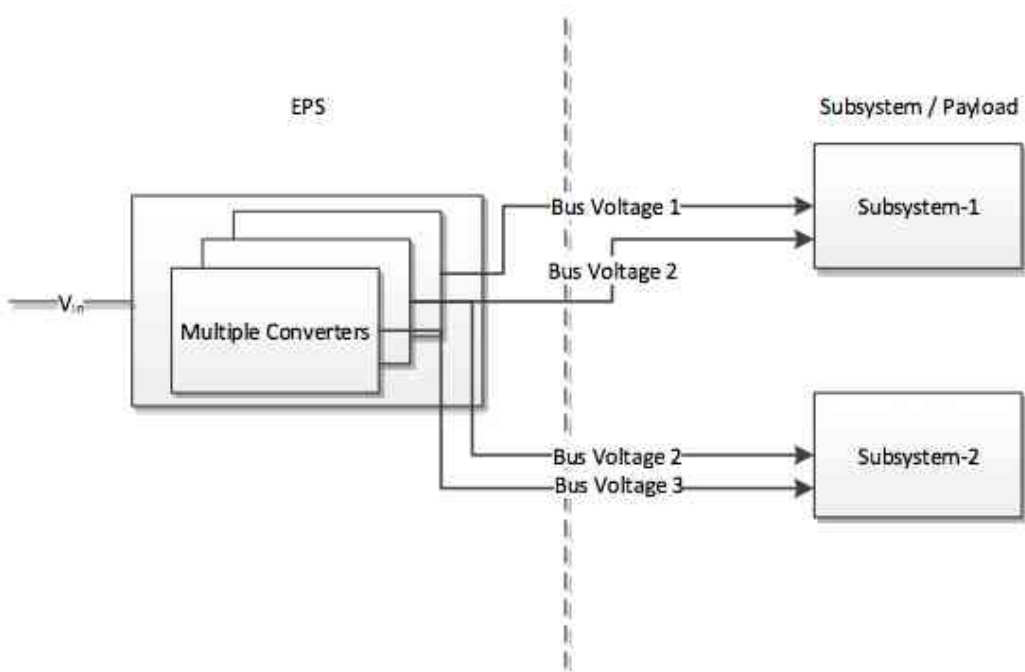


Figure 3.1: Centralized power system. EPS supplies multiple bus voltages for subsystems and payloads

The distributed power systems (DPA) deliver intermediate voltage next to the point of load (POL) where further regulation is done if needed. Basic configuration of a distributed power system is shown in Figure 3.2. Advantages of such a system are the possibility to match the DC-DC converter to the load and achieve better efficiency. Also heat generated in converters distributes more uniformly throughout the whole system. Obvious disadvantages are that more DC-DC converters are needed and subsystem/ payload manufacturers have to further regulate the voltages in their systems. (Chakraborty, 2006)

The intermediate bus architecture voltage conversion has one more conversion step compared to DPA systems. IBA delivers bus voltage to bus converter which converts the voltage more suitable to point-of-load converter and performs the isolation when the bus voltage is high. Due the extra conversion step, efficiency is usually lower than in DPA solutions, but non-isolated POL regulators are much cheaper when conversion can be made from already isolated voltages.

Traditional spacecrafts have been using distributed power systems with a single voltage bus, where subsystems and payloads are responsible for further regulation if needed at the POL. Smaller spacecrafts use 28 volts as a de facto industry standard voltage. However, most of the CubeSats rely on the centralized power architecture. (Burt, 2011) When using single voltage bus, isolating converters are seldom used, as bus voltages are of small magnitude in the CubeSat power systems.

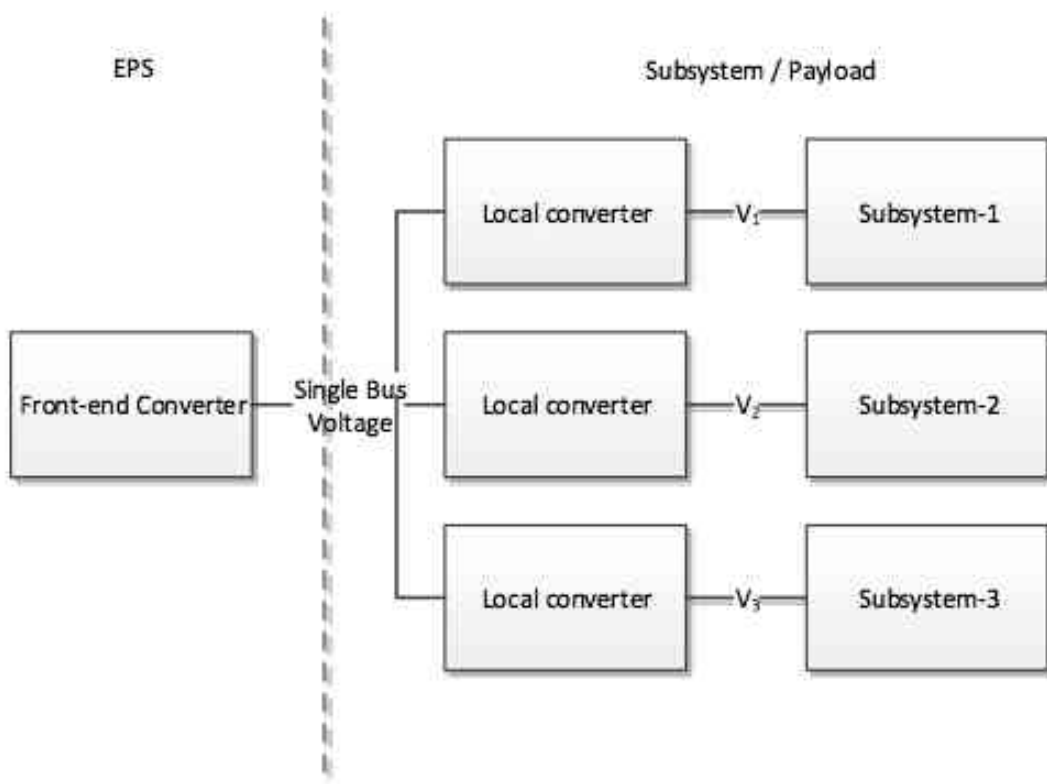


Figure 3.2: The block diagram of a distributed power system

An important issue in power systems is the possibility to use more converters than the minimum required by load. Usually $(m+r)$ converters are used, where m is the minimum amount required by load and r is number of redundant units. In most applications one extra unit is enough. An obvious disadvantage, when using redundant converters is increased complexity of the circuit.

The parallelization of multiple converters provides several benefits. The most important for space applications is that parallelization offers fault tolerance through hardware redundancy as converters can operate also individually. Another advantage is sharing the load between multiple power stages. Load sharing leads to lower currents on the components, extending their lifetime as the temperature stays lower. Parallelization also allows using components designed for lower currents. This leads to the possibility of using smaller and less expensive components. (Luo & Batarseh, 2005)

Some type of control is needed to distribute currents evenly to all of the converters, because parallel modules are not identical due to finite manufacturing tolerances. Therefore several methods have been developed for controlling the currents flowing through power converters. There are lot of differences between complexity and current-sharing performance between these methods. Methods are often divided into two categories: droop methods and active current sharing methods. Luo et al.

presents in their article “A classification and evaluation of paralleling methods for power supply modules” classification for different paralleling methods for power supplies. The classification diagram is shown in Figure 3.3. (Luo et al., 1999)

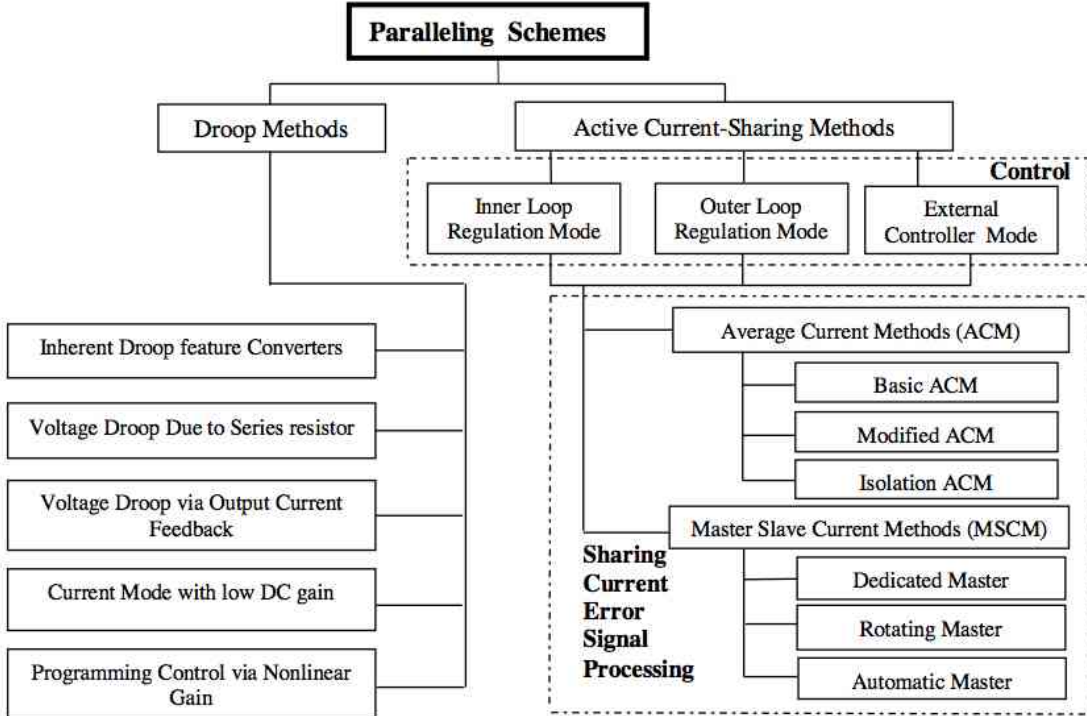


Figure 3.3: Classification diagram for paralleling methods (Luo et al., 1999)

3.1 DC-DC converters

DC-DC converters are necessary to transform battery voltage suitable for spacecraft subsystems and payloads. There exist several different types of DC-DC converters with different characteristics. Each type has its advantages and disadvantages typical for the device in question. Important parameters when choosing the suitable DC-DC converter are voltage conversion ratio range, maximum output power, efficiency, number of components needed and required footprint size. Power conversion efficiency is extremely important parameter in battery powered equipment, where the amount of stored energy is limited. Better efficiency leads to lower energy consumption, lowering the battery utilization and lengthening battery lifetime. High efficiency also reduces the heat dissipation and helps manufacturing smaller components without the need for large heatsinks. Also one often neglected effect is that low temperature reduces conduction losses in metals caused by positive temperature coefficient resistive behaviour.

3.1.1 Linear voltage converters

The oldest method for DC-DC voltage conversion is using linear voltage converters also known as resistive dividers. They dissipate excessive power into a resistor causing a voltage drop. Therefore they are not ideal in terms of conversion efficiency, especially when difference between U_{out} and U_{in} is large, because power loss P_{loss} is determined by Equation:

$$P_{loss} = V_{drop} * I, \quad (1)$$

where V_{drop} is the voltage drop of the resistor and I is the current through the resistor.

The advantages in using linear converters are a fairly simple implementation and the lack of large, space consuming passive components. There are two types of linear voltage converters, the series and the shunt converters. The power conversion efficiency is proportional to voltage conversion ratio when using the series or shunt linear voltage converters. In addition it is also proportional to the output power when using the shunt converter. Linear series voltage regulators are used in applications with low difference between U_{out} and U_{in} because in such cases they achieve a moderately high efficiency as the voltage drop is fairly small. (Wens & Steyaert, 2011)

LDO-regulator (Low-dropout regulator) is one type of linear regulator which utilizes open collector or open drain topology. That kind of topology enables saturation of transistor and voltage drop from the unregulated voltage to the regulated voltage may be as low as the saturation voltage across the transistor. LDOs are a viable option if subsystems or payloads current usage is low. The advantage of using a low-dropout regulator is reduced part count increasing the reliability and reducing footprint size as amount of external components is smaller.

3.1.2 Inductive DC-DC converters

Inductive DC-DC converters consist of one or more inductors and capacitors and at least one switch. The reason to use inductors instead of capacitors to store the charge is that inductors are less lossy. By using these components on different topologies various types of DC-DC converters can be created, e.g. a step-down (buck), step-up (boost) or buck-boost converter.

These types of converters belong to the group of switched-mode DC-DC converters like charge-pumps that are introduced briefly in Chapter 3.1.2.4. Switching power supplies offer better efficiency than traditional power supplies using linear voltage regulators. High efficiency is required in space application as the power production is usually limited. Another advantage compared to linear regulators is the possibility to provide output voltages higher than input (e.g. step-up converter) and inverted voltages (e.g. buck-boost, charge pumps).

Trade-off between higher or lower switching frequency has to be considered. Higher switching frequency reduces footprint of circuit because smaller capacitors and inductors can be used. On the other hand efficiency is reduced because using higher frequencies causes more switching losses. Therefore compromise between small footprint and desired efficiency has to be made.

There are inductive DC-DC converter IC (Integrated Circuit) packages available on the market from many chip manufacturers. The purpose of such IC is to monitor the output voltage and maintain it in desired level. This can be achieved using voltage or current-mode control. In voltage-mode control (Figure 3.4), error-amplifier samples the output voltage and subtracts it from a reference voltage (V_{ref}). The result gives an error signal V_c , which is compared to fixed external ramp signal. Comparator outputs a digital PWM (Pulse width modulation) signal to control the switch(es). Change in the output voltage affects the error signal and the comparator alters the duty cycle to reduce the error signal to zero. Current-mode control (Figure 3.5) uses the sensed inductor-current ramp instead of fixed ramp signal to generate the PWM signal. Therefore two loops are needed when using current-mode control. (Li, 2009) In most cases the circuit designer has to choose only

inductor(s), capacitor(s) and several resistances to set parameters of the converter. (Skvarenina, 2002; Erickson, 2007)

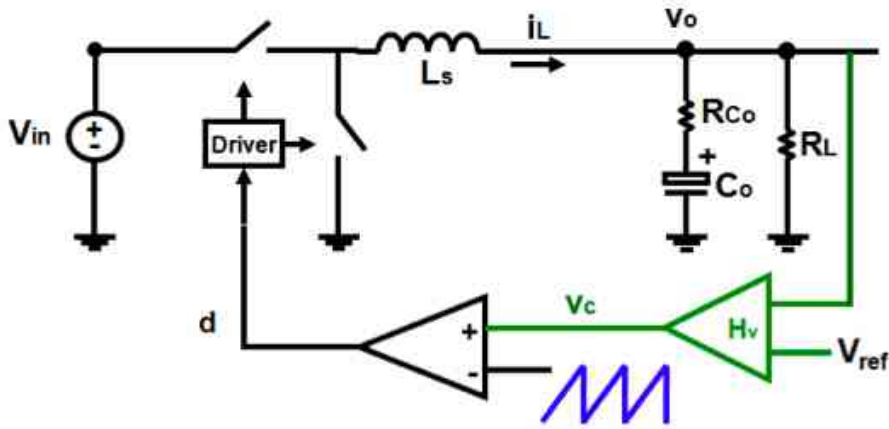


Figure 3.4: Circuit diagram of voltage-mode control (Li, 2009)

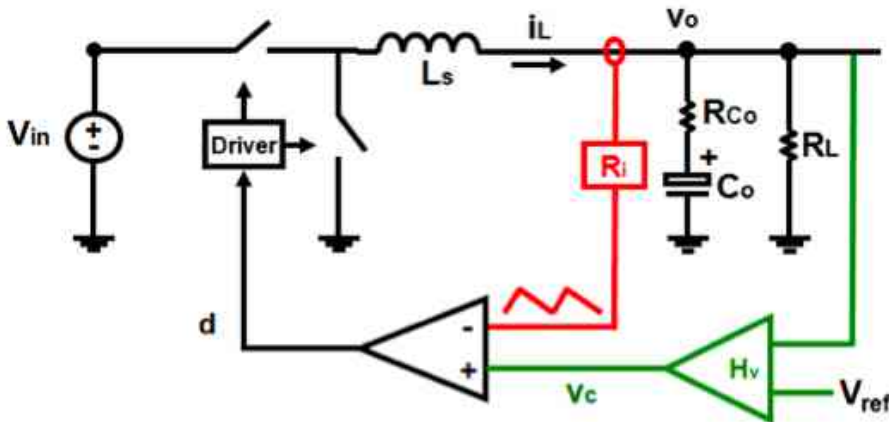


Figure 3.5: Circuit diagram of current-mode control (Li, 2009)

3.1.2.1 Step-down converters

Step-down (buck) converters are used to transform higher voltage to lower. Buck converters typically achieve efficiency rates between 70 to 95%. A buck converter consists of switch network which reduces the DC component of the voltage and a low pass filter to remove high-frequency harmonics. (Erickson, 2007)

A typical buck converter circuit is illustrated in Figure 3.6. Usually power MOSFET and diode is used to realize the switches, but other kind of semiconductor switches can be used as well. If MOSFET is used instead of the diode, better efficiency is achieved due to the smaller voltage drop. In that case the converter is called a synchronous buck converter. Output voltage can be adjusted by changing the duty-cycle between 0 and 1. Output capacitor in the circuit is used to smooth out the current and voltage transition caused by the switching part of the converter. Inductor acts as an energy reservoir when the switch is closed and transfers the stored energy to the capacitor when the switch opens. (Skvarenina, 2002; Erickson, 2007)

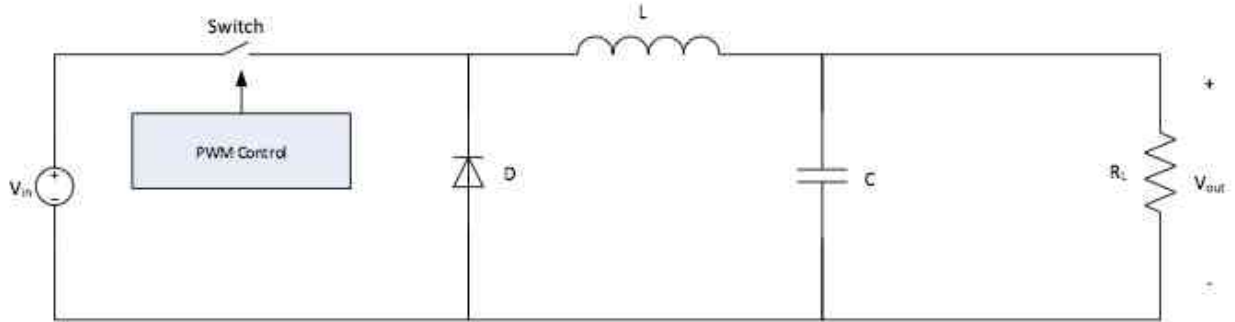


Figure 3.6: Circuit diagram of a typical step-down converter

3.1.2.2 Step-up converters

A step-up converter is used to boost input voltage to higher output voltage and is therefore also called a boost converter. Boost converter components are arranged differently compared to step-down converters. A typical boost converter is illustrated in Figure 3.7. When the switch is closed, current flows from the input through the inductor and the energy is stored in the inductor's magnetic field. At this point there is no current flowing through the diode and load is supplied by the charge of capacitor. When the switch is opened, the voltage of inductor adds to the source voltage and current flows from the inductor to load and to the capacitor recharging it. (Skvarenina, 2002)

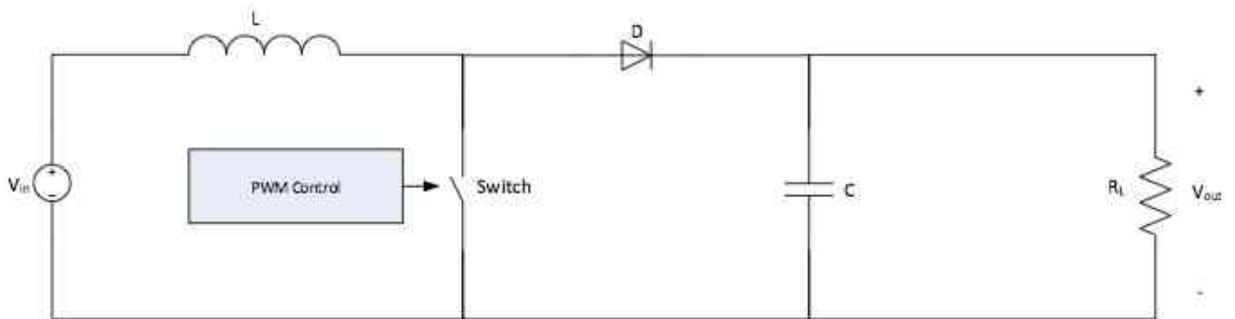


Figure 3.7: Circuit diagram of a typical step-up converter

3.1.2.3 Buck-boost converters

Buck-boost converters are practical when input voltage varies below or above the desired output voltage. This is common especially in different kinds of portable equipment, for example single lithium-battery discharges from 4.2V to 3.0V. Thus the system is not able to provide an output voltage of 3.3 V in all situations if single buck or boost converter is used.

A circuit diagram of a typical buck-boost converter is shown in Figure 3.8. When the switch is closed, current starts to flow from source to inductor, storing energy in its magnetic field. The current does not flow through the reverse biased diode, but the capacitor supplies the load. Opening the switch forward biases the diode and current flows from inductor to the load and capacitor

recharging it. As in buck and boost converters, output voltage can be adjusted by changing the duty-cycle between 0 and 1.

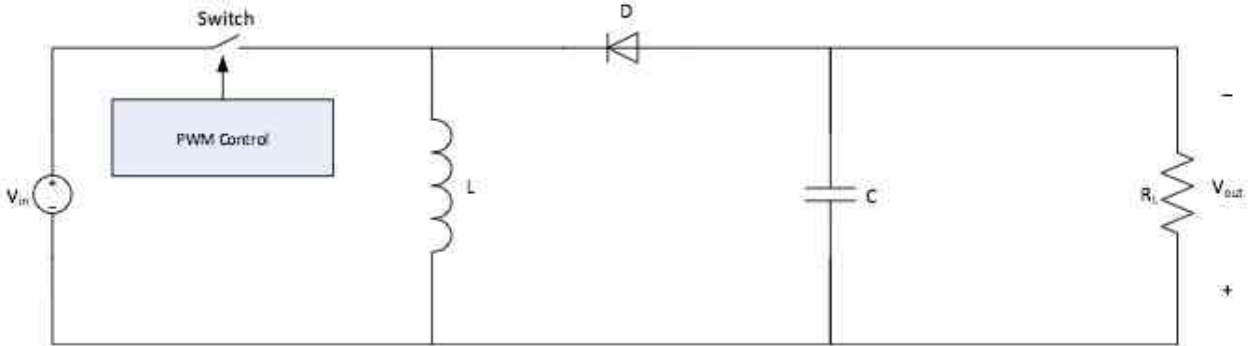


Figure 3.8: Circuit diagram of a typical buck-boost converter

3.1.2.4 Charge pumps

Charge-pumps are DC-DC converters, which use a capacitor to store the energy as electric charge. Converters of this type are usually used in voltage multiplying applications. Capacitors used should have low ESR-value to minimize the losses. It should also be able to handle large ripple currents. Charge-pumps can step-up, step-down and invert the voltage.

Charge-pumps are cheaper and more compact than converters using inductors. Disadvantage when using charge-pumps in battery powered systems is that charge-pump efficiency is highly dependent on the input voltage. Another disadvantage is that they can supply only low currents. For example Texas Instruments manufactures charge-pumps delivering current up to 300 mA (TI, 2013). Therefore, charge-pumps are usually not the best option for centralized power architectures, but may be well suited for Point-of-load (POL) regulation for systems with small power requirements and where the input voltage is regulated.

3.2 Protection circuits

Protection circuits are needed to protect loads from anomalies caused by various environmental reasons such as single event upsets and latch-ups. Such circuits also protect the power system itself from subsystem or payload failures. Most common protection circuits are current limiters which are used to limit the current in possible short circuit situation.

Single event latch-ups (SEL) occur when a high energy particle hits the component. SEL can be noticed by monitoring the current of the supply and if sudden increase in current consumption is detected, the protection circuits' responsibility is to disconnect the affected system from the electrical power system and inform the system of the anomaly. Fast response to such an event may save the system from permanent damage. The circuit can be set for automatic retry or latch-off mode. If latch-off is chosen, the microcontroller sends a command to the protection circuit to connect loads back to the system. Also batteries need overcharging or undercharging protection circuits as battery capacity is heavily affected on those conditions.

4 Solar cells

4.1 Solar cell theory

A solar cell is an electrical device that converts energy in light into electricity using the photovoltaic effect. The simplest equivalent circuit of a solar cell can be modelled as a current source and a diode connected in parallel. The output of the current source is directly proportional to the light coming to the cell. This kind of circuit represents an ideal solar cell and is presented in Figure 4.1. V is voltage across the output terminals and the diode, I_L is photogenerated current, I_d is saturation current of the diode and I is output current. I_d can be obtained by using the Shockley diode equation for an illuminated pn-junction:

$$I_d = I_S \left(e^{\frac{V_D}{nV_T}} - 1 \right) \quad (2)$$

Where I_d is the current through the diode, I_S is the reverse saturation current, V_D the voltage across the diode and n is the quality factor of the cell. V_T is the thermal voltage kT/q , where k is the Boltzmann's constant, T is the temperature in Kelvins and q is the charge of electron.

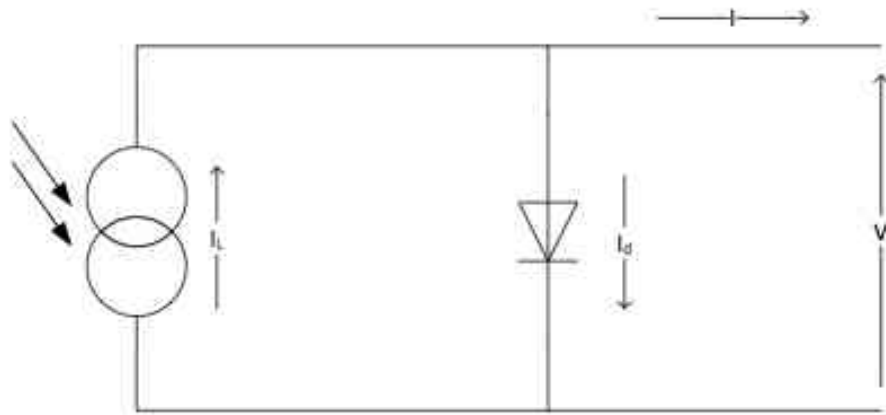


Figure 4.1: Model of the ideal solar cell

Thus output current I is:

$$I = I_L - I_d \quad (3)$$

By substituting Eq (2) to Eq (3), the result is the characteristic equation of the ideal solar cell:

$$I = I_L - I_S \left(e^{\frac{V_D}{nV_T}} - 1 \right) \quad (4)$$

A more realistic solar cell model can be achieved by adding (Walker, 2001):

- Temperature dependence of the diode saturation current I_O
- Temperature dependence of the photogenerated current I_L
- Series resistance R_s
- Shunt resistance R_{sh} in parallel with diode
- Using two diodes in parallel to get two independent saturation currents
- Diode quality factor n may be variable parameter

This equivalent circuit is presented in Figure 4.2. Figure represents the Mottet model of a solar cell, which is also referred as the two diode model (van den Berg & Kroon, 2002). In the figure I is the output current, I_L is the photogenerated current, I_d is the saturation current of the diffusion diode (D_1), I_r is the saturation current of the recombination diode (D_2), I_{sh} is the current through shunt resistor, V_j is the voltage across the diode and shunt resistor and V is the voltage across the output terminals.

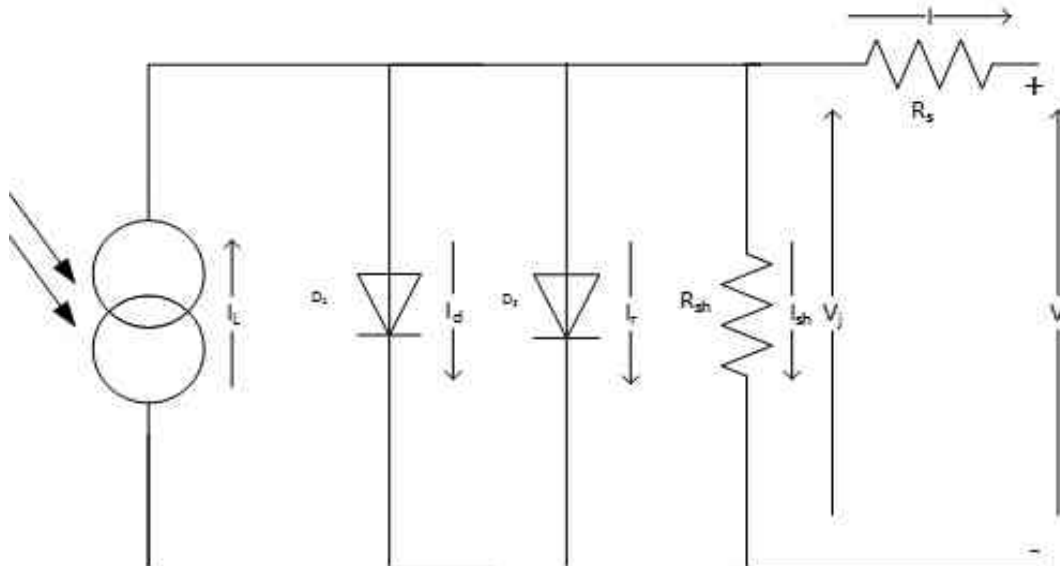


Figure 4.2: Mottet model of the solar cell

Equivalent Kirchhoff equations for the circuit presented in Figure 4.2 are (van den Berg & Kroon, 2002; De Luca, 2011):

$$V_j = V + IR_s \quad (5)$$

$$I = I_L - I_d \left(e^{\frac{V_j}{V_T}} - 1 \right) - I_r \left(e^{\frac{V_j}{2V_T}} - 1 \right) - \frac{V_j}{R_{sh}} \quad (6)$$

The current relationship to temperature is (De Luca, 2011):

$$I_d = C_d * T^{\frac{5}{2}} * e^{\frac{E_g}{n_1 * T}} \quad (7)$$

$$I_r = C_r * e^{\frac{E_g}{n_2 * k * T}} \quad (8)$$

Where C_d and C_r are constants independent from temperature, T is temperature and E_g is the energy of the prohibited band gap (De Luca, 2011):

$$E_g = E_{g0} - \frac{\alpha * T^2}{T + \beta_e}, \quad (9)$$

where E_{g0} , α and β are material constants and T is temperature.

4.2 Maximum power point tracking

Due to the non-linear current-voltage relationship of the solar cell there is a specific point on current-voltage curve ($I-V$), where the solar array operates with maximum efficiency producing maximal output power. This point is called the maximum power point (MPP). Figure 4.3 shows $I-V$ curve and power-voltage ($P-V$) curve for Azur Space 3G30C cell modelled with Matlab using the data available on the manufacturer's datasheet (Azur Space, 2012a). Values used to estimate the curves are shown in Table 4. Matlab code is based on model presented by Walker in 2001 and modified to be usable with Azur Space cells. Model is simplified model of the solar cell neglecting the shunt resistance and the recombination diode (Walker, 2001). Matlab code is presented in Appendix A.

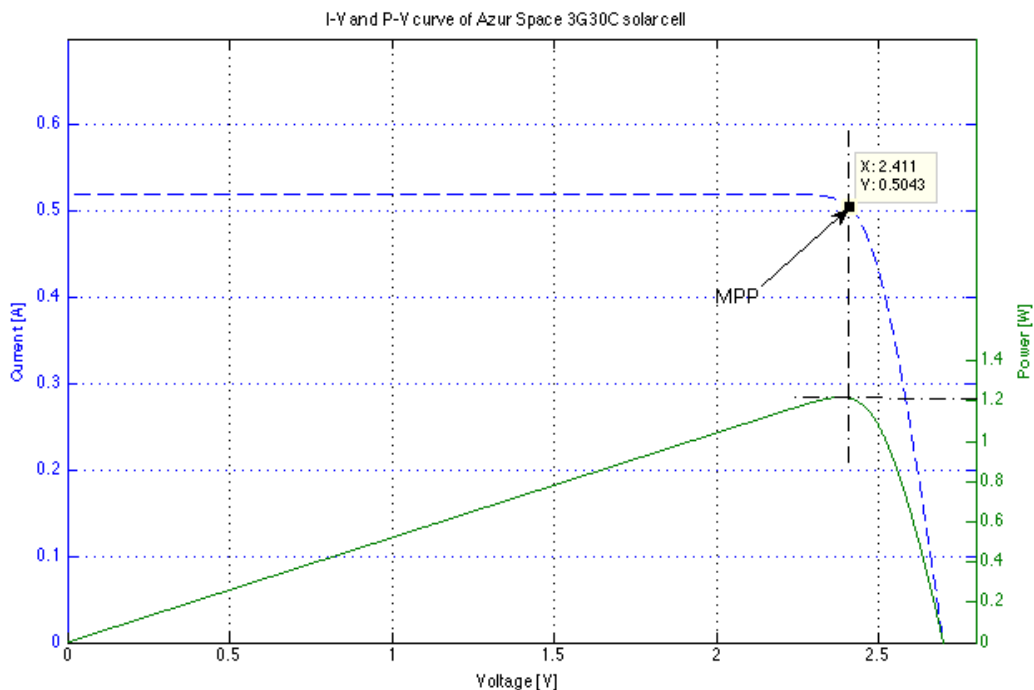


Figure 4.3: $I-V$ curve and $P-V$ curve of Azur Space 3G30C cell ($T=28^\circ\text{C}$, $E=1367 \text{ W/m}^2$). Power curve can be used to determine the MPP

The idea of maximum power point tracking (MPPT) is to adjust the operating point in a way that maximum power is achieved. The MPP location depends on multiple parameters including total solar insolation coming to the cell, orientation to the sun, temperature, aging of the cell and type of cell used. (Hohm & Ropp, 2003) $I-V$ curves for 3G30C cell in respect to temperature are presented in Figure 4.4. Rise of the temperature increases the MPP current (I_{MPP}) and decreases the voltage on MPP (V_{MPP}). The figure shows that higher temperatures decrease cells efficiency as the voltage decreases more rapidly than the current rises.

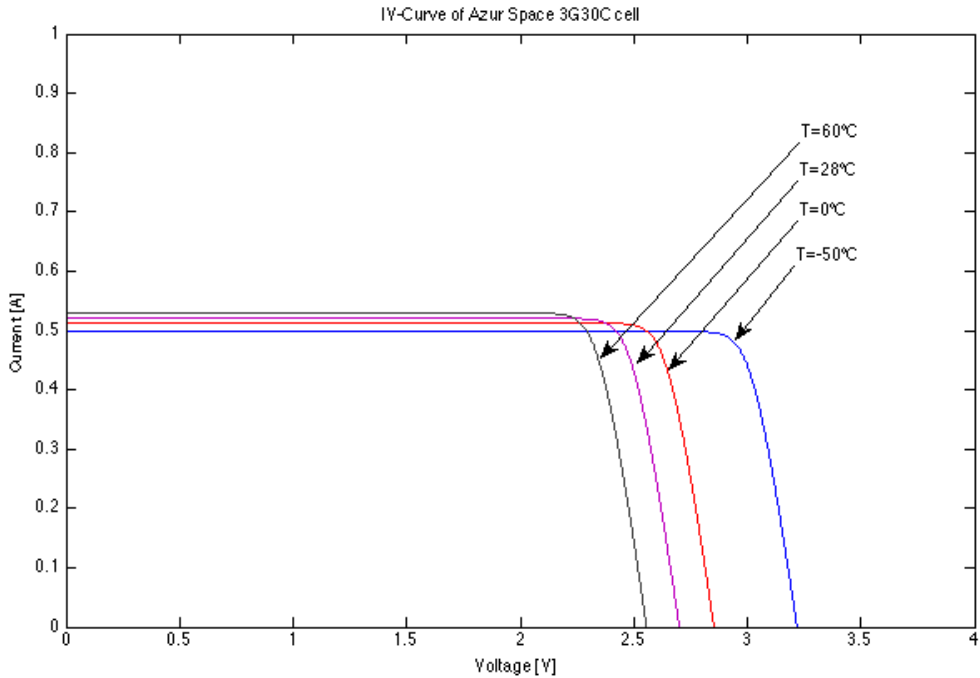


Figure 4.4: $I-V$ curves of Azur Space 3G30C cell in respect to temperature

Solar arrays can be connected directly to the load using the Direct Energy Transfer (DET) method (Figure 4.5). The array operates at the MPP when the conditions are ideal and the load is properly matched with the array. In reality conditions are not ideal, while satellite's angle towards the Sun changes on its orbit around the Earth and the amount of solar flux arriving to solar cells varies significantly. Also temperature variation and degradation of the solar cells have large effects on the MPP position. Therefore MPP-tracking methods are needed to find the power point in varying conditions. In most cases MPPT functionality is achieved by using a series converting device between the load and the solar array (Figure 4.6). MPPT-controller maintains the solar arrays operating point at the MPP by changing the array's operating voltage.

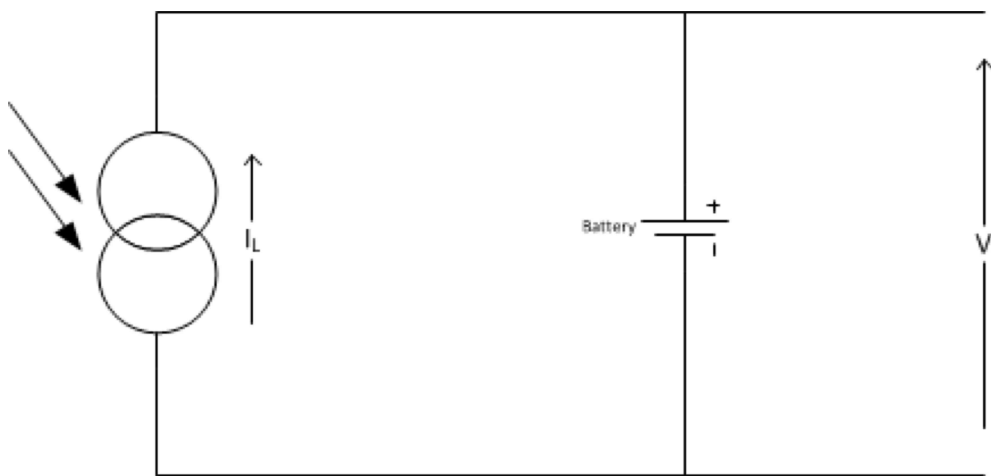


Figure 4.5: Direct energy transfer based system. A battery is connected directly to the solar array

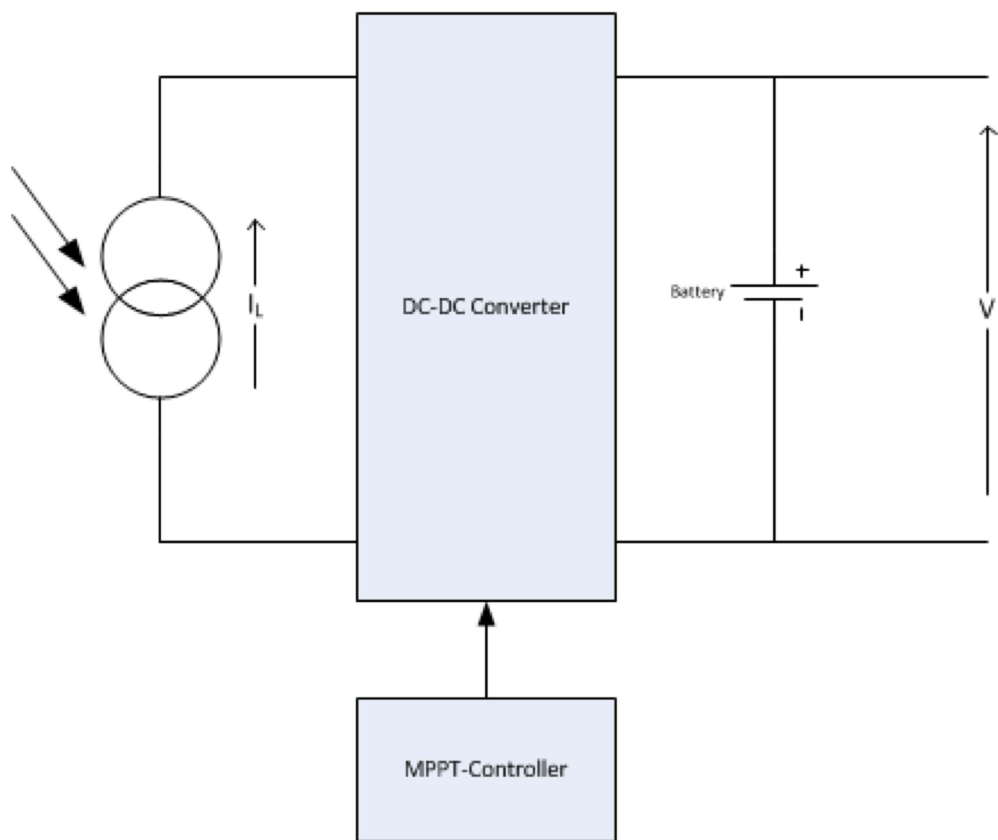


Figure 4.6: System based on the maximum power point tracking. Loads are connected to the array using a series converter device

MPPT adjusts DC-DC converters ratio in such a way that the solar panel operates at the MPP. Duty cycle (D) when using a buck converter is calculated using Eq (10).

$$D = \frac{V_{battery}}{V_{panel}}, \quad (10)$$

where $V_{battery}$ is the battery voltage and V_{panel} is the solar panel voltage at maximum power point.

4.3 MPPT algorithms

There are various MPPT algorithms available to suit different purposes. Algorithms have differences on e.g. efficiency, complexity and response time. Following subchapters describe briefly the most common ones.

4.3.1 Perturb-and-observe

The perturb-and-observe (P & O) algorithm is the most widely used algorithm for MPPT because of its simplicity and efficiency. It is based on the fact that power increases when the operating point is moving towards the MPP. If total power production increases when changing voltage, the operating point is closer to the MPP. This method can cause oscillations to power output because it cannot accurately determine the point where the MPP is actually reached. It can also function erroneous if irradiance levels are changing rapidly. Therefore, more advanced versions of the P & O algorithms are developed to reduce oscillations. Literature suggests various methods, e.g. adding a waiting period between the measures or using a three-point weighting comparison. Drawbacks in these methods are increased complexity and reduced response time. (Hohm & Ropp, 2003)

The P & O algorithm can be implemented by using the flow chart presented in Figure 4.7. First the product of $V(k)$ and $I(k)$ are calculated to get the total power at the beginning. Then the voltage is perturbed by small increment and a new power measurement is done. The difference between power measurements shows if change has happened towards or away from the MPP. In other words if $P(k) - P(k-1) < 0$ then direction of perturbation has to be changed. Tracking direction is forward if power and voltage increases. (Onat, N. 2010)

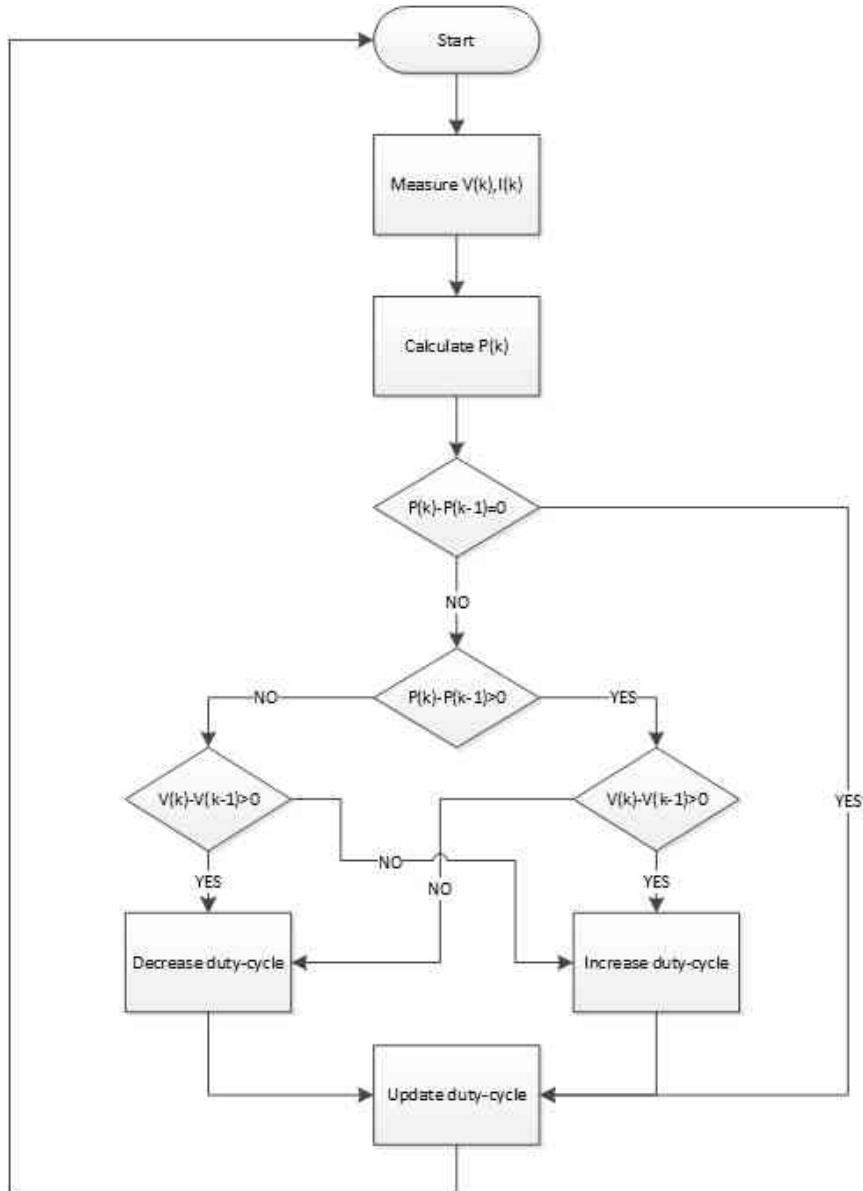


Figure 4.7: Flow diagram of the perturb-and-observe algorithm

4.3.2 Incremental conductance

The incremental conductance (IC) algorithm measures the derivative of the current with respect to voltage to determine the MPP. The maximum power point is achieved when:

$$\frac{dI}{dV} = -\frac{I}{V}, \quad (11)$$

where $\frac{dI}{dV}$ presents incremental conductance of the array and $-\frac{I}{V}$ is the negative instantaneous conductance.

The IC method has an advantage over the P & O method as it can determine in which direction the voltage has to be changed to achieve the MPP. (Onat, N. 2010)

The operating voltage of the solar array has to be increased, when

$$\frac{dI}{dV} > -\frac{I}{V} \quad (12)$$

and decreased if

$$\frac{dI}{dV} < -\frac{I}{V} \quad (13)$$

to achieve maximum power point.

A controller based on incremental conductance algorithm maintains the operating point until a change of current is observed and then it calculates a new power point.

4.3.3 Parasitic capacitance

The parasitic capacitance (PC) algorithm is similar to the incremental conduction method. The difference between PC and IC-methods is that PC also takes into account the solar cells' parasitic junction capacitance, which is used to model charge storage in the p-n junction of solar cells.

By adding the parasitic junction capacitance (C_p) and series resistance to the characteristic equation of the ideal solar cell Eq (4) produces the following:

$$I = I_L - I_S [e^{\frac{(V_p + IR_s)}{nV_r}} - 1] + C_p \frac{dv_p}{dt} = F(v_p) + C_p \frac{dv_p}{dt}, \quad (14)$$

where $F(v_p)$ presents the current as the function of array voltage and $C_p \frac{dv_p}{dt}$ presents the current in the parasitic capacitance.

Incremental conductance of the array can be defined as $\frac{dF(v_p)}{dv_p}$ and instantaneous conductance as $-\frac{F(v_p)}{v_p}$. By multiplying the equation by array voltage v_p to get the array power and differentiating the result, the equation for the array power at the MPP is:

$$\frac{dF(v_p)}{dv_p} + C_p \left(\frac{V'}{V} + \frac{V''}{V'} \right) + \frac{F(v_p)}{v_p} = 0 \quad (15)$$

The first term of this equation represents incremental conductance, the second term voltage oscillation due to the parasitic capacitance and third term instantaneous conductance. Equation simplifies to the incremental conductance Equation when $C_p = 0$. (Hohm & Ropp, 2003):

$$\frac{dI}{dV} + \frac{I}{V} = 0 \quad (16)$$

4.3.4 Constant voltage and constant current

The constant voltage (CV) and constant current (CC) algorithms are based on the fact that V_{mpp} / V_{oc} and I_{mpp} / I_{sc} ratios are approximately constant. The constant voltage algorithm is the more popular one as open-circuit voltage (V_{oc}) is often easier to measure than short-circuit current I_{sc} .

$$\frac{V_{mpp}}{V_{oc}} \cong K < 1, \quad (17)$$

where V_{mpp} is the voltage at the maximum power point and V_{oc} is the open-circuit voltage of the cell.

When using the CV-algorithm, the maximum power point can be determined by isolating the solar array temporary from the MPPT-system and measuring the V_{oc} voltage. Then the MPP can be determined by using Eq (17) to calculate V_{mpp} , if K is known. The constant voltage flow diagram is presented in Figure 4.8. (Hohm & Ropp, 2003)

The value of K differs depending on the type of solar cell used. Therefore K has to be measured and circuit matched for different types of cells. Another drawback is that power production is halted momentarily when the V_{oc} measurement is made.

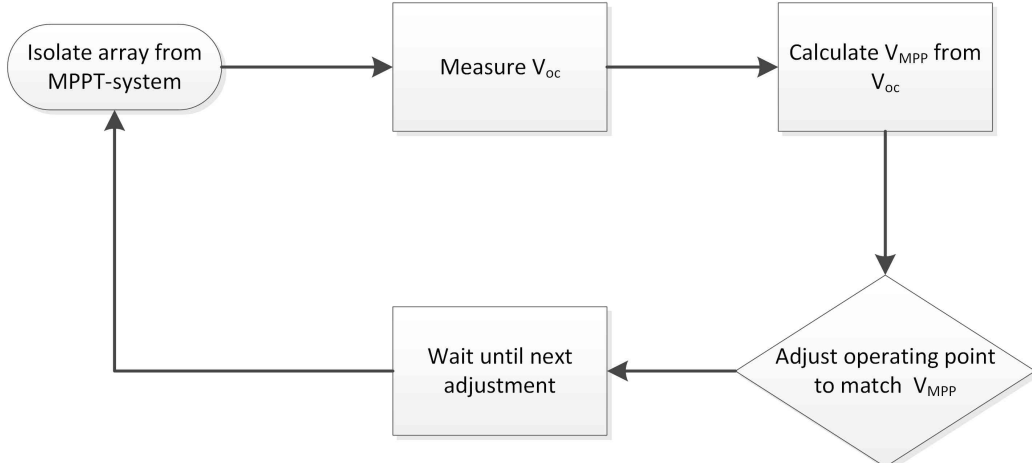


Figure 4.8: Flow diagram of constant voltage MPPT-algorithm

4.3.5 Comparison of different methods

The efficiency of MPPT-algorithm can be calculated by:

$$\eta = \frac{\int_0^t P_{actual}(t) dt}{\int_0^t P_{max}(t) dt}, \quad (18)$$

where P_{actual} is a measured power of PV-array and P_{max} is the maximum power the array can produce.

The perturb & observe, the incremental conductance and the parasitic capacitance algorithms are so called “hill climbing” algorithms. These methods can be used to track the true maximum power point. But as stated earlier, the basic P & O algorithm usually cannot track the exact point and starts to oscillate around it when conditions vary.

Nevzat Onat presents in his review article a survey of different Maximum Power Point Tracking technologies and the results are presented in Table 3. (Onat, 2010) As the power production is sufficiently low in CubeSats, power consumption of the power point tracking circuit should be as small as possible to minimize its effect on overall efficiency. Using low complexity algorithms often leads to lower power consumption. A simpler design also takes less space on PCB and increases reliability in most cases. As low complexity and high efficiency are required properties, parasitic capacitance seems a viable option. Also response time is an important characteristic in a rapidly changing environment. Especially in space applications the rotation of a satellite may cause fast irradiance changes when the attitude of the satellite is not controlled.

Table 3: Comparison of different MPPT-algorithms (Onat, 2010)

Comparison parameters	MPPT Algorithms					
	Perturb & observe	Modified P&O	Artificial intelligence	Constant voltage (current)	Incremental conductance	Parasitic capacity
Efficiency (%)	81.5–85	93–96	>95	88–89.9	73–85	99.8
PV Panel depending operation	No	No	Yes	Yes	No	No
Exactly MPP determination	Yes	Yes	Yes	No	Yes	Yes
Analog or digital control	Both	Digital	Both	Analog	Digital	Analog
Periodic tuning requirement	No	No	No	Yes	No	No
Convergence speed	Varies	Fast	Fast	Medium	Varies	Fast
Complexity	Low	Medium	High	Low	Medium	Low
Measured parameters	Voltage, current	Voltage, current	Varies	Voltage (current)	Voltage, current	Voltage, current

5 Solar cell selection and solar panel design

Solar panels are composed by connecting solar cells to form strings. The number of cells in series determines the voltage and the number of cells in parallel determines the current of the panel. The goal in terrestrial solar panel design is to minimize the cost per produced energy unit. Therefore, expensive high efficiency solar cells which are manufactured by using the latest technology are not generally used as price per Wh is high. However, in space applications it is important to maximize the amount of generated power as there are strict limits in size and weight budgets. Also the launch costs per kilogram are high. In CubeSat applications the number of cells is usually restricted by available space on surface of the satellite. Limitation of surface space may be avoided by using deployable solar panels, but that increases the complexity of the system. The basic principle is to choose panels with the highest efficiency. The best option considering this is to choose triple junction cells with BOL (Beginning of life) efficiency over 28 %. There are many options available on the market as many manufacturers have produced space-graded cells, which also have flight heritage. Most of the CubeSats have been using cells manufactured by Emcore, Spectrolab, CESI or Azur Space.

5.1 Selecting suitable solar cells for Aalto-1

The solar panels for Aalto-1 are manufactured by using Azur Space triple junction 3G30C GaInP/GaAs/Ge solar cells with an integrated by-pass diode. The cells are space qualified with BOL efficiency of 29.5 % in AM0 conditions and they provide approximately 1.2W of power per cell on BOL. Specifications for the cells are presented in Table 4 and a picture of the solar cell (3G30C) assembly 3G30A is shown in Figure 5.1. A technical drawing of 3G30A assembly is presented in Figure 5.2 (Azur Space, 2012a)

Comparisons of the cells between different manufacturers were made and Azur Space 3G30C cells were chosen because of the following reasons:

- long flight heritage; used in many CubeSat projects
- good availability
- short lead times
- competitive price for solar cell assemblies (SCA) including solar cells, interconnectors, cover glass and integrated bypass diode
- small price difference between cells of 28 % and 30 % efficiency classes

When cells are connected in series, the same amount of current flows through every cell. If some of the cells in a string are shaded, its voltage is negative and the cell consumes power instead of producing it. To avoid that, bypass diodes are used. They allow the current to pass around shaded cells and therefore voltage loss does not occur. If Azur Space 3G30C cell gets shaded, the bypass diode turns to forward bias mode and the current flows through it instead of the cell.

The open circuit voltage (V_{oc}) of Azur Space 3G30C solar cell is 2.7 V (BOL). The maximum load current is 520.2 mA for 30.18 cm² cells. The voltage is 2411 mV and the current is 504.4 mA at the maximum power point. (Azur Space, 2012a)

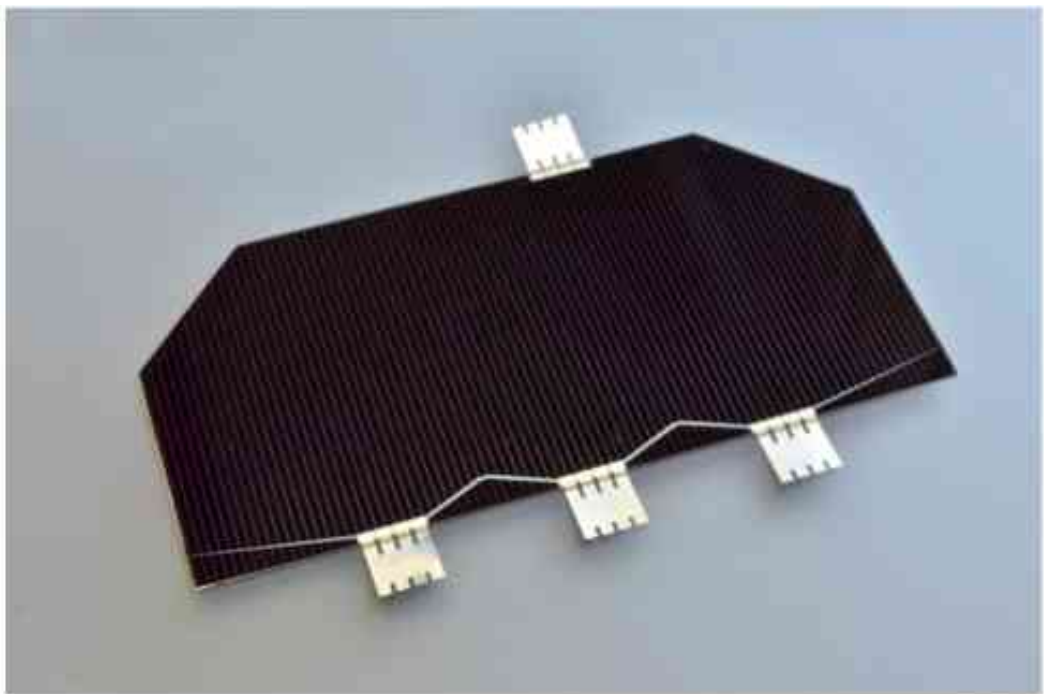


Figure 5.1: Azur Space 3G30A Solar cell assembly (Azur Space, 2012b)

Table 4: Specification of the Azur Space 3G30C solar cell (Azur Space, 2012a)

Electrical Data				
	BOL	2.5E14	5E14	1E15
Average Open Circuit Voltage V_{oc} [mV]	2700	2616	2564	2522
Average Short Circuit Current I_{sc} [mA]	520.2	518.5	514.0	501.9
Voltage at Maximum Power Point V_{mpp} [mV]	2411	2345	2290	2246
Current at Maximum Power Point [mA]	504.4	503.2	500.6	486.6
Average Efficiency [%] $\eta_{bare}(1367 \text{ W/m}^2)$	29.5	28.6	27.8	26.5
Average Efficiency [%] $\eta_{bare}(1353 \text{ W/m}^2)$	29.8	28.9	28.1	26.8
Temperature Gradients				
Open Circuit Voltage $\Delta V_{oc}/\Delta T$ [mV/ $^{\circ}\text{C}$]	-6.0	-6.2	-6.2	-6.3
Short Circuit Current $\Delta I_{sc}/\Delta T$ [mA/ $^{\circ}\text{C}$]	0.32	0.35	0.31	0.39
Voltage at MPP $\Delta V_{mp}/\Delta T$ [mV/ $^{\circ}\text{C}$]	-6.1	-6.3	-6.3	-6.4
Current at MPP $\Delta I_{mp}/\Delta T$ [mA/ $^{\circ}\text{C}$]	0.28	0.27	0.20	0.29

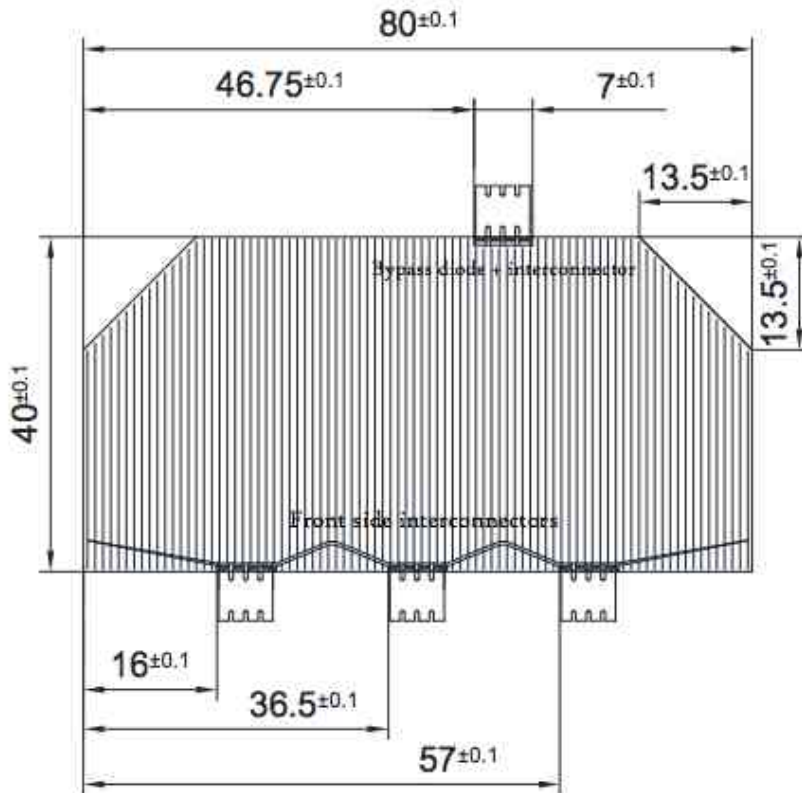


Figure 5.2: Technical drawing of the Azur Space 3G30A-cell (dimensions in millimetres) (Azur Space, 2012b)

5.2 Bonding of the solar cells

5.2.1 Methods used for connecting cells to strings

Soldering cells to form strings becomes challenging when the cells are extremely thin like Azur Space 3G30C cells, which are approximately 150 µm thick without a coverglass. Cells can break in the process or crack later due to the damage caused by the process. Hence the soldering has to be done in a reliable way. The soldering can be done in numerous ways, e.g. by using soldering iron, lasers, wave soldering or reflow soldering. Also using metallized epoxy may be used to connect cells to the strings. (TASC, 2002)

Different values for coefficient of thermal expansion (CTE) between the cell and the interconnector used to connect cells causes stress to the connection, which can later form cracks on the cells. Solder containing lead has a lower melting point than lead-free solder. Therefore, it is suggested to use leaded solder as the temperature differential between the cell and the interconnector decrease when lower temperatures are used when soldering. Interconnectors used in Aalto-1 and Aalto-2 solar panels are manufactured from Kovar with a silver coating to minimize CTE and they are only 25 µm thick. Interconnectors are also bent in such a way that they offer stress relief.

5.2.2 Methods used for solar cell bonding to substrate

There are several options which may be used to attach solar cells on the surface of the satellite. Solar cells may be attached straight on to the satellite's body or to a substrate between the body and the cells. Solar cells have to be isolated from conductive surfaces and this is done in most cases by applying polyimide (Kapton®) tape on top of the surface. In Aalto-1 case, PCB is used as substrate material for the cells. PCB solar panels shall be screwed on to Aalto-1 aluminium body.

Both methods have advantages. Using PCB as a substrate eases assembling, while PCBs can be attached one by one on each side of the satellite. On the other hand, the use of PCBs increases the weight of the structure. The PCB-method is usually chosen for larger CubeSats, because manufacturing panels individually is easier than bonding the cells straight on to the satellite's surface. It is the easier way especially due to the reason that when the cells are attached to the substrate, removing them is in most cases impossible.

In most cases, cells are attached to the substrate by using silicone (elastomer) adhesives. Some of these adhesives have good outgassing properties and are suitable for space use, but low outgassing space-graded silicones are fairly expensive in general. Silicones offer good bonding strength combined with elasticity, which gives protection against shocks, vibrations and mismatch of thermal coefficients. In some of the earliest CubeSats cells were soldered to PCB, but this method has many disadvantages e.g. the lack of protection against vibration and large differences between CTEs.

Another option to attach solar cells is to use NuSil CV4-1161-5 adhesive tape. It is double sided tape made of same material as Kapton® and therefore has good outgassing properties. This is a new method having significantly less flight heritage. During the study the only CubeSat launched using the NuSil CV4-1161-5 was AeroCube-3. The bonding method is going to be used also in U.S. Naval Postgraduate School's NPS-SCAT CubeSat. The description of the method used for NPS-SCAT can be found from Lawrence Dorn Jr. Master's thesis "NPS-SCAT: Electrical Power System". (Dorn, 2009) Due to the limited flight heritage of NuSil CV4-1161-5 adhesive tape and lack of information available, the silicone adhesive was chosen for Aalto-1 solar cell bonding. In both methods any attempt to remove cells from the substrate after attaching will result in the destruction of the cells.

5.2.3 The method used for Aalto-1

After a long review process and comparing methods previously used in CubeSats, it was decided to use silicone adhesives for bonding solar cells to Aalto-1 solar panels. Valuable information and general procedure of the process was obtained from AAUSat-1 and ESTCube-1 teams and process was further modified to be more suitable for Aalto-1 panels.

Wacker RTV-S 691 and NuSil CV-2568 elastomers are widely used for attaching solar cells because of the materials good outgassing properties. They are considered as the best options for Aalto-1 final solar cell bonding. At first Dow Corning SILASTIC® RTV silicone 9161 was used, but as there was no proof that outgassing would not harm the optical surfaces, it is not used in manufacturing final solar panels. It has been used for practising the bonding process as it has similar properties but much lower price than space-graded silicones. Figure 5.3 shows different layers and their thickness used in manufacturing Aalto-1 solar panels. Thickness of coverglasses used on Aalto-1 solar cells is approximately 100 µm. Figure 5.4 shows prototype of the Aalto-1 solar panel.

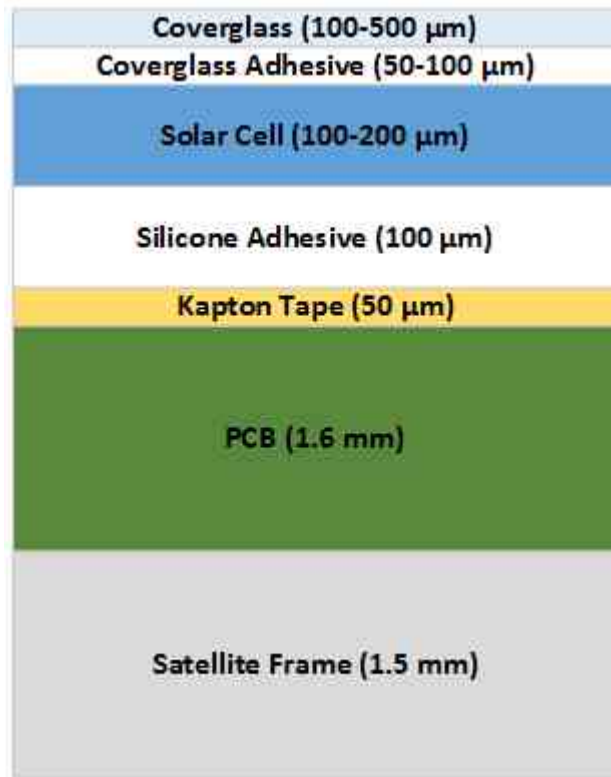


Figure 5.3: Aalto-1 solar panel composition

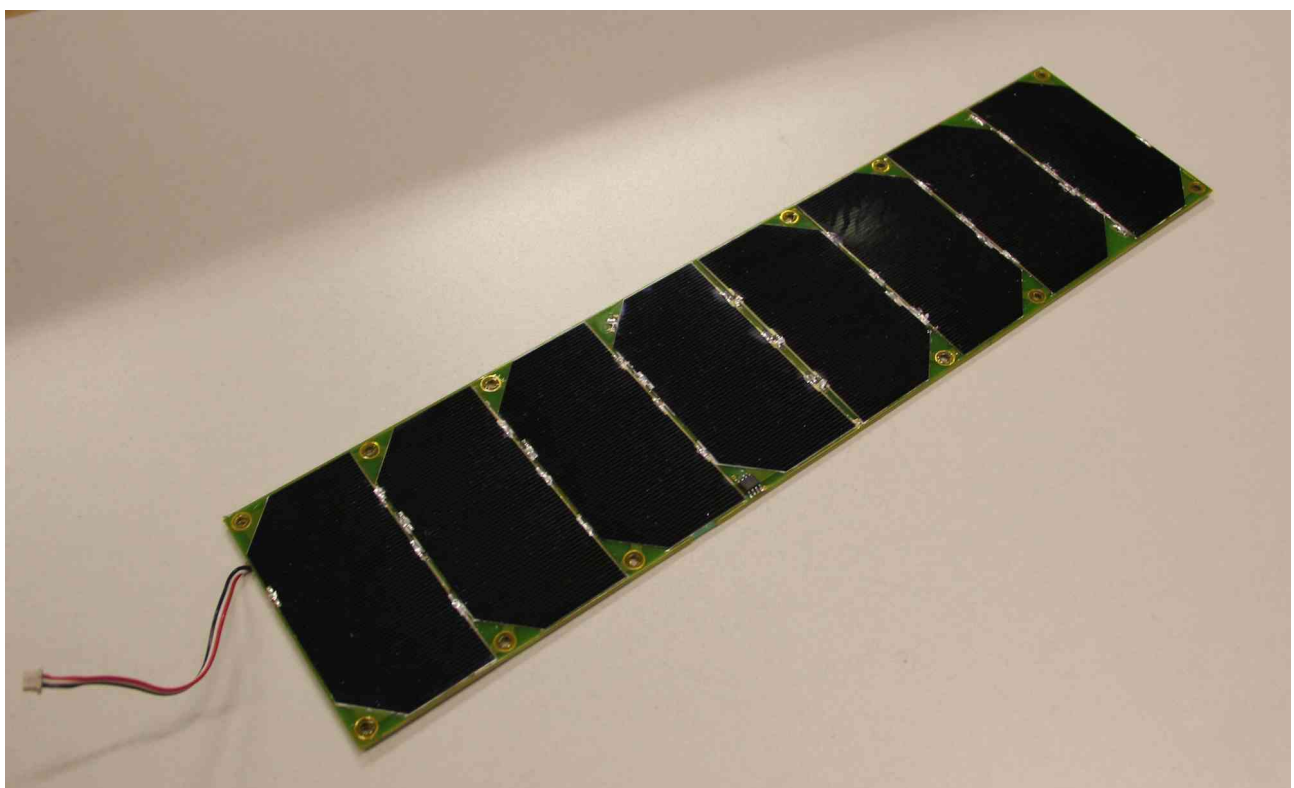


Figure 5.4: Aalto-1 solar panel prototype

Solar panel PCBs have connection points for solar cells and temperature sensors. Panels also have integrated sun sensors for improved attitude determination. Therefore six pins per panel are needed to connect panels to the satellite bus. Two of the pins are used for the sun sensor data and one as operating voltage for the sun sensor. Three of the pins are used for solar panel V+, GND and temperature. Temperature sensor and pins needed for delivering power generated by solar cells are connected to Clyde Space EPS-board using Hirose power connectors. To ease the assembly, PCBs are attached to the satellites surface using screws.

5.3 Solar panels for Aalto-2

A similar approach as used in Aalto-1 solar panel manufacturing is used for Aalto-2 panels. Solar panels have integrated sun sensors and the cells are bonded to PCB substrate using silicone adhesive. The usable surface area of Aalto-2 limits the maximum amount of solar cells to five on each long side except for the GPS antenna side if 40.00 ± 0.1 mm x 80.00 ± 0.1 mm cells with total cell area of 30.18 cm^2 manufactured by Azur Space are used. Only four cells can be fitted on the GPS antenna side. This means that a maximum open circuit voltage for 5 cell strings is approximately 13.5 V at BOL and for 4 cell strings 10.8 V according to Table 4. More information about Aalto-2 solar panels is presented in Chapter 6.3.1.

6 Electrical power system requirements

The first step of the CubeSat EPS design process is to consider requirements of the satellite subsystems and payloads. The process involves determining requirements originating from mission requirements, space environment and CubeSat standards. The EPS has to be reliable, efficient and meet power requirements defined by the specific mission. Reliability is one of the most important aspects to consider, as the satellite is impossible to repair when on orbit. Also size and mass constraints must be fulfilled.

When designing the EPS for the nanosatellite several things have to be considered:

- Mission time
 - important parameter for dimensioning battery capacity
 - has effect on power budget as solar cells degrade over time
 - determines the level of radiation protection needed
- Orbit parameters
 - has effect on power production and battery usage
 - determines the eclipse duration
 - impacts the level of radiation protection needed
- Functional requirements by payloads and subsystem
- Temperature range, robustness and price of the components

Some of the requirements derive from CubeSat design specification (CDS, 2009). Following CDS requirements have to be taken in account in EPS design:

“

2.1 General Requirements

2.1.5 Total stored chemical energy shall not exceed 100 Watt-Hours.

2.1.6 No hazardous materials shall be used on a CubeSat.

2.1.7 CubeSat materials shall satisfy the following low out-gassing criterion to prevent contamination of other spacecraft during integration, testing, and launch.

2.1.7.1 Total Mass Loss (TML) shall be < 1.0 %

2.1.7.2 Collected Volatile Condensable Material (CVCM) shall be < 0.1%

2.1.7.3 Note: A list of NASA approved low out-gassing materials can be found at:
<http://outgassing.nasa.gov>

2.1.8 The latest revision of the CubeSat Design Specification shall be the official version (<http://cubesat.calpoly.edu/pages/documents/developers.php>), which all CubeSat developers shall adhere to.

2.3 Electrical Requirements

Electronic systems shall be designed with the following safety features.

2.3.1 No electronics shall be active during launch to prevent any electrical or RF interference with the launch vehicle and primary payloads. CubeSats with batteries shall be fully deactivated during launch or launch with discharged batteries.

2.3.2 The CubeSat shall include at least one deployment switch on the designated rail standoff (shown in Figure 5) to completely turn off satellite power once actuated. In the actuated state, the deployment switch shall be centered at or below the level of the standoff.

2.3.4 The CubeSat shall include a Remove Before Flight (RBF) pin or launch with batteries fully discharged. The RBF pin shall be removed from the CubeSat after integration into the P-POD. “

These requirements demand the use of low outgassing non-hazardous materials and requires that the EPS have interfaces for remove before flight and deployment switches. Remove before flight interface is supposed to keep the satellite powered off while awaiting launch. This is necessary to prevent a slow discharge of batteries during transportation or when waiting for launch as it might take a while before launch permission will be given. The requirement can be fulfilled by isolating the battery from the electronic circuits.

The deployment switch, which is often called a separation switch is a CDS requirement to prevent current floating in the satellite while in launch vehicle. This can be accomplished by disconnecting batteries from the bus. The deployment switch is usually a spring activated device on the bottom of the satellite which closes the circuit between the battery and the DC/DC converter inputs when the satellite ejects the launch pod.

6.1 Requirements for Aalto-1

The first preliminary requirements for the Aalto-1 EPS were determined in 2010 after the project started. Specifications have been updated several times during the design phase. Reasons for the updates are the changes in payloads and subsystems. Timo Nikkanen made a survey over various COTS (Commercial off-the-shelf) systems in his Bachelor's thesis and GomSpace NanoPower 30U was suggested for the control board for Aalto-1 and GomSpace BP-4 for the battery board (Nikkanen, 2010). But when the requirements of subsystems and payloads were more carefully specified, Clyde Space 3U EPS was evaluated as the best option for the Aalto-1. In late 2010 negotiations were started with Clyde Space to procure a modified version of the Clyde Space EPS. Modifications to Clyde Space's standard product were needed to fulfil the requirement of 12 V bus and to have option to shut down the payloads through EPS if necessary.

More detailed EPS requirements for the Aalto-1 nanosatellite are defined in Appendix B.

6.2 Requirements for Aalto-2

As QB50 project is at a fairly early phase, the launch parameters or requirements of payloads are not accurate. As the mission parameters are subject to change at this point, possible changes in requirements have to be taken in account when considering EPS functionalities. Therefore the EPS-board shall be designated in such a way that there is enough flexibility for future changes. There is no previous experience on building electrical power systems for nanosatellites in Aalto University and therefore design has to be made from beginning.

An important requirement is to ensure the electrical and mechanical compatibility with the COTS-systems. The reason for this is to have a backup plan in case the designed system does not pass the qualification tests. Therefore the requirements are determined for a common power system for 2U CubeSat. The mission time for the Aalto-2 is only three months and the planned orbit is low, approximately 350-400 km high. This provides easier radiation environment compared to the Aalto-1 mission. The requirements for Aalto-2 EPS are presented in next chapters and listed more extensively in Appendix C.

6.2.1 Top level requirements

The EPS shall be able to provide sufficient power to fulfil requirements of subsystems and payloads using common regulated voltages 3.3 V, 5 V and unregulated battery voltage between 3.5 V – 4.15 V (TBD). If one of the loads require a voltage which differs from the common voltages, regulation shall be done on the load by using a point-of-load converter. The EPS board shall have integrated batteries to minimize the mass of the system. The data interface of the EPS shall be able to deliver telemetry data to OBC and have functionality to telecommand the power system using I²C or CAN bus (TBD). The system's electrical and mechanical interfaces shall be CubeSat Kit compatible. Used materials shall have TML < 1.0% and CVCM < 0.1%. Components shall be chosen in such a way that the components stay in their operating rate while the system is operating and in their survival range at all other times.

As the output voltage of 4 to 5 solar cell in series at maximum power point is in the range of 8.5 – 14.5 V when operating between -40 to +60 degrees Celsius, the EPS shall be able to operate at the same input voltage range.

6.2.2 Functional requirements

The EPS shall have the following functionalities:

- Low battery voltage and overcharge protection
 - Charging with hysteresis. Stop supplying power to loads, if battery voltage is lower than 3.4 and power up when voltage exceeds 3.6 volts
- Functionality to reset 3.3V and 5V power buses
- Ability to supply solar panel current telemetry for rough attitude determination.
- Blocking diodes in input to prevent solar cells act as load when not illuminated
- Remove before flight (RBF) and separation switch interfaces
- Shall be able to deliver telemetry data determined in Chapter 6.2.3.

Each solar array needs a blocking diode to prevent them from acting as a load when not illuminated. A blocking diode causes voltage drop across the terminals, consuming energy. Low forward voltage drop Schottky diode or ideal diode IC may be used to minimize the voltage drop.

6.2.3 Telemetry and telecommand

Telemetry is used to monitor the power usage of the satellite and to give valuable information about the condition of the EPS. Telemetry data can be used to make decisions about shutting down unnecessary systems in case of low battery or anomalies in power production. The EPS shall be able to send at least the following telemetry to OBC on request:

- Solar panel voltages and currents
- Solar panel temperatures
- Battery voltage
- Battery temperatures
- SOC (State of Charge) of the battery
- Output voltage levels and currents

The EPS shall have a functionality to reset the satellite on request. Function turns off the 3.3 V and 5 V converters for a predetermined time.

6.3 Power and mass budget of the Aalto-2 EPS

It is important to determine the power and mass budget at the beginning of the EPS design to determine the characteristics of the system. When the available space for the solar cells and the orbital parameters are known, power production can be estimated.

6.3.1 Total power production of the solar panels

Irradiance on different sides of the satellite changes when the orientation to the sun changes. In Figure 8.2 is an example of irradiation curves for different sides of the satellite when the -X plane of the satellite is pointing to nadir and +Z is the direction of the satellite's velocity vector. The figure shows power production during two orbits for satellite having 4 solar cells on each long side. Simulation is done using STK (Systems Tool Kit) and the orbital parameters defined in the QB50 interface control document (Singaray et al., 2013). The figure describes power production only at the beginning of the mission as orbit changes due to the satellite's orbital decay. Solar cells used for the simulation are 30% efficiency class triple junction 3G30C cells (GaInP/GaAs/Ge) manufactured by Azur Space Solar Power GmbH. The STK-model of the satellite is presented in Appendix D.

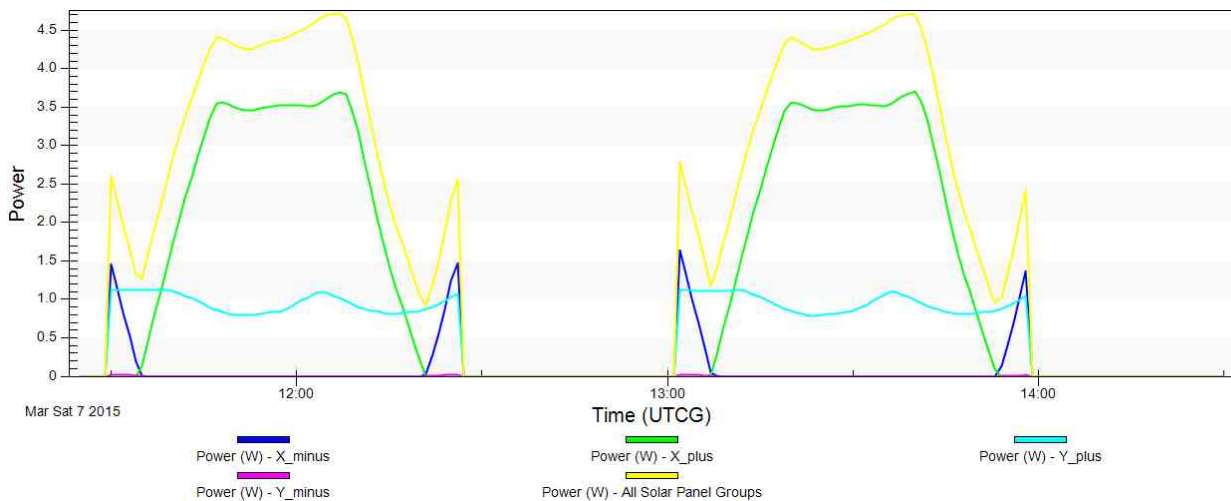


Figure 8.2: Power production of Aalto-2 over two orbits when using 4 solar cells per panel

For Aalto-2 the estimated orbit average power production is 2.5 W when panels containing 4 solar cells are used on each long side of the satellite. The Table 7 shows that using 4 cells per panel is able to fulfil subsystem and payload power requirements with a small margin. But when conversion losses are taken in account, the margin is minimal. Therefore, using 5 cells on +Y and -Y sides and 4 cells on +X and -X sides is suggested as only 4 cells are possible to fit on the panel on +X side while the GPS antenna is taking space. The reason to use 4 cells also on -X side is to have the same cell configuration on panels connected to same battery charging regulator (BCR). With this configuration and adjusting the attitude in such way that panel containing 5 cells is illuminated most of the time, orbit average power production will be between 3.0W – 3.5W. Table 5 presents the proposed solar cell configuration.

Table 5: Proposed solar cell configuration for Aalto-2

Side	No. of cells	Voltage at MPP (BOL)	
+X	4	9.6	GPS-antenna side
-X	4	9.6	Nadir side
+Y	5	12.1	
-Y	5	12.1	

For increased power production it is also possible to add one more BCR and to increase the number of cells on -X side to five. One possibility is also to put the GPS antenna to -Z side of the satellite and then it is possible to have 5 cells on each panel. Then maximum power is achieved by changing the attitude in such way that two 5 cell sides are illuminated. That increases the power production due the fact that illuminated area is increased.

6.3.2 Power consumption of the subsystems and payloads

An estimate of power consumption for Aalto-2 is presented in Table 6. The table shows the orbit average power consumption for the subsystems and the QB50 payload in different operation modes. The power usage of subsystems is weighted using their duty-cycles to get the orbit average consumption of the system. The power usage of the communication system (COM) is based on 10 minutes of transmission per orbit, but accurate utilization is not known yet and depends on available ground stations to communicate with. The antenna deployment system (ADS) is turned on for less than 60 seconds 30 minutes after ejecting the launch POD and the power consumption during the antenna deployment phase is presented in the post deployment column of Table 6. As the orbit average power production is estimated to be between 3.0 - 3.5 watts, the power budget is positive with large margin, even if 20% losses in storing and regulation of the energy are used as shown in the Table 7.

Table 6: Estimated power consumption of Aalto-2 for different operation modes (A2-SYS-DD-01-v1. 2013)

Load	Power consumption (mW)	Number of Units on	Average Duty Cycle by Mode (%)			Post Deployment (< 60 sec)
			Safe-mode	Recovery mode	Payload Operation mode	
OBC	200	1	100	100	100	100
ADCS	500	1	100	100	80	0
EPS	100	1	100	100	100	100
GPS	160	1	10	0	20	0
COM.ADS	6000	1	0	0	0	100
COM.UHF	400	1	0	100	100	0
MEC	0	1	0	0	0	0
QB50 Payload	1000	1	0	0	70	0
Sum loads (mW)			816	1200	1832	6300

Table 7: Power budget for Aalto-2 (A2-SYS-DD-01-v1. 2013)

Operation mode	Safe-mode	Recovery mode	Payload Operation mode
Avg. power generated per orbit (mW)	3000	3000	3000
20% losses in storage and regulation (mW)	-600	-600	-600
Power consumed by subsystems and payloads (mW)	-816	-1200	-1832
Power margin (mW)	1584	1200	568

The required battery capacity can be determined by calculating:

$$DOD[\%] = \frac{\text{Power consumption}[W] * \text{Eclipse period}[h]}{\text{Capacity}[Wh]} * 100\% \quad (19)$$

When the worst case power consumption is approximated to be 2.45 W, the total power drawn from the battery during 35 minutes of eclipse is 1.43 Wh. To assure battery lasting through the whole mission, maximum depth of discharge shall be less than 15 %. To fulfil this requirement, the battery capacity shall be at least 9.5 Wh.

6.3.3 Size and mass budget

Compatibility with COTS systems is important to ensure that the mechanical and electrical interfaces are compatible between each subsystem and payload. The PC/104 is common size used in CubeSats and following PC/104 standard is seen as a good engineering practise to ensure compatibility with other manufacturers' systems. PCBs based on CubeSat Kit standards are compatible with COTS manufactures e.g. GomSpace, ISIS, Pumpkin, Clyde Space and AllSpace products. CubeSat Kit compatible PCB dimensions are presented in Figures 6.1, 6.2 and 6.3. (CSK-SPEC, 2007; PC/104, 2008) The Aalto-2 EPS-board follows CubeSat Kit PC/104 form factor which defines PCB size to be 90.17 mm x 95.89 mm. (Figures 6.1, 6.2)

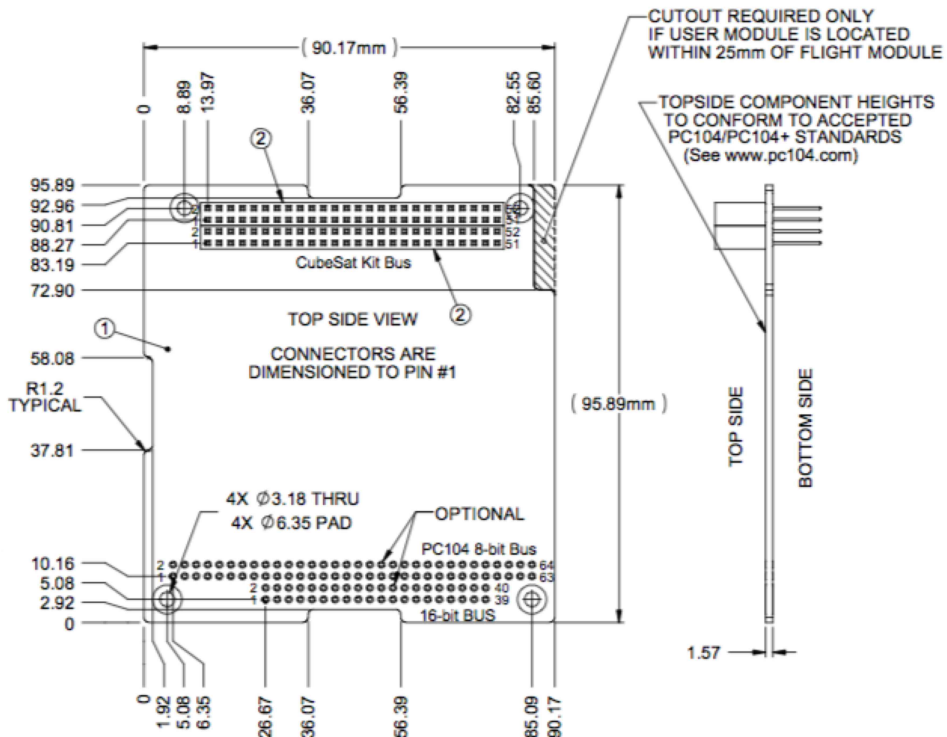


Figure 6.1: Technical drawing of CubeSat Kit compatible PCB showing the top side (not in scale) (CSK-SPEC, 2007). Dimensions are in millimetres.

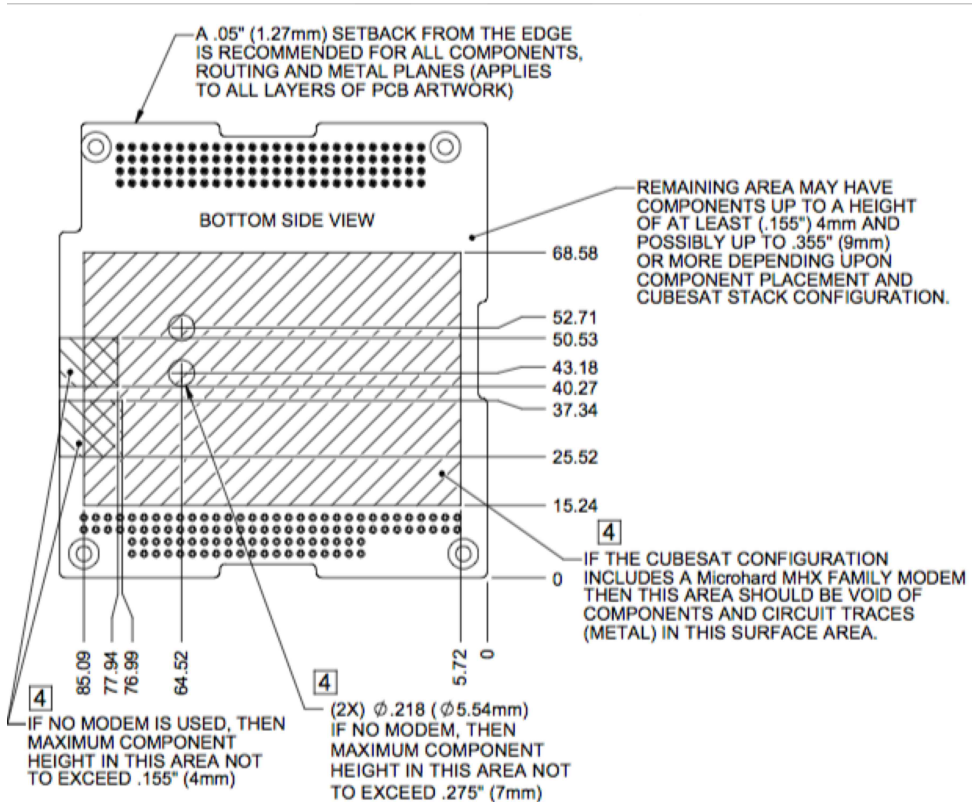


Figure 6.2: Technical drawing of CubeSat Kit compatible PCB showing the bottom side (not in scale) (CSK-SPEC, 2007). Dimensions are in millimetres.

CubeSat Kit PC/104 specification also defines maximum component height to be less than 11.05 millimetres measured from top of PCB as presented in Figure 6.3. As batteries are located on top side of the EPS-board, maximum height is exceeded and the specification is not followed on this point. The maximum height for components on the top side is determined to be 22.10 mm. Change in height does not affect to the compatibility with different manufacturers systems, when taller CubeSat Kit connector and spacers are used.

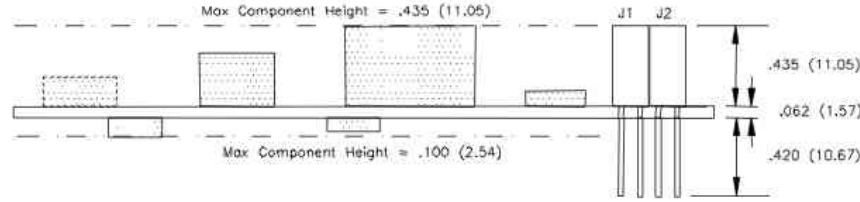


Figure 6.3: Technical drawing of CubeSat Kit compatible PCB (side view, not in scale) (PC/104, 2008). Dimensions are in inches (millimetres)

Mass is one of the most limiting factors when making design choices as the QB50 has a 2 kg mass budget for 2U CubeSats participating in the project instead of the current 2U standard of 2.6 kg. (CDS, 2009; Singarayar et al., 2013) Due to this fact it is important to determine the maximum mass allowed for the EPS and to estimate the mass of the system using a sufficient margin. The mass budget for Aalto-2 is presented in Table 8. The mass of the different EPS parts is based on Aalto-1 experience. The EPS mass consists of solar cell SCAs (Solar cell assemblies, including solar cells, interconnectors, cover glass and integrated bypass diode), PCBs used as substrates for cells, adhesive used in bonding cells, the EPS control board and batteries. EPS.SOL refers to solar panels and EPS.REG to the control board and batteries in the Table 8.

Table 8: Mass budget of Aalto-2 satellite (A2-SYS-DD-01-v1, 2013)

SUBSYSTEM	Mass (g)	Contingency (g)	Mass with contingency (g)	Fraction (%)
OBC	90	9	99	5
ADCS	180	18	198	10
EPS.SOL	300	30	330	16,6
EPS.REG	180	18	198	10
GPS	40	4	44	2,2
TT&C.ADS	100	10	110	5,5
TT&C.UHF	100	10	110	5,5
MEC	270	27	297	15
PAYOUT	500	100	600	30,2
Total	1760	226	1986	100
Target mass		0	2000	
Mass margin			14	0,7

The mass budget is tight and several actions have to be taken to meet the mass requirements:

- Integrating batteries to EPS control board
- Dimensioning the battery capacity to meet the mission requirements without excessive margin to keep the battery mass low
- Using a lighter substrate for the solar cells than in Aalto-1 case

Integrating batteries to the control board of EPS saves tens of grams of mass as the total weight of PCB and two CubeSat Kit bus connectors is 42 grams. Increasing the depth of discharge, a smaller battery can be used thus reducing the battery weight. Higher DOD (Depth of Discharge) shortens the lifetime of the battery, but this can be tolerated as the total cycles will stay low because of the short mission time. Less than 15 % DOD is achieved when using 10 Wh battery at BOL.

The weight of the solar panels can be reduced by using a thinner substrate or substrate material with lower density. The option of buying panels from reliable vendor is also a possibility. Clyde Space COTS 2U panels weigh only 69 grams per piece. (Clyde Space, 2012) Standard COTS panels are not suitable and modified versions are needed, due to the requirement of having the sun sensors on the panels.

6.4 Pinout and CubeSat Kit connector

Aalto-2 is using a 104-pin CubeSat Kit bus connector to stack the PC/104 boards electrically together. The pinout for EPS-board is selected to be compatible with the COTS-systems to ensure compatibility. The pinout for the connectors are presented in Table 9. Power pins 3 and 5 in header 1 used for powering up the QB50 payload are equipped with MOSFET switches to have a possibility to disconnect the payload from the EPS in case of a payload malfunction (TBD).

Table 9: Aalto-2 EPS pinout (A2-SYS-DD-01-v1, 2013)

Pins used by COTS EPS hardware		
Power pins required by payload		
		Header
Header 1		2
+5 V (switch TBD)	2	+5 V
+3.3 V (switch TBD)	3	+3.3 V
	4	
	5	
	6	
	7	
	8	
	9	
	10	
	11	
	12	
	13	
	14	
	15	
	16	
	17	
	18	
	19	
	20	
	21	
GND	22	
	23	
	24	
	25	
	26	
GND	27	
	28	
	29	
	30	
	31	
	32	
	33	
	34	
	35	
	36	
	37	
	38	
	39	
I2C DATA	40	
	41	
I2C CLK	42	
	43	
	44	
	45	
	46	
	47	
	48	
	49	
	50	
		Header
Header 2		
+5 V	1	
+3.3 V	2	
GND	3	
	4	
	5	
	6	
	7	
	8	
	9	
	10	
	11	
	12	
	13	
	14	
	15	
	16	
	17	
	18	
	19	
	20	
	21	
	22	
	23	
	24	
	25	
	26	
	27	
	28	
	29	
	30	
	31	
	32	
	33	
	34	
	35	
	36	
	37	
	38	
	39	
	40	
	41	
	42	
	43	
	44	
	45	
	46	
	47	
	48	
	49	
	50	

7 Aalto-1 EPS architecture

The Aalto-1 EPS control board and the battery board are COTS components bought from Clyde Space. Clyde Space EPS-boards have extensive flight heritage with over 240 units sold. Clyde Space products have been found reliable and robust. The EPS Control Board is a modified version of Clyde Space COTS product CS-3UEPS2-NB and the battery board is a modified version of their standalone 30 Wh battery CS-SBAT2-30. The maximum voltage of the battery pack is 8.3 V, when fully charged. Extra functionalities to standard products are the 12 V regulator, the dead man's switch to reset the satellite in case of the OBC or I²C anomaly and 10 commandable switches with latch-up protection providing the possibility to disconnect the loads reliably in case of a subsystem/payload failure. Latch-up protection activates when the set current limit is exceeded for a predetermined time. The OBC is able to send ON/OFF commands to the EPS through the I²C bus to control the switches. One of the switches has a timer to turn on the antenna deployment system's (ADS) 12 V line 30 minutes after exiting the launch POD. This is used as a redundant system for ADS built-in timer circuit to activate the ADS in case of timer circuit failure. A delay in the ADS activation is needed as the CDS states that deployables shall not be activated in the first 30 minutes after exiting the P-POD.

The dead man's switch is realized by having a timer on microcontroller of the EPS. The EPS resets 3.3 V, 5 V and 12 V buses of the satellite, if the EPS is unable to receive "alive" signal sent by OBC. The signal is sent every 4 minutes through I²C line in standard configuration, but the time interval may be set between 4 and 10 minutes.

A simple block diagram of Aalto-1 EPS is presented in Figure 7.1. Solar panels provide power to the battery charge regulators (BCRs) used to charge batteries. The power condition modules (PCM) are responsible for regulating the voltages produced by solar panels and battery. Another function of the PCMs is to protect the power outputs against system anomalies.

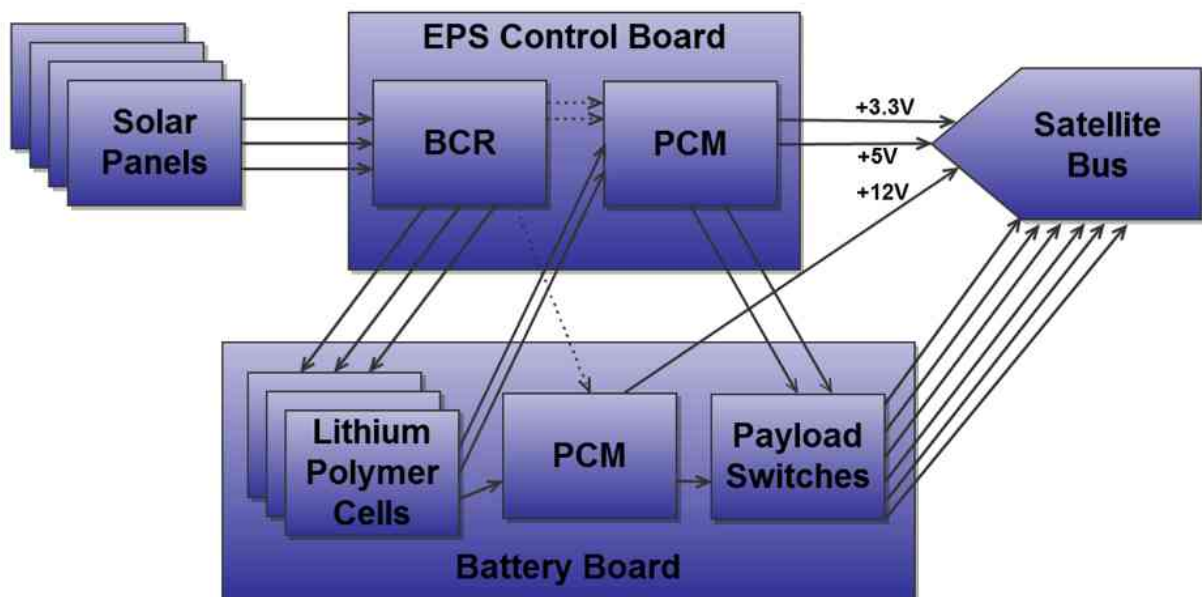


Figure 7.1: Block Diagram of Aalto-1 EPS

The Aalto-1 has solar panels on each four long sides of the satellite and the panels are connected to three Battery Charge Regulators (BCR) on Clyde Space EPS-board. BCRs are independent from each other, so failure in one of the regulators does not cause total loss of power. Solar panel configuration is presented in Table 10.

Table 10: Solar panel configuration of Aalto-1

Side	No. of cells	Voltage @ MPP (V)	Max power (W)
+X	3	7.2	3.65
-X	8	19.3	9.73
+Y	8	19.3	9.73
-Y	6	14.5	7.30

8 Aalto-2 preliminary EPS architecture

Most of the subsystems shall be built in-house for the Aalto-2. As stated earlier the EPS shall have basic functionalities and to be reliable. The EPS uses COTS components and the reliability requirements are achieved by hardware redundancy. Failure prone parts: DC-DC converters, battery charge regulators, maximum power point tracking (MPPT) controllers and batteries will be multiplied. The Aalto-2 prototype utilizes two MPPT-controllers, redundant inductive DC-DC converters for 3.3 V and 5 V voltage buses and parallel battery strings in case one fails. Using centralized power architecture instead of the distributed architecture is suggested for Aalto-2. It reduces weight and makes subsystem development easier, as common voltages are delivered to systems. Block diagram of the Aalto-2 EPS prototype is presented in Figure 8.4. Individual blocks are explained further in the next chapters and the reasons for choosing the components are justified.

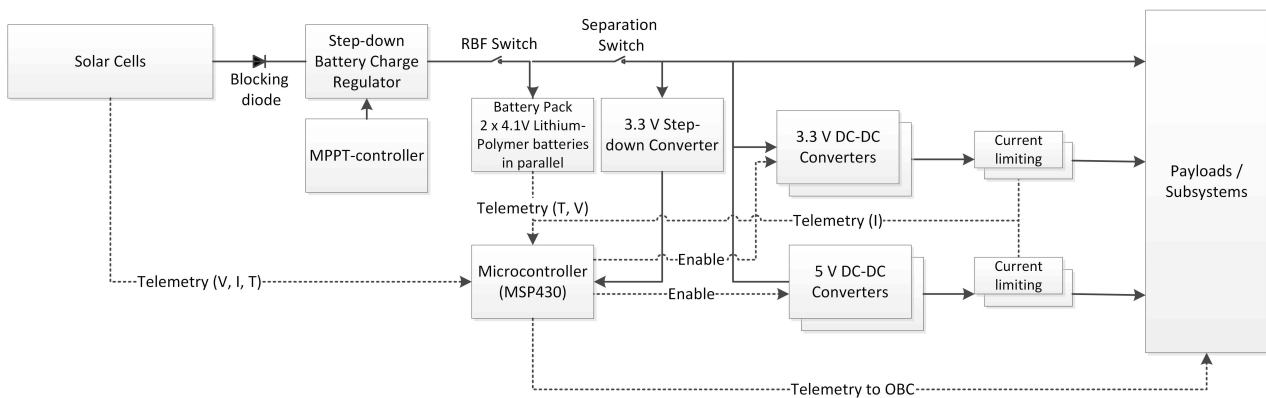


Figure 8.1: Block diagram of the Aalto-2 EPS-prototype

There are several options to realize battery charging and power distribution to the subsystems and payloads. Five Azur Space 3G30C solar cells in series provide voltage of 12.1 V at solar panel output on maximum power point in AM0 conditions ($T=28^{\circ}\text{C}$, $W=1367 \text{ W/m}^2$). A blocking diode is necessary on the EPS board's input to prevent solar panel acting as load. This decreases the voltage coming to battery charging regulator's input, and to minimize losses a low voltage drop diode is required. A buck type battery charge regulator is needed to charge the battery to 4.15 volts. Battery voltage has to be further regulated to 3.3 volts using the buck converter and to 5 volts using a boost (or buck-boost) converter to be suitable for the subsystems/ payloads.

8.1 Microcontroller

The microcontroller's primary functions are to collect and deliver telemetry data to the Aalto-2 on-board computer and to control the DC-DC converters. As the microcontroller has an independent power supply, it can be used to reset voltage buses by shutting down converters and turning them back on. Figure 8.2 presents the system used for Aalto-2 EPS. Current monitoring notices possible latch-ups by measuring the current supplied by the converters and shuts down the converter(s) momentarily if anomaly is detected. An integrated circuit for current limiting is also used to ensure that current does not exceed allowed limits.

Using a microcontroller also gives a possibility to employ similar “dead man's switch” as used in the Aalto-1 satellite. In Aalto-1, the microcontroller of the EPS is set to listen “alive” signal sent

frequently by the On-Board computer. If the signal is not received in a predetermined time interval, EPS resets the voltage buses.

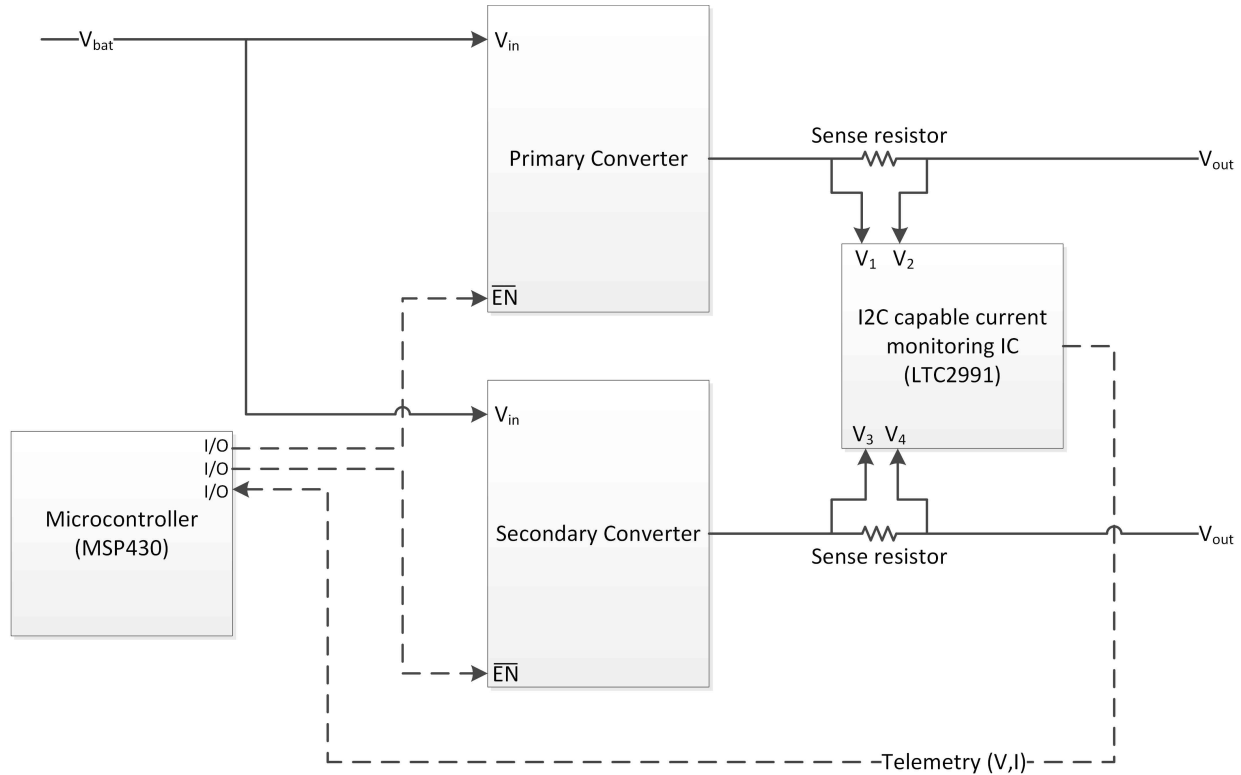


Figure 8.2: Converter selection using microcontroller

The converters are connected in such a way that in case of the failure of the microcontroller, the input of the regulators enable pin stays high and EPS is able to provide power to the systems. This functionality is realized by using N-channel enhancement-mode MOSFET as a switch. It connects enable pin of the regulator to ground when microcontrollers output sends logic high. When the microcontroller's output is low or floating, MOSFET is not conducting and the regulator operates normally as enable pin is in high state. R_2 is used as a pull-down resistor to ensure that the device is in a defined logic state even in a microcontroller failure situation. The system is presented in Figure 8.3. This configuration is chosen as one of the design goals was that single point failure shall not stop the power distribution to the systems. However, reduced maximum power available and loss of functionalities are tolerated. Microcontroller failure leads to loss of telemetry data, reset functionality and the possibility to switch between the regulators. None of these functions are critical for the EPS to operate, but a failure in the microcontroller may lead to high depth of discharge of the battery as the on-board computer does not receive telemetry anymore and cannot make a decision to change the satellite's operation mode to a safe-mode to save power.

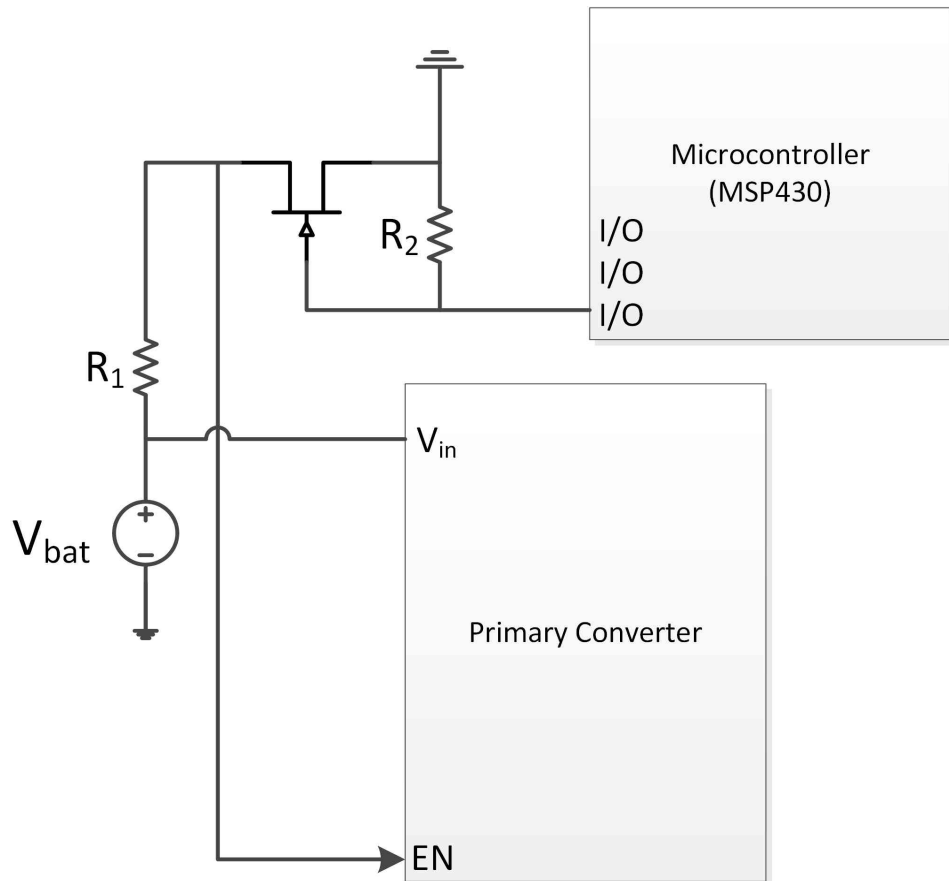


Figure 8.3: MOSFET switch providing enable functionality for primary converter in case of microcontroller failure

The proposed microcontroller for the Aalto-2 EPS is Texas Instrument's MSP430-F1611 as it consumes low power and has a lot of flight heritage, due to the reason that it is used in flight computers produced by Pumpkin Inc. It is powered from battery bus using step-down converter TPS62122 as suggested in Texas Instruments Application Report SLVA335C. (TI, 2012) Another reason for favoring the use of MSP430 is the reason that it is used in several Aalto-1 and Aalto-2 subsystems and there is already knowledge on interfacing and programming it. Microcontroller hardware or software is not developed as a part of this thesis, but suitable pins to connect I/O lines are given for testing and further implementation.

8.2 Selection of DC-DC converters

Voltage conversion is made to 3.3 V and 5 V from battery voltage floating between 3.5 to 4.15 volts. The inductive DC-DC converters have high efficiency in this kind of application and were therefore chosen to convert battery voltage suitable for subsystems and payloads. Charge-pumps are not considered as an option as their maximum current is too low for the application.

Several commercial step-down converters were compared and the choice was made between different options. The important parameters were e.g. efficiency, maximum output current, a small foot-print size and an easy solderability. Specifications are listed here and derating margins in Table 2 shall be taken into account when considering the suitability.

Specification for the 3.3 V converters

- Input voltage: 3.5 V to 4.4 V
- Output voltage: 3.3 V (+/- 0.1 V)
- Maximum output current $\geq 0.8 \text{ A}$
- Temperature range of -40...+85°C
- Efficiency > 88%, when $I_{LOAD} = 0.5 \text{ A}$

Specification for the 5V converters

- Input voltage: 3.5V to 4.4V
- Output voltage: 5 V (+/- 0.1 V)
- Maximum output current $\geq 0.8 \text{ A}$
- Temperature range of -40...+85°C
- Efficiency > 90%, when $I_{LOAD} = 0.5 \text{ A}$

Linear Technology LTC1875 was chosen to be used as 3.3 V buck converter for several reasons:

- High efficiency for the estimated load
- Suitable V_{in} and V_{out} for the application
- Easy soldering as the package is 16-SSOP
- Synchronous rectification with built-in switch (diode is replaced with switch to increase efficiency)
- Small footprint in total, as low amount of external components needed

Linear technology LTC3122 was chosen for 5 V boost converter for the following reasons:

- Suitable input voltage range 1.8 V to 5.5 V
- Large thermal pad
- High efficiency, when $V_{in} = 4.2 \text{ V}$, $V_{out} = 5 \text{ V}$, $I_{out} = 0.1 - 1 \text{ A}$
- Switch built-in
- Easy soldering as the package is 12-MSOP
- Synchronous rectification with built-in switch

To achieve redundancy of paralleled converters, they shall be paralleled in a way that prevents current flowing back to the converter in failure situation. A simple way to achieve this is to use OR'ing diodes on converter outputs to employ the droop method. Figure 8.5 shows the configuration used. The problem with using normal diodes is their large forward voltage drop, causing significant power loss. To minimize the power loss, “ideal diodes” are used in Aalto-2 EPS prototype. Ideal diodes used are actually based on MOSFET switches with low on-state resistance. The first prototype employed two Linear Technologies LTC4411 ideal diodes per voltage bus. In the next version of the EPS, LTC4411 is replaced by LTC4413 to save space on the PCB. LTC4413 has two independent ideal diodes built-in to 3x3 mm DFN package.

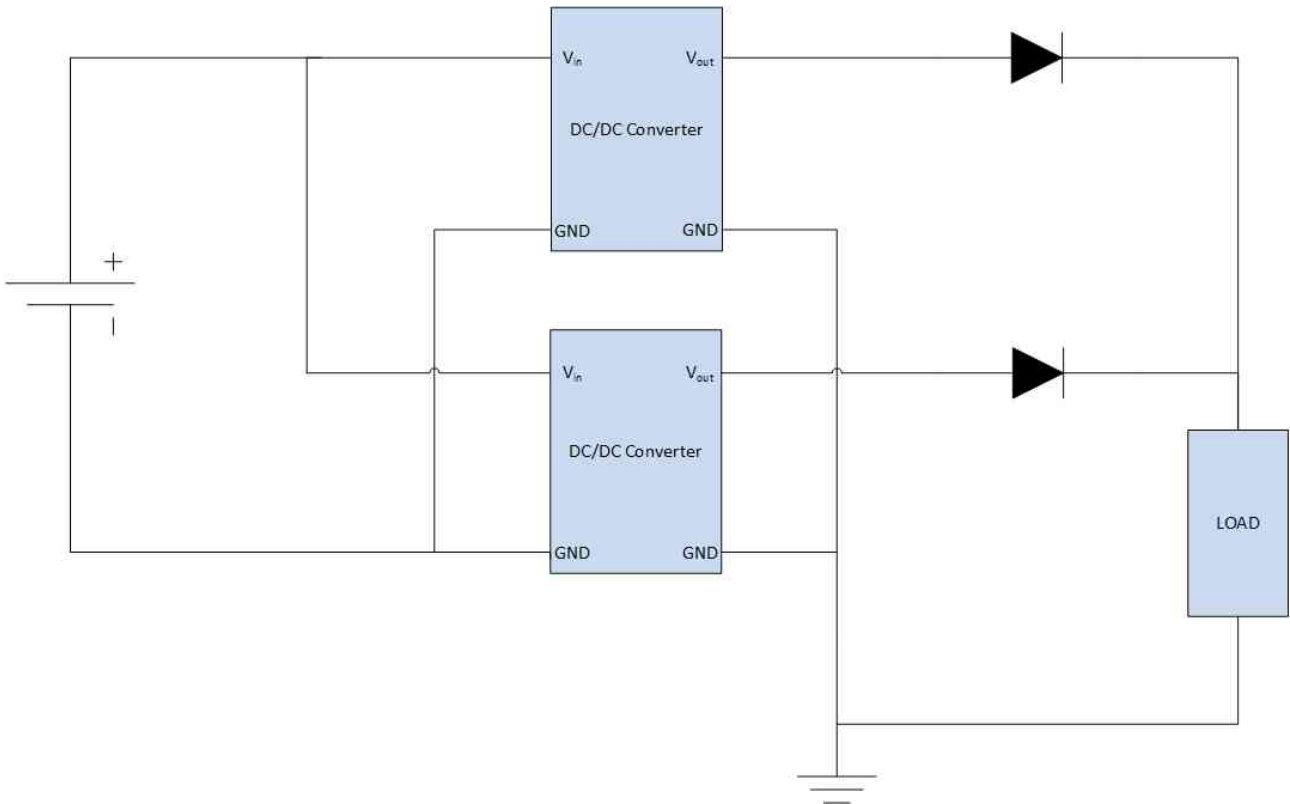


Figure 8.5: Paralleling DC-DC converters

8.3 Maximum power point tracking

At the beginning of the Aalto-2 project it was decided to use MPPT or similar technology to achieve the best possible efficiency from the solar panels. Due to the complexity of most solutions to utilize MPPT and to speed-up and ease the design process, decision of using IC with a built-in MPPT was made. There are many advantages: reduced footprint size, less complexity on design, easily achievable redundancy etc. The small footprint size brings the possibility to use several MPPT controllers operating individually for hardware redundancy. Using dedicated IC provides autonomous MPPT-tracking increasing fault tolerance compared to a system which utilizes microcontroller to track the power point. Different available options for MPPT IC are presented in Table 11.

Table 11: Survey of MPPT capable integrated circuits (AVNET, 2011; Linear, 2012; STM, 2012)

Supplier	Part Number	Panel Voltage	Output Voltage	Max Charge Current	Integrated FETs	MPPT Type	Topology	Package	Comments
Texas Instruments	BQ24650	5-28 V	2.6 - 26 V	10 A	No	Temperature compensated fixed point voltage	Buck	QFN-16	
Texas Instruments	BQ24210	3.5 – 7 V		800 mA	Yes	None		WSON-10	
STMicroelectronics	SPV1020	6.5 – 40 V	$V_{in} - 40$ V	9 A	Yes	Perturb & Observe	Boost	PowerSSO-36	
STMicroelectronics	SPV1040	0.3 – 5.5 V	2 – 5.2 V	1 A	Yes	Perturb & Observe	Boost	TSSOP8	
National Solar Magic	SM72442, SM72295	Programmed	9-100 V	Programmed	No	Proprietary algorithm	Buck, Boost	TSSOP-28 SOIC-28	Programmable chipset, Both SM72242 and SM72295 needed
NXP Semiconductors	MPT612	Programmed	5 – 50 V	Programmed	No	Proprietary algorithm	Buck or Boost	LQFP48	MPPT only
Linear Technology	LTM8062 / LTM8062A	4.95 - 32	< 18.8 V	2 A	Yes	Temperature compensated fixed point voltage	Buck	77-Lead LGA	
Linear Technology	LT3652	4.95 – 32 V	< 14.4 V	2 A	Yes	Temperature compensated fixed point voltage	Buck	DFN12, MSOP-12	

Suitable options for MPPT controller were STMicroelectronics SPV1020, Texas Instruments BQ24650 and Linear Technologies LT3652 for the solar cell configuration shown in Table 5. The LT3652 was chosen to employ the MPPT control because of a smaller footprint compared to the BQ24650 and a built-in buck converter to regulate the voltage to 4.15 V. LT3652 input regulation loop maintains the panel at peak output power by varying the battery charging current. Also LTM8062 was considered as an option, but LT3652 was chosen because ICs are available in MSOP-12 package. Manufacturing and finding the possible defects is easier for the ready product as solder joints except for the GND pin are visible. SPV1020 was not chosen because of the need of one more conversion stage to regulate the voltage suitable for batteries. The biggest drawback in using LT3652 is that the IC offers only fixed point voltage, which is not a real MPPT method. The method approximates the MPP and the true maximum power point is not achieved. But as the operating point can be adjusted by using temperature compensation, operation point will be near the maximum power point also in different temperature conditions.

Using a fixed voltage point may lead to problems as single cell damage takes down the whole solar cell string as the controller cannot measure a new operation point. Another disadvantage in using LT3652 is the fact that used solar panels and the MPPT circuit have to be matched to each other. That also brings another problem: solar panels on opposite sides should have V_{mpp} in the same range as opposite side solar panels are connected to the same controller. This problem can be solved by using more controllers. Adding more controllers is possible as there is available space on PCB and foot-print for LT3652 circuitry is fairly small. In current configuration two LT3652 modules are needed as panels on +X and -X sides are connected to one MPPT-controller and panels on +Y and -Y sides to another as shown in Figure 8.6. This is possible as the panels are illuminated from only one side at the time when the Albedo radiation is neglected as it is fairly small.

Radiation effects have to be taken into account when using fixed point voltage if the design is used for longer missions. When solar cells degrade, the power point might be set above panels open circuit voltage point, leading to zero power production. Because of this, the power point has to be determined to be near maximum point when end of mission is approaching. This leads to using a non-optimum power point when the solar cell characteristics are in BOL condition. But as mission time for Aalto-2 is only 3 months and the orbit altitude is low, the total induced dose will be fairly small and significant degradation is not expected.

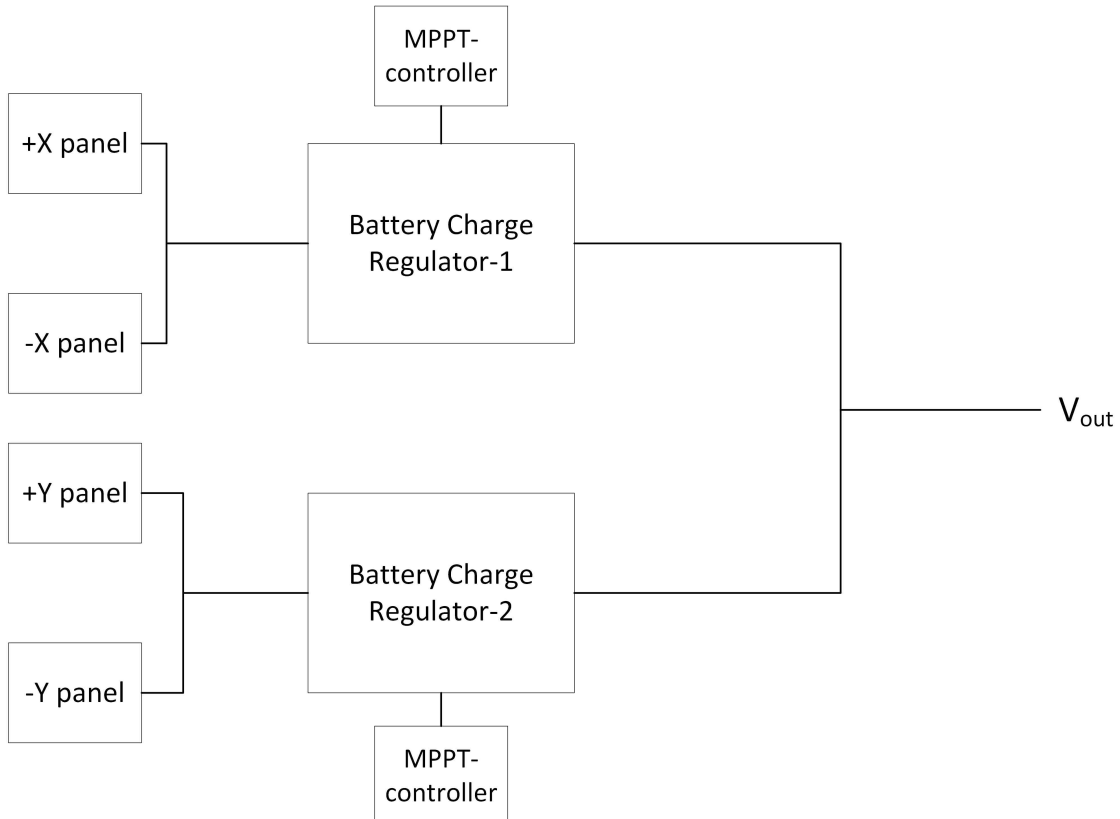


Figure 8.6: Solar panel connections to battery charge regulators

8.4 Protection circuits

Latch-up protection for the DC-DC converters is accomplished by using current limiting IC and monitoring the current on 3.3 V and 5 V power buses using shunt resistors. The microcontroller is responsible of measuring currents flowing to the loads and if the current limit is exceeded longer than the predetermined time interval (TBD), the affected power bus is turned off momentarily. After such an anomaly, converters are powered on sequentially to detect if the fault is caused by the converter.

The EPS is also using a Maxim Integrated MAX890L current-limited P-channel MOSFET switch as the over-current protection circuit. It can be used for 3.3 V and 5 V lines as its operating voltage range is between 2.7 V and 5.5 V. The allowed pass-through current can be chosen between 240 mA - 1200 mA. If the current exceeds the preset value, the IC starts to decrease the output voltage. The output voltage drops to zero when the preset current exceeds 1.5 times the set value. MAX890L also has a thermal shutdown function and shuts down with hysteresis when the component temperature exceeds 135°C and turns back on when the temperature decreases under 125°C. (MAX890L, 2011)

If the current limit is set to 1 A, the power output from regulated 3.3 V or 5 V buses is not sufficient for the Antenna Deployment System (ADS) to operate as the peak power requirement is approximately 6 to 7 W, if ADS designed for Aalto-1 is used. The ADS operates only once for less than 60 seconds at the beginning of the mission. Therefore it is suggested that the ADS is powered directly from the battery bus. After the antennas are deployed, current flow through the ADS stops

and it is shown as an open circuit to the EPS. Another option is to have own output for the ADS between the current limiting and the regulator output.

It is suggested to have current limitation on loads also to prevent a short circuit situation. If the subsystem or payload is short circuited when connected to a common power bus, other systems connected to the same bus are affected. The problem is solved in Aalto-1 by adding dedicated voltage lines to payloads and subsystems. If the Aalto-2 subsystem/payload providers are unable to provide latch-up protection for their systems, a similar system can be implemented. This requires additional switches on the EPS-board, which can be used to connect those loads. In such a scheme, the bus voltage is delivered to specific pins through a switch. The current through the switch is monitored and is turned off, if the current exceeds the predetermined value.

8.5 Telemetry

Current and voltage information is measured using LTC2991 Octal I²C voltage, current, and temperature monitoring circuit from Linear Technology. The component has a built-in analog-to-digital converter, 8 inputs for voltage data and I²C support to transfer the measurement results to the microcontroller. Preliminary design has also measurement pins on the board to verify the results. The current is calculated by measuring the voltage over known value sense resistor and by using Ohm's law. The telemetry data is sent to the OBC using CAN bus or I²C (TBD) on request.

8.6 Remove before flight and separation switch interfaces

The remove before flight (RBF) switch and the separation switch interfaces are accomplished by connecting pins in header 2 (Table 9). When the output of the BCR is shorted (pins H2.41-H2.42) with positive pin of the battery (H2.45-H2.46), the batteries connect to LT3652 charging circuit. The batteries are connected to the DC-DC converters, when the batteries' positive pin is shorted with 3.3 V and 5 V regulators input (H2.35-H2.36).

It is possible to connect the pins by using a normally closed (NC) single pole, single throw switch (SPST). SPST-switch used for the separation switch is positioned in such a way, that a spring-loaded pusher plate on the bottom of the launch POD keeps the switch pressed down, when the satellite is inside of the POD. After the satellite ejects the launch POD, the switch is released, connecting the terminals. RBF switch is released before inserting the CubeSat to the POD.

8.7 Battery selection and design

Choosing the batteries used in Aalto-2 do not belong to the scope of this thesis, but a survey of basic demands for batteries was made.

Lithium-ion and Lithium-ion polymer batteries are most commonly used in CubeSat application due to their high gravimetric (Wh/kg) and volumetric (Wh/l) energy densities (Table 12). The batteries are one of the main components, which determine the maximum mission time as the charge-discharge cycles are limited. Therefore, choosing batteries with sufficient capacity is important. As the Aalto-2 mission length is short, total cycles will stay low. The satellite will enter in eclipse approximately 16 times per day and therefore the partial cycle count is approximately 1440 cycles for the whole 3 month mission period.

*Table 12: Comparison of different battery types
(Elbrecht et al. 2011)*

Battery Type	Ni-MH	Li-Ion	Li-Po	LiFePO ₄
Weight Energy Density Wh/kg	30-80	100-250	130-200	90-110
Volumetric Energy Density Wh/dm ³	140-300	250-360	300	220
Nominal Voltage	1.2V	3.6V	3.7V	3.3V
Voltage Limits	1..1.3V	2.7..4.1V	3..4.2V	2.5..4.2V
Charge Current	low	high	high	high
Discharge Current	low	high	high	high
Charge Temperature Range	-10..45°C	0..45°C	0..45°C	-30..60°C
Discharge Temperature Range	-20..60°C	-20..60°C	-20..60°C	-30..60°C
Robustness	Medium	low	low	high
Charge Cycles	500-1000	400-1200	400-1200	2k...7k

High discharge rate and depth of discharge (DOD) speeds up the deterioration of the battery capacity. Lowering the discharge rate is possible by using two battery cells in series, which doubles the battery voltage and halves the needed current to get the same amount of output power when compared to a single battery. Also using two batteries in parallel relieves the stress by doubling the current carrying capacity of the batteries. When using LT3652, the voltage from 4 solar cells is not sufficient to charge the battery to charge-termination voltage of 8.3 V without extra boost converters. Therefore, Aalto-2 uses batteries in parallel leading to a voltage of 4.15 V when fully charged. Another reason for choosing the voltage of 4.15 V is that only two batteries (1s2p) is needed to have two independent power paths, compared to need of four batteries if 8.3 V configuration is required. Using a configuration of two battery strings in parallel with two cells per string (2s2p) would double the mass of batteries. The capacity of the battery is to be dimensioned in such a way that DOD is less than 15 %. This requirement is achieved by using batteries with total capacity of 10 Wh. Two Panasonic CGR18650HG Li-ion or similar batteries (TBC) are connected in parallel to meet the capacity requirement. The exact model depends on the availability of the product and results of the qualification tests. Weight of the CGR18650HG is 42 grams, the nominal voltage is 3.6 V and the standard capacity is 1800 mAh.

Oversupply and undervoltage protection for the battery is needed to maintain the battery capacity as li-ion batteries are highly sensitive to overcharge. Also high depth of discharge reduces the battery lifetime dramatically as stated earlier. The recommended operating temperature for most lithium-ion batteries is between 0 °C and 40 °C. When the battery temperature is below 0 °C its capacity is greatly reduced as the equivalent series resistance increases. Therefore, it is necessary to use a heater for the batteries to maintain desired temperature when the satellite is on eclipse. There are several vendors manufacturing suitable heaters for aerospace use. For example US based company Minco manufactures thin flexible polyimide insulated heaters in various sizes. Also tailor-made heaters are available. The heater can be autonomous or controlled by the EPS microcontroller. An example of the circuitry to connect heater is presented in Figure 8.7. The circuit has two redundant power paths. The both paths have two N-channel MOSFETs in series to increase reliability.

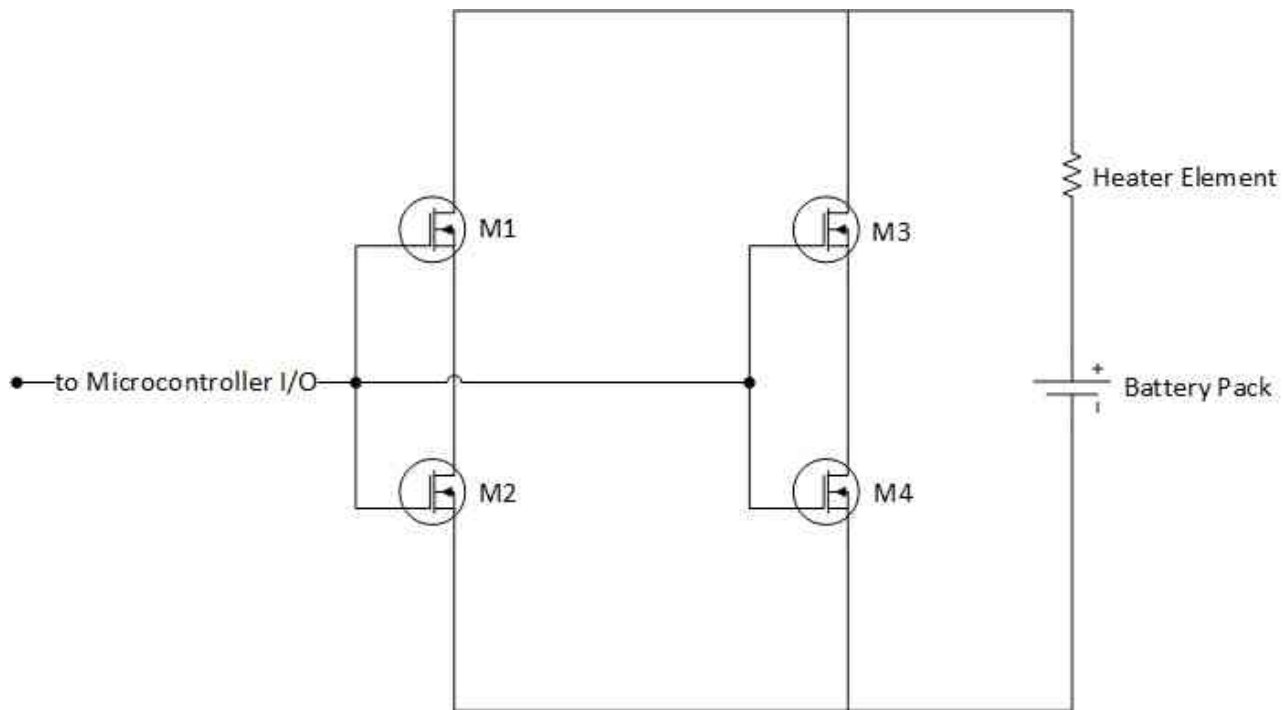


Figure 8.7: Example of redundant battery heater circuitry controlled by EPS-microcontroller

8.8 Component selection (passive)

The passive components used in the flight model of the EPS are selected in a way that the design survives in the space environment. This includes using components which are radiation-tolerant and able to handle the space vacuum. Therefore, film resistors, X7R/X8R ceramic capacitors and hermetically sealed tantalum capacitors are used. X7R or X8R ceramic capacitors are suggested for the flight model as they have a vast temperature range (X7R: -55/+125 °C, X8R: -55/+150 °C). If very low value capacitors are needed, C0G ceramic capacitors may be used. Otherwise, the operational temperature range for the components shall be at least on the industrial range between -40°C to 85°C.

9 Functional testing of the Aalto-2 EPS prototype

9.1 General about testing

Testing is an important task to verify that the developed system can meet the defined requirements. Tests required for the equipment used in space are generally divided into functional, qualification and acceptance tests. Functional tests are used to ensure that the system provides the functionalities defined in the requirements. Testing that the regulator on the EPS-board can supply the defined voltage is a basic example of functional tests.

Qualification tests are used to ensure that the system is able to operate in an environment it is designed for and meets the requirements. Qualification tests generally use slightly broader ranges than defined in the requirements to have a safety margin. An example of qualification test is to test that the EPS can operate on a defined temperature range. Functional and qualification tests are usually done to qualification models (QM) or proto flight models (PFM). Acceptance tests are performed to the products which are ready to be shipped to the customer. Such models are often referred to as flight models (FM). There is no need to stress the FM beyond its limits as functional and qualification tests are already done to the device.

Engineering model shall be made for Aalto-2, which is used to verify that functionalities are operating as supposed. After the EM passes the required tests, QM or PFM will be manufactured, which will be used for qualification tests. The Appendix C shows the requirements for the design and in which model the requirement shall be fulfilled.

The Aalto-2 EPS model tested in the next chapters is considered a prototype model, because the final passive components are not chosen, the routing of the signals is not optimal, nor the microcontroller is integrated on the board. As the designing of the Aalto-2 EPS is in early phase, only functional tests are done to the prototype. Suitable testing facilities are not easily accessible and it is not beneficial to test the prototype thoroughly at this point as testing takes a lot of resources in terms of time and money.

Nevertheless, thermal-vacuum tests are better to be performed for the first prototypes to ensure that components can tolerate the space environment. This saves a lot of time as there is no need for redesign in a later phase if components are found unusable for space. Also radiation tests are important especially if the design is reused for longer missions. Testing shall be performed to all components susceptible to radiation induced damage, if there is no proof of flight heritage. The following parameters of radiation hardness shall be measured:

- total ionizing dose (TID); absorbed dose, which a component can tolerate without significant changes in characteristics
- displacement damage
- SEE; how the component survives from single event effects caused by high energetic particles

Vibrational and shock test shall be done to the qualification or proto flight model to ensure that the batteries are properly connected to the board. CDS require that the flight model shall be tested according to GSFC-STD-7000 standards, when the launch vehicle is not known. (CDS, 2009; GSFC-STD-7000A:2013) Environmental testing shall be made in the early phase after the first prototypes to make sure that the design is feasible.

9.2 Test results

Functional tests include measuring the ripple and offset of the regulators and their efficiencies using various resistive loads. Also testing of battery charging functions and operation of over-current protection are included in functional testing phase. Microprocessor functionalities for enabling or disabling individual DC-DC converters are simulated using Arduino.

9.2.1 DC-DC Converters

The prototype following the block diagram in Figure 8.1 was built (Figure 9.1) and DC/DC converters were tested using Agilent E3464A power supply to provide power to regulators.

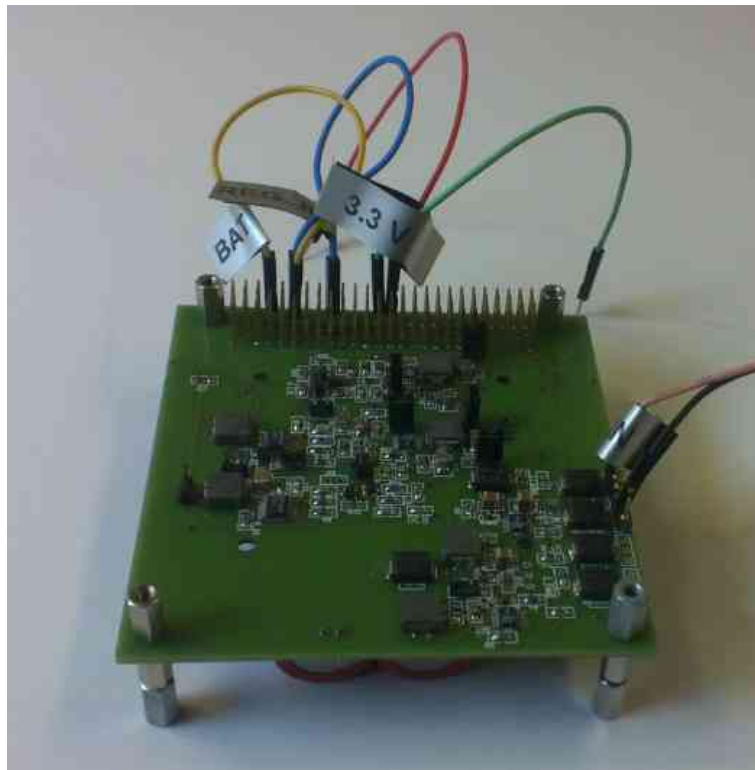


Figure 9.1: Aalto-2 EPS-prototype

A variable load was connected to the output of regulators. All regulators were tested in individual and parallel operation. Regulators are operating parallel in normal operation mode and the redundant one is shut down only in case of malfunction. LTC4411 ideal diodes were used to connect parallel outputs to the voltage bus. Figure 9.2 shows the measurement setup.

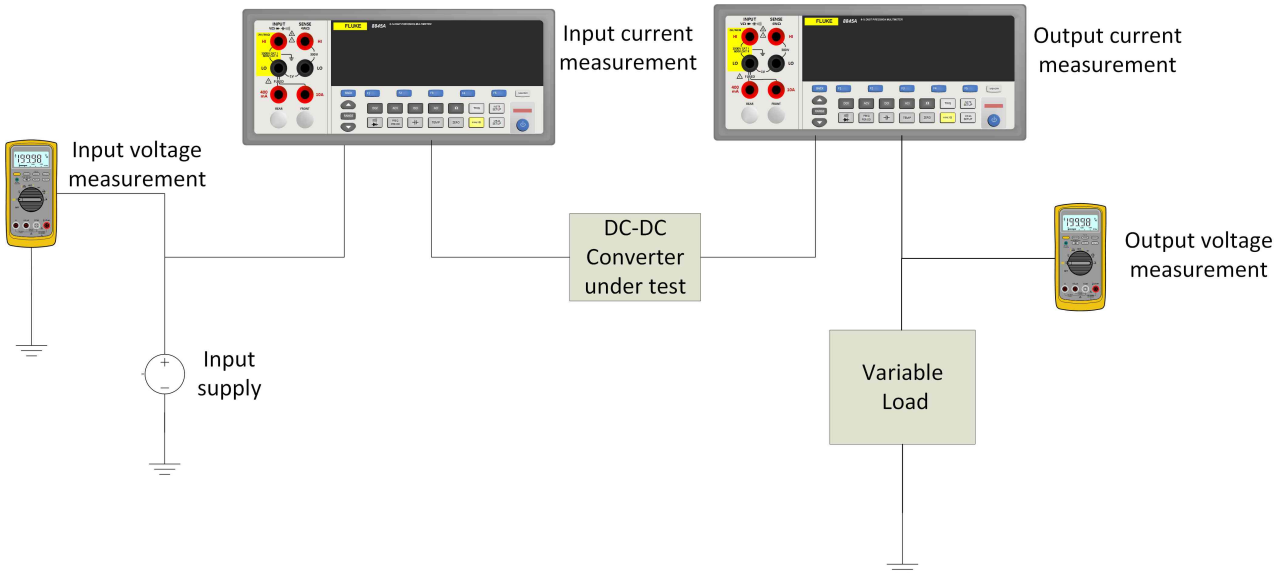


Figure 9.2: Measurement setup for DC-DC converters

The test results show that the system is able to provide at least 0.8 A of current for 3.3 V and 5 V buses which was required in Aalto-2 requirements (ELEC-003, Appendix C). Also the efficiency is > 92 % for 3.3 V when both regulators are operating parallel at 550 MHz frequency in burst mode fulfilling the efficiency requirement of > 88 %, when $I_{LOAD} = 0.5$ A (Table 15). When regulators were measured individually (Tables 13, 14), instability and large drop in output voltage were noticed for LTC1875-1 (Table 13) when higher output currents were needed. This is likely caused by a design flaw leading to an insufficient trace width to V_{in} pin. Otherwise the measured efficiency values are of same scale in comparison to manufactures values presented in Figure 9.3. Also the figure shows the efficiency rising slightly as the battery voltage decreases. It is due the reason that buck converter's dynamic losses decrease as the input voltage decreases.

Table 13: Measurement results of 3.3 V regulator LTC1875-1

U_{in} [V]	I_{in} [mA]	U_{out} [V]	I_{out} [mA]	Efficiency [%]
4,1	0	3,37	0	N/A
4,1	200	3,34	231	94,09
4,1	400	3,31	456	92,03
4,1	600	3,3	671	90,01
4,1	800	2,56	925	72,20

Table 14: Measurement results of 3.3 V regulator LTC1875-2

U_{in} [V]	I_{in} [mA]	U_{out} [V]	I_{out} [mA]	Efficiency [%]
4,1	0	3,35	0	N/A
4,1	200	3,35	231	94,32
4,1	400	3,35	446	90,99
4,1	600	3,35	645	87,73
4,1	800	3,35	850	86,68

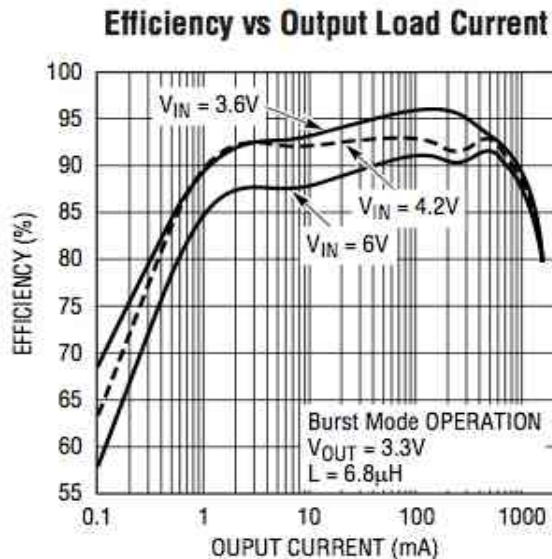


Figure 9.3: LTC1875 efficiency curve (LTC1875, 2001)

Table 15: Measurement results of 3.3 V regulators LTC1875-1 and LTC1875-2 operating in parallel

U_{in} [V]	I_{in} [mA]	U_{out} [V]	I_{out} [mA]	Efficiency [%]
4,1	0	3,32	0	N/A
4,1	200	3,34	231	94,17
4,1	400	3,31	456	92,12
4,1	600	3,29	693	92,68
4,1	800	3,30	850	85,52

Measured efficiencies of the 5 V regulators were lower than stated in the manufacturer's datasheet (Figure 9.4) and lower than the requirement of $> 90\%$, when $I_{LOAD} = 0.5$ A. Measurement results in Tables 16, 17 and 18 show that efficiency drops rapidly on larger loads. When regulators are operating individually, the output stays in regulation and output voltage is 5 V (± 0.05 V). The regulators are operating in fixed frequency PWM-mode at 1 MHz. The efficiency can be increased by lowering the operating frequency. Datasheet also states that adding schottky diode between the switch and the V_{out} pins may increase the efficiency as much as 4%. Also by widening the vias and improving the routing to decrease copper losses, over 90 % efficiency can be achieved.

Table 16: Measurement results of 5 V regulator LTC3122-1

U_{in} [V]	I_{in} [mA]	U_{out} [V]	I_{out} [mA]	Efficiency [%]
4,1	0	5,05	0	N/A
4,1	200	5,04	149	91,49
4,1	400	5,05	284	87,45
4,1	600	5,04	424	86,78
4,1	800	5,03	573	87,87
4,1	1000	5,03	697	85,51

Table 17: Measurement results of 5 V regulator LTC3122-2

U_{in} [V]	I_{in} [mA]	U_{out} [V]	I_{out} [mA]	Efficiency [%]
4,1	0	4,99	0	N/A
4,1	200	5	151	92,07
4,1	400	5,04	286	87,89
4,1	600	5	438	89,02
4,1	800	5,03	508	77,90
4,1	1000	N/A	N/A	

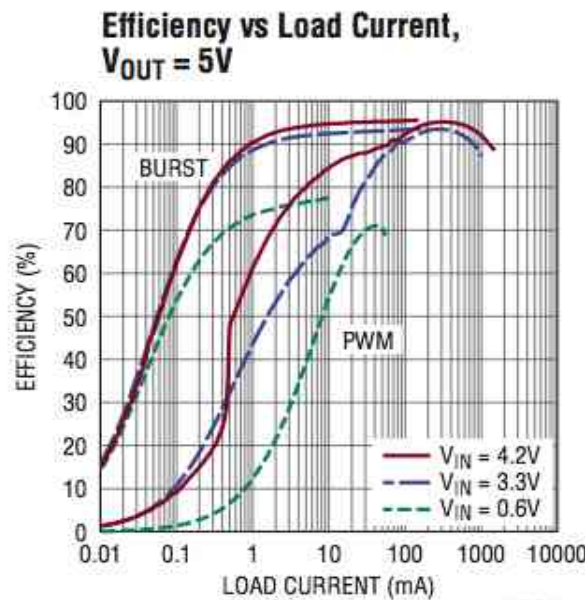


Figure 9.4: LTC3122 efficiency curve from manufacturers datasheet (LTC3122, 2012)

Table 18: Measurement results of 5 V regulators LTC3122-1 and LTC3122-2 operating simultaneously

U_{in} [V]	I_{in} [mA]	U_{out} [V]	I_{out} [mA]	Efficiency [%]
4,1	0	5,04	0	N/A
4,1	200	5,09	148	91,87
4,1	400	5,14	290	90,89
4,1	600	5,2	408	86,24
4,1	800	5,07	562	86,87
4,1	1000	5,05	682	84,00
4,1	1200	5,06	796	81,87

9.2.2 Maximum power point tracking and battery charging capabilities

The battery charging capability was tested by using various input voltages and measuring the efficiency of the charging circuit. As the Aalto-2 solar panels were not ready yet, I-V curve of panels were simulated by connecting a power supply to the EPS board's input. Battery charging was tested by connecting a rheostat to the battery bus and input and output voltages and currents were measured using different sized loads. The results are presented in Table 19. The input current is highly dependent on the illumination level of the panel and therefore EPS was tested using different input currents. The loss caused by the blocking diode between the output of the power supply and input of the regulator is decreasing the efficiency slightly (Table 21).

Table 19: EPS battery charging efficiency

U_{in} [V]	I_{in} [mA]	P_{in} [mW]	U_{out} [V]	I_{out} [mA]	P_{out} [mW]	Efficiency [%]
11,6	101	1171,6	3,86	229	883,94	75,45
11,5	204	2346	3,75	483	1808,84	77,10
11,34	300	3402	3,79	705	2669,84	78,48
11,5	406	4669	3,92	931	3651,38	78,20
11,75	511	6004,25	4,01	1142	4579,42	76,27
11,8	608	7174,4	4,02	1327	5330,56	74,30

The measured efficiency was lower than targeted. As the efficiency is between 74-78 %, 20 % losses in storage and regulation determined in power budget (Chapter 6.3.2, Table 7) cannot be met. Total efficiency between the solar panel input and the output of 3.3 V and 5 V buses can be calculated using Equation:

$$\eta_{tot} = \eta_{BCR} * \eta_{bat} * \eta_{reg}, \quad (20)$$

where η_{tot} is efficiency between the solar panel input and the regulator output, η_{BCR} is the battery charging regulators efficiency, η_{bat} is the battery charge efficiency and η_{reg} is the efficiency of the regulator. Charge efficiency of lithium-ion batteries is approximately 97-99 %.

The efficiency from solar panel input to 5 V bus in typical load condition is calculated using Equation 20.

$$\eta_{tot} = \eta_{BCR} * \eta_{bat} * \eta_{reg} = 68 \% \quad (21)$$

where $\eta_{BCR} = 76\%$ (Table 19, $U_{in} = 11,75$ V, $I_{in} = 511$ mA), $\eta_{bat} = 98\%$ and $\eta_{reg} = 91\%$ (Table 18, $I_{load} = 290$ mA).

For 3.3 V voltage bus, the overall efficiency in typical load situation, between solar panel input and output of the regulators is:

$$\eta_{tot} = \eta_{BCR} * \eta_{bat} * \eta_{reg} = 67\%, \quad (22)$$

where $\eta_{BCR} = 76\%$, $\eta_{bat} = 98\%$ and $\eta_{reg} = 92\%$ (Table 15, $I_{load} = 456$ mA).

As the solar panels are not operating on exact maximum power point, total conversion efficiency will be even lower than this. The battery charging efficiency was tested also using Linear Technology's evaluation board DC1568A using LT3652EDD. It was modified to use a battery float voltage of 4.2 V. The measured efficiency is slightly better, but some of the increase on the efficiency originates from the fact that the board does not have blocking diode. Results for DC1568A are presented in Table 20.

Table 20: Test results for LT3652EDD evaluation board DC1568A

U_{in} [V]	I_{in} [mA]	P_{in} [mW]	U_{out} [V]	I_{out} [mA]	P_{out} [mW]	Efficiency [%]
12,07	100	1207,40	4,18	219	916,1	75,87
12,05	201	2422,25	4,18	470	1964,6	81,11
12,02	301	3618,02	4,18	714	2983,1	82,45
11,99	409	4905,14	4,18	968	4042,4	82,41
11,96	507	6065,24	4,17	1189	4962,9	81,83
11,94	602	7187,28	4,17	1404	5857,5	81,50
11,91	700	8333,50	4,17	1615	6734,6	80,81
11,89	809	9622,25	4,07	1868	7610,2	79,09

As total efficiency stays low, it is suggested that another options for battery charge regulators are investigated. Temperature compensation functionality of the LT3652 was not tested at this point. It has been postponed until the new trade-off between available options for battery charging is completed.

Table 21: Power loss over blocking diode

I_{in} [mA]	Voltage over blocking diode [V]	Blocking diode power loss [mW]
101	0,29	29,19
204	0,30	61,40
300	0,31	93,00
406	0,32	128,70
511	0,32	165,56
608	0,33	200,64

An easy way to accomplish better efficiency in battery charging is to lower the input voltage by using a different approach in connecting the cells to the system. On Estonian ESTCube-1 1U CubeSat all of the cells are connected in parallel and approximately 90 % efficiency to charge the batteries to 4.17 V is achieved. ESTCube-1 MPPT tracking and battery charging is based on STMicroelectronics SPV1040. (Ilbis, 2013) The solar cells on ESTCube-1 are the same as are

supposed to be used in Aalto-1 and Aalto-2 nanosatellites. SPV1040 uses P & O algorithm for MPPT and therefore degrading of the cells does not affect on finding the maximum power point.

The parallel cell configuration suitable for Aalto-2 is shown in Figure 9.5. Figure shows cells on +X side and -X side of the satellite. Cells on +Y and -Y sides are connected in a similar way, except one more cell is connected to both controllers as the +Y and -Y side panels have 5 cells. Total of 4 MPPT/battery charge controllers are needed in total. The advantage in this configuration is the large amount of redundancy as there is 16 independent solar cells in parallel connected to 4 controllers. Other advantages are flight heritage and good efficiency. Largest drawback is increased footprint. The efficiency of SPV1040 was verified on Aalto University using STEVAL-ISV006V2 evaluation board. The battery was charged to 4.15 V and 87 % efficiency was measured. It is suggested that LT3652 is replaced with SPV1040 in future versions of the EPS.

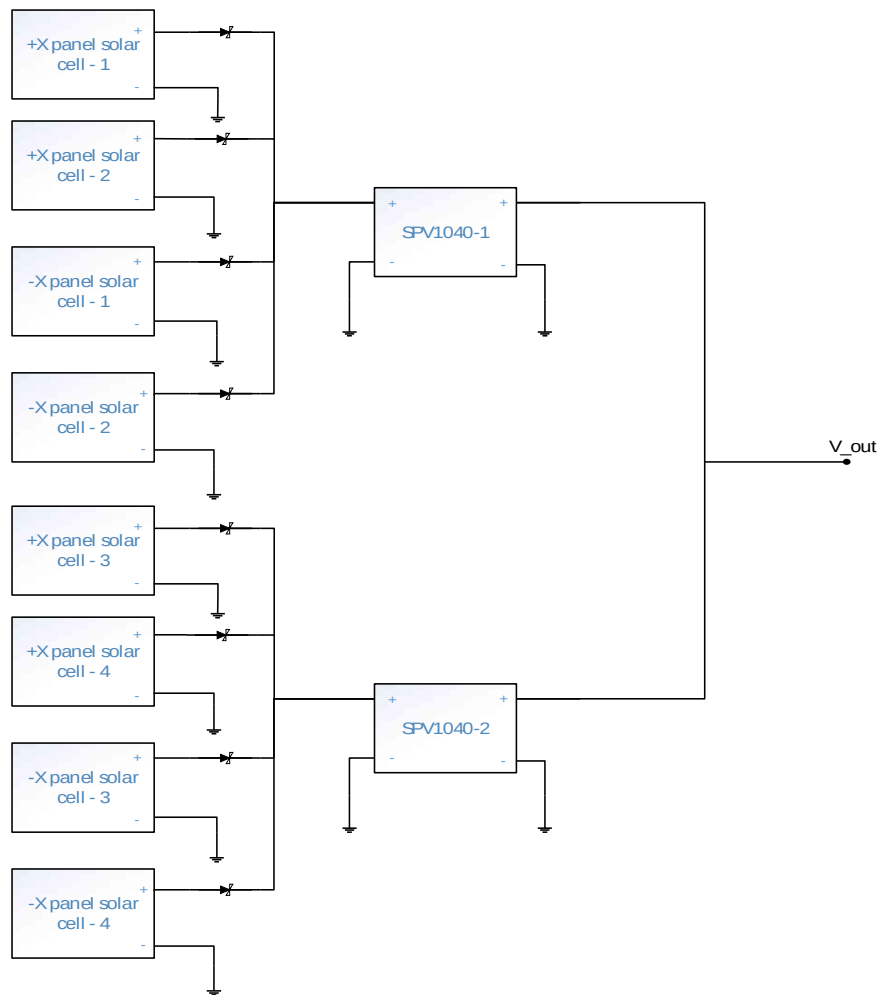


Figure 9.5: Solar cells connected in parallel

9.2.3 Over-current protection

Operation of the MAX890L over-current protection circuit was tested. The current limit was set to 0.8 A. The circuit operated as supposed to and the output voltage dropped when current climbed over the set limit. Voltage drop over MAX890L was measured using various pass-through currents. Measurement results are presented in Table 22.

Table 22: Measurement results of MAX890L ($V_{in} = 3.3$ V)

I [mA]	Voltage over MAX890L [V]	Power loss [mW]
200	0,05	10
300	0,07	22,2
400	0,10	40
500	0,13	63,5
600	0,15	90,6
700	0,18	122,5
800	0,21	168

Power loss in MAX890L is large when using higher currents. Losses originate from the on-resistance of the component which is approximately 75 to 150 mohms according to the datasheet. Therefore, it shall be considered if MAX890L is the best option to employ over-current protection or is using current telemetry and shutting down regulators as stated in Chapter 8.4 adequate. Another option is to replace the component with component having lower on-resistance in order to lower losses.

9.2.4 Burn-in testing

The prototype was tested using burn-in test in room temperature for a pre-determined time. The test helps to find out if there's manufacturing errors in the components or problems in assembling phase. The burn-in test was realized by connecting a 4.5 W load to 5 V output and a 2.5 W load to 3.3 V output. The board was powered for 7 days. Afterwards the EPS-board characteristics were measured and compared to earlier results. There was no change noticed in characteristics.

10 Summary and future work

In this master thesis, requirements were determined for Aalto-1 and Aalto-2 electrical power systems and a prototype of the EPS for Aalto-2 was developed. Requirements for Aalto-1 are listed in Appendix B and for Aalto-2 in Appendix C. The next subchapters summarize the outcomes of the thesis work and actions to be taken for future development of Aalto-2 EPS.

10.1 Summary

Mass budget of 2 kilograms for Aalto-2 satellite sets great challenges to the project. To speed up Aalto-2 design process, Aalto-1 subsystems are used whenever it is possible. Aalto-1 designs have to be modified to be as light as possible and in some cases totally new approaches has to be thought of. Low mass budget of 200 grams reserved for EPS forces to make new design choices. The maximum battery weight shall be less than 120 grams including the packaging and connection to the board. This does not leave much room for different battery configurations, when redundant battery configuration is required. To achieve redundancy, paralleling batteries is needed and 1s2p configuration is chosen. Using 2s2p configuration would exceed the mass budget, if light-weight batteries could not be found. The chosen battery voltage determines options for the DC/DC converters as conversion steps needs to be minimized to keep the design simple and to maximize the efficiency.

As the EPS board has not yet gone through environmental tests, there is no proof that the design survives in the space environment. But as Aalto-2 is under Earth's radiation belts in a fairly low orbit, the total amount of ionizing radiation will be small and should not pose a problem to the components. A more severe case is if high energetic particles penetrate some of the subsystems or the payload causing a latch-up. This possibility is taken into account by adding redundancy and latch-up protection for the voltage buses to the system. After a reliable method to attach the batteries to the board has been found, vibration or shock effects should not cause problems either. The system is modular and it is easy to change individual blocks of the system. If more risk is allowed and redundancy is not needed in some parts of the system, the EPS can easily be modified to a non-redundant system.

It was noticed that the battery charging efficiency was much lower than anticipated. Therefore, it is suggested to investigate if another MPPT capable battery charging regulator is more suitable for the purpose. MPPT-algorithms which rely on measurements of the panels BOL characteristics does not work optimally for longer missions as the solar panel characteristics degrades over time because of the environmental effects. Method which could estimate the new power point after solar panel degradation would be a better option, especially for longer missions. For Aalto-2 mission a fixed power point with temperature compensation is feasible as a short mission time leads to minimal degradation of the solar cells. If the current design is used, the power budget and the battery capacity have to be recalculated.

One option for achieving better efficiency is connecting all the solar cells in parallel as described in Chapter 9.2.2. The configuration requires 4 SPV1040 MPPT-controllers (Table 11) in total as the cells on opposite sides can be connected to the same controller. SPV1040 uses P & O algorithm for MPPT and therefore degrading of the cells does not affect on finding the maximum power point. SPV1040 has been used on EPS of Estonian 1U CubeSat ESTCube-1, which is operational on orbit in more harsh conditions than expected for Aalto-2. Advantages in using SPV1040 are flight

heritage, good efficiency and the large amount of redundancy as the cells are divided to 16 individual strings. The largest drawback is increased footprint.

Efficiency and operation of 3.3 V and 5 V regulators were satisfactory, although the 5 V converter did not meet the requirement of 90 % efficiency. Over 90 % efficiency can be achieved by updating the component placement and improving the routing of the board. Also the voltage drop on larger loads for 3.3 V converter can be fixed by following the manufacturer's instructions on component placement more carefully. Using MAX890L chip for limiting the current seems unnecessary, when the same functionality can be made by monitoring output currents of the converters and shutting them down if necessary.

Test results for Aalto-1 EPS are not presented in this thesis as delivery of the engineering model of the EPS was postponed several times.

10.2 Future work

The Aalto-2 EPS prototype needs improvements on several fields. The most important tasks for the future development of the Aalto-2 EPS is to integrate the batteries on the EPS control board and design the digital interface to control the EPS board. Functions needed for the digital interface is controlling the converters based on telemetry data and delivering the telemetry to the on-board computer of the satellite. The new trade-off between LT3652 and SPV1040 is necessary before continuing the solar panel design as it affects to solar cell configuration on the panel.

A decision has to be made, whether it is necessary to have option to turn off the payloads or subsystems on the EPS side. Such switches are easy to implement if necessary, but redundant power paths with latch-up protection require a small amount of extra footprint space on the board. Also the decision whether the antenna deployment system based on Aalto-1 ADS design is used or if it is better and simpler to use a microcontroller controlled MOSFET switch similar to the battery heater connection presented in Figure 8.7.

For the engineering model of the routing of the board has to be improved and vias on the board shall be widened to decrease losses and improve the conduction of the heat away from the DC/DC converter ICs. After the EM is completed, the FMECA shall be conducted to the design to notice points which have to be improved or corrected for the flight model.

References

A2-SYS-DD-01-v1. 2013. Interface Control Sheet. Aalto-2 project internal document.

Amy, R.A. Aglietti, G. S. Richardson, G. 2009. Reliability analysis of electronic equipment subjected to shock and vibration – A review. *Shock and Vibration*, vol. 16, no. 1 (2009), pp. 45-59. IOS Press. DOI 10.3233. ISSN: 1875-9203 (Online).

Azur Space, 2012a. 30% Triple Junction GaAs Solar Cell, Type: TJ Solar Cell 3G30C. Issued 17th April 2012. Available at www.azurspace.de. [Accessed 2nd November 2012].

Azur Space, 2012b. 30% Triple Junction GaAs Solar Cell Assembly, Type: TJ Solar Cell Assembly 3G30A. Issued 19th April 2012. [Accessed 20th November 2012].

AVNET, 2011. Avnet Energy Harvesting & Off-Grid Solar. Applications Selector Guide. AVNET electronics marketing. Available at <http://www.em.avnet.com/solar> [Accessed 8th October 2012]

Bjorndahl, W.D. McMullen, E. 1999. Plastic packaging in circuit board assemblies for space applications. 1999 IEEE Aerospace Conference Proceedings, vol. 2, pp. 295-302.

Brandhorst Jr., H.W. Rodiek, J.A. 2008. Space solar array reliability: A study and recommendations. *Acta Astronautica*, vol. 63, no. 11–12 (2008), pp. 1233-1238.

Burt, R. 2011. Distributed Electrical Power Systems in Cubesat Applications. Master's Thesis. Utah State University, Electrical and Computer Engineering. 83 pages.

CDS. 2009. CubeSat Design Specification. Rev 12, California Polytechnic State University, Aug 2009. Available at http://www.cubesat.org/images/developers/cds_rev12.pdf. [Accessed 20th October 2012]

Chakraborty, S. 2006. Analysis an Design of a Digitally Controlled Source Based Multi-output Converter. 178 pages. Proquest

Chen, Y. Li, P. 2011. The “popcorn effect” of plastic encapsulated microelectronic devices and the typical cases study. 2011 International Conference on Quality, Reliability, Risk, Maintenance, and Safety Engineering (ICQR2MSE), p.482-485, 17-19 June 2011 doi: 10.1109/ICQR2MSE.2011.5976658

CSK-SPEC. 2007. CubeSat Kit PCB Specification rev A5. Pumpkin incorporated. Updated to revision A5 19 June 2007. Available at http://www.cubesatkit.com/docs/CSK_PCB_Spec-A5.pdf. [Accessed 10th November 2012]

De Luca, A. 2011. Architectural Design Criteria for Spacecraft Solar Arrays, Solar Cells - Thin-Film Technologies, Prof. Leonid A. Kosyachenko (Ed.), ISBN: 978-953-307-570-9, InTech, Available at <http://www.intechopen.com/books/solar-cells-thin-film-technologies/architectural-design-criteria-for-spacecraft-solar-arrays> [Accessed 20th April 2013]

Dorn, L.T. Jr. 2009. NPS - SCAT: Electrical Power System, M.Sc. Thesis, Naval Postgraduate School, Monterey, CA, September 2009. 103 pages.

Elbrecht, A. Dech, S. Gottscheber, A. 2011. 1U CubeSat Design for increased Power Generation. 1st IAA Conference on University Satellites Missions and CubeSat Workshop in Europe Roma, Italy, 24-29 January 2011

Erickson, R. W. 2007. DC-DC Power Converters. Article in Wiley Encyclopedia of Electrical and Electronics Engineering. DOI: 10.1002/047134608X.W5808.pub2. John Wiley & Sons, Inc.

ESA. Outgassing database. Available at http://esmat.esa.int/Services/outgassing_data/outgassing_data.html. [Accessed 24th July 2012]

ESCIES. 2012. The European Space Components Information Exchange System database. Available at <https://escies.org/epplcomponent/list> [Accessed 18th December 2012]

Fortescue, P (Editor). Swinerd, G (Editor). Stark, J. (Editor). 2011. Spacecraft Systems Engineering, 4th edition. ISBN 978-0-470-75012-4. 752 pages. Wiley.

GSFC-STD-7000A. 2013. GSFC-STD-7000A. General Environmental Verification Standard (GEVS). Published 4/22/2013. NASA. Available at <http://standards.gsfc.nasa.gov/gsfc-stds.html>.

Hohm, D. P. and Ropp, M. E. (2003), Comparative study of maximum power point tracking algorithms. Prog. Photovolt: Res. Appl., 11: 47–62. doi: 10.1002/pip.459

Jacques, L. 2009. Thermal Design of the Oufiti-1 nanosatellite. Master's Thesis. Faculty of Applied Sciences. University of Liège. 142 pages. Available at <http://orbi.ulg.ac.be/handle/2268/76017>. [Accessed 17th June 2012]

Ilbis, E. 2013. ESTCube-1 electrical power system – design, implementation and testing. Bachelor's Thesis. University of Tartu. Faculty of Science and Technology, Institute of Physics. 88 pages.

Kestilä, A. Tikka, T. Peitso, P. Rantanen, J. Näsilä, A. Nordling, K. Saari, H. Vainio, R. Janhunen, P. Praks, J. Hallikainen, M. 2013. Aalto-1 nanosatellite - technical description and mission objectives. *Geosci. Instrum. Method. Data Syst.*, vol. 2, no. 1 (2013), pp. 121 – 130. Copernicus Publications. Available at <http://www.geosci-instrum-method-data-syst.net/2/121/2013/gi-2-121-2013.pdf> [Accessed 26th February 2013]. DOI 10.5194/gi-2-121-2013

LaBel, K.L. Gates, M.M. Moran, A.K. Marshall, P.W. Barth, J. Stassinopoulos, E. Seidleck, C. Dale, C. 1996. Commercial Microelectronics Technologies for Applications in the Satellite Radiation Environment. *Proceedings 1996 IEEE Aerospace Applications* (1996), pp. 375–390.

Li, J. 2009. Current-mode control: modeling and its digital application. Diss. Virginia Polytechnic Institute and State University. 197 pages.

Linear. 2012. Linear Technologies company webpage. Available at <http://www.linear.com>. [Accessed 20th December 2012]

LTC1875. 2001. Linear Technologies LTC1875 Datasheet. Available at <http://www.linear.com>. [Accessed 22nd December 2012]

LTC3122. 2012. Linear Technologies LTC3122 Datasheet. Available at <http://www.linear.com>. [Accessed 22nd December 2012]

Luo, S., Ye, Z., Lin, R. L., & Lee, F. C. 1999. A classification and evaluation of paralleling methods for power supply modules. In *Power Electronics Specialists Conference, 1999. PESC 99. 30th Annual IEEE* (Vol. 2, pp. 901-908). IEEE.

Luo, S. & Batarseh, I. 2005. A review of distributed power systems part I: DC distributed power system. *IEEE Aerospace & Electronic Systems Magazine*, vol. 20, no. 8 (2005), pp. 5-16.

MAX890L. 2011. Maxim Integrated company webpage. Available at <http://www.maximintegrated.com/datasheet/index.mvp/id/1526>. Page last modified: 2011-04-18 [Accessed 19th December 2012]

Messenger, S.R., Summers, G.P., Burke, E.A., Walters, R.J. & Xapsos, M.A. 2001. Modeling solar cell degradation in space: A comparison of the NRL displacement damage dose and the JPL equivalent fluence approaches?. *Progress in Photovoltaics: Research and Applications*, vol. 9, no. 2, pp. 103-121.

NASA. 2012. Outgassing Data for Selecting Spacecraft Materials Online. Updated 22nd March 2012. Available at <http://outgassing.nasa.gov/>. [Accessed 24th July 2012]

NASA-PD-ED-1201. PRACTICE NO. PD-ED-1201 EEE Parts Derating. Available at <http://engineer.jpl.nasa.gov/practices.html#reliability>. [Accessed 24th November 2012]

Nikkanen, T. 2010. Nanosatelliitin energiajärjestelmä. Bachelor's Thesis. Aalto University. School of Electrical Engineering. 30 pages.

Näsilä, A. Kestilä, A. Hakkarainen, A. Komu, M. 2012. Aalto-1, Experiment Interface Document, version 5. A1-SYS-EID-01-v5. Version 5 issued 30th March 2012

Onat, N. 2010. Recent developments in maximum power point tracking technologies for photovoltaic systems. International Journal of Photoenergy, vol. 2010, Article ID 245316, 11 pages. Hindawi Publishing Corporation. DOI:10.1155/2010/245316.

PC/104. 2008. PC/104 Specification Version 2.6 October 13, 2008. PC/104 Consortium. Available at www.pc104.org. [Accessed 12th September 2012]

Rauschenbach, H. S. 1980. 'Damage equivalent 1 MeV fluence caused by electrons and protons due to trapped particles, to silicon cells protected by 150 µm fused silica covers and infinitely thick rear shielding' [Figure] Solar Cell Array Design Handbook, Van Nostrand Reinhold, New York in Fortescue et al. 2011, Spacecraft Systems Engineering, 4th edition, ISBN 978-0-470-75012-4. 752 pages. Wiley

Singarayar, F. Reinhard, R. Asma, C. Bernal, C. Weggelaar, W. Kataria, D. 2013. QB50 System Requirements and Recommendations, Interface Control Documents, Issue 3. Issued 5 February 2013. Available at www.qb50.com. [Accessed 7th February 2013]

Skvarenina, T. L. (Editor) 2002. The Power Electronics Handbook. ISBN 9780849373367. 664 pages. CRC Press.

Srour, J. R. McGarrity, J. M. 1988. Radiation Effects on Microelectronics in Space. Proceedings of the IEEE, vol. 76, no. 11. (1988), pp. 1443-1469.

STM. 2011. STMicroelectronics SPV1001 datasheet. Available at <http://www.st.com/st-web-ui/static/active/en/resource/technical/document/datasheet/CD00287228.pdf> [Accessed 15th August 2013]

STM. 2012. STMicroelectronics company webpage. Available at <http://www.stm.com>. [Accessed 20th December 2012]

TASC. 2002. Triangular Advanced Solar Cells (TASC) datasheet. Available at http://www.spectrolab.com/DataSheets/PV/PV_NM_TASC_ITJ.pdf. [Accessed 20th September 2012]

TI. 2012. Powering the MSP430 from a High Voltage Input using the TPS62122. Texas Instruments Application Report SLVA335C–October 2009–Revised January 2012. Available at <http://www.ti.com> [Accessed 27th November 2012]

TI. 2013. Products for Charge Pump (Inductorless). Available at <http://www.ti.com/lscds/ti/power-management/charge-pump-inductorless-products.page> [Accessed 3th February 2013]

van den Berg, E. & Kroon, M. 2002. Algorithms and performance of a space dedicated solar array modelling tool. In Proceedings of 6th European Space Power Conference held 6-10 May, 2002 in Porto, Portugal. European Space Agency, ESA, pp. 527-532

Walker, G. 2001. Evaluating MPPT converter topologies using a matlab PV model. J. Elect. Electron. Eng., Australia, vol. 21, no. 1, pp. 45–55 (2001)

Wens, M & Steyaert, M. 2011. Design and Implementation of Fully-Integrated Inductive DC-DC Converters in Standard CMOS. ISBN 978-94-007-1435-9. 322 pages. Springer.

Appendix A

Matlab code for estimating MPP location of Azur Space 3G30C solar cells:

```
function Ia = AzurSpace(Va,insolation,TaC)
% Model of Azur Space 3G30C, 29.5 % efficiency cells @ BOL. To simulate
% different illumination, temperature and degradation conditions
% Usage: Ia = AzurSpace(Va,insolation,TaC), where
% Va = array voltage
% Ia = array current
% insolation = solar radiation energy on a given surface area (AM0=1367W/m2)
% TaC = Temperature in Celsius degrees
% Usage example: AzurSpace(0:0.1:3.2,1367,28)

% Reference: G. Walker, "Evaluating MPPT converter topologies using a
% Matlab PV model", Journal of Electrical & Electronics Engineering,
% Australia, IEAust, vol. 21, No. 1, 2001, pp. 49-56

k = 1.38e-23; % Boltzmann's constant
q = 1.60e-19; % Charge of an electron

K0=0.00032; %Temperature coefficient dIsc/dT
K1=-0.006; %Temperature coefficient dVoc/dT

% "diode quality" factor, =2 for crystalline, <2 for amorphous, chosen to
% fit the curve
n = 1.5;

% Band gap voltage, 1.12eV for xtal Si, ?1.75 for amorphous Si.
% Source for chosen value: Architectural Design Criteria for Spacecraft Solar
Arrays
Vg = 1.42;
Ns=1; % number of series connected cells (diodes)
Tref = 273 + 28; % reference temperature
Voc_T1 = 2.7 % Open Circuit voltage @ T=28C
Isc_T1 = 0.5202; % Short Circuit current @ T=28C

% MPP
Vmp_T1 = 2.411; % MPP-voltage at T = 28C
Imp_T1 = 0.5044; % MPP-current at T = 28C

% Temperature in Kelvins
TaK=273+TaC;

% insolation in Watts/m2
insolation=insolation/1367;

Iph_T1 = Isc_T1 * insolation; %Iph at reference temperature
a = 0.28e-3/Isc_T1 % Change in Iph per degree
Iph = Iph_T1 * (1 + a*(TaK - Tref)); %Photogenerated current Iph at selected
temperature
Vt_T1= k*Tref/q; %A*kT/q
Id_T1 = Isc_T1 / (exp(Voc_T1/(n*Vt_T1))-1) % Diode saturation current of Diode 2
at T=28C
b = Vg * q/(n*k)

% Diode saturation current at selected temp
Id = Id_T1 * (TaK/Tref).^(3/n) .* exp(-b.* (1./TaK - 1/Tref))
Rs=0.304 % Chosen to match the curve
Vt_Ta= n*1.38e-23*Tref/(1.60e-19) %n*kT/q

% Solve for Ia: f(Ia) using Newton's method:
Vc = Va/Ns;
Ia = zeros(size(Vc)); %Iav=Ia;
```

```

for j=1:5;
Ia = Ia - (Iph - Ia - Id.* (exp((Vc+Ia.*Rs)./Vt_Ta)-1)) ./ (-1 -
(Id.* (exp((Vc+Ia.*Rs)./Vt_Ta)-1)).*Rs./Vt_Ta)
end

% Plotting functions
% Change of axis may be needed, if values are changed
% Draw I-V curve
figure(1)
plot(Va,Ia);
title('IV-Curve of Azur Space 3G30C cell');
xlabel('Voltage [V]');
ylabel('Current [A]');
axis([0 4 0 1]);
grid
hold all;

% Draw I-V and P-V curve on the same figure
figure(2)
y=Ia.*Va; [AX,H1,H2] = plotyy(Va,Ia,Va,y,'plot');
set(get(AX(1),'Ylabel'), 'String','Current [A]')
set(get(AX(2),'Ylabel'), 'String','Power [W]')
title('IV-Curve & PV-Curve of Azur Space 3G30C cell');
xlabel('Voltage [V]');
ylabel('Current [A]');
zlabel('Power [W]');
set(H1, 'LineStyle', '--')
set(H2, 'LineStyle', '-')
axis(AX(1), [0 2.8 0 0.7])
axis(AX(2), [0 2.8 0 3])

grid
hold all;

```

Appendix B

Requirements for Aalto-1

ID	Requirement	Procedure	Result	Success Criteria	Compliance (pass / fail)	Notes
MEC-001	The system mass shall be no more than 372 g (Control Board 91 g+ battery board 281g)	Weight measurement		Mass < 372 g		EM battery board not fully populated
MEC-002	Mechanical interface of the EPS board shall be CubeSat Kit compatible	Verification, measurement of dimensions		Connectors fit, drill holes positioned right, dimensions ok		
MEC-003	Mechanical interface of the battery shall be CubeSat Kit compatible, except height shall be no more than 20.44 mm from the top of PCB	Measurement of dimensions		Connectors fit, drill holes positioned right, dimensions ok		
MEC-004	All dimensional tolerances shall be within ± 0.1 mm	Measurement of dimensions		Offset < 0.1 mm		
MEC-005	The EPS shall be able to withstand the launch environment	Verification from supplier		Manufacturers assurance		
MEC-006	The EPS shall be able to withstand the LEO environment for at least 2 years.	Verification from supplier		Manufacturers assurance		
MEC-007	Design life of the EPS shall be more than 4 years	Verification from supplier		Manufacturers assurance		
MEC-008	The EPS shall use materials which fulfils NASA outgassing requirements of TML < 1.0%, CVCM < 0.1%	Verification from supplier		Materials list		
MEC-009	The EPS shall be possible to store for >120 days without degradation	Verification from supplier		Manufacturers assurance		
MEC-010	The EPS-control board shall be able to withstand an operating temperature of -40 to +85 °C	Functional testing, thermal cycling/ Verification from supplier				
MEC-011	The Battery-board shall be able to withstand operating temperature of -10 to 50°C	Functional testing/ Verification from supplier				
MEC-012	The supplier shall conduct verification to present the EPS meets all the following requirements. – Functional tests – EMC tests – Thermal vacuum cycling with acceptance levels – Mechanical tests with acceptance levels – Vibration – Shock	Verification from supplier		Test reports delivered		

ELEC-001	The EPS shall provide 3.3 V, 5 V and 12 V regulated voltage buses.	Functional testing		Voltages are present and connected to right pins.		
ELEC-002	3.3 V and 5 V regulated voltage buses shall provide at least 1.5 A of current and 12 V bus at least 0.8 A of current	Functional testing		Provides enough current for payloads / subsystems		
ELEC-003	The EPS shall provide an unregulated voltage line which floats following the battery voltage	Design check, functional testing		Battery bus voltage delivered to CubeSat Kit connector		
ELEC-004	The regulated voltage range shall be within $\pm 1\%$ of stated value across the full load range	Functional testing		Voltages are $\pm 1\%$ range of nominal		
ELEC-005	All voltage lines shall have overcurrent protection	Functional testing		Voltage line trips if maximum current is exceeded		
ELEC-006	The electrical interface shall be CubeSat Kit compatible	Design check, functional testing		Pinout matches		
ELEC-007	The EPS shall have 10 commandable switches to turn off payloads / subsystems in case of failure	Functional testing		Switches operational		
ELEC-008	Commandable switches shall be able to be commanded through I ² C	Functional testing		Enable / disable operational		
ELEC-009	The pinout shall follow A1-EPS-IF-02-v5-FINAL.pdf document provided to manufacturer	Design check, functional testing		Pinouts follows the documentation		
ELEC-010	The ADS pin shall have 30 minute timed ON function	Functional testing		Voltage line dedicated to ADS activates 30 minutes after powering the system on		
ELEC-011	The EPS shall utilize Maximum Power Point Tracking	Design check, functional testing		Solar Simulator / Real Panels		
ELEC-012	The Battery shall have BOL capacity of 30Wh	Verification from supplier		Manufacturers assurance		Only FM model
ELEC-013	The battery shall have a heater which activates when battery temperature is too low	Design check, functional testing		Activates If $T_{battery} < 0^\circ C$		
ELEC-014	Battery heater shall be deactivated when $T_{battery} > 5^\circ C$	Functional testing		Deactivates when $T_{battery} > 5^\circ C$		
ELEC-015	Battery shall have undervoltage / overvoltage protection	Functional testing		Charging ends when $V_{BAT} > 8.3 V$ and battery stops supplying current when $V_{BAT} < 6.2 V$ (TBD)		
ELEC-016	After undervoltage protection has activated, battery shall not reactivate until the battery voltage has risen to safe level	Functional testing		After undervoltage lockout situation battery activates when $V_{bat} \approx 7V$ (TBD)		
ELEC-017	The EPS shall not cause any significant interference to other systems	Functional testing for the assembled satellite		Connect systems and test the operation		
ELEC-018	The EPS shall have blocking diode to ensure that non-illuminated solarpanel does not consume power	Design check, functional testing		Test if current flowing to non-illuminated solarpanel		
ELEC-019	The EPS shall have interface for kill switch and separation switch	Design check, functional testing		Kill switch can be connected and EPS stops supplying power when activated		
ELEC-020	The Solar panels shall have at least 490 cm ² of conductive surface	Design check, measuring the amount of conductive				

		surface			
TM & TC-001	The EPS shall send at least the following telemetry on request: - Solar panel voltages - Solar panel currents - Solar panel temperatures - Individual battery cell voltage levels - Individual battery cell currents - Battery temperature of each battery individually - Battery charge/discharge status for each battery - Output voltage levels - Output currents	Functional testing		Telemetry available and values right	
TM & TC-002	The EPS shall provide instant solar array currents to have possibility to use values as a rough attitude indicator	Design check, functional testing		Telemetry values provided on demand and without significant delay	
TM & TC-003	Telemetry and telecommand shall use I ² C data bus	Design check		Sends telemetry and responds to commands	
TM & TC-004	EPS shall connect in slave mode to I ² C data bus	Design check, functional testing		Operates in slave mode	
TM & TC-005	EPS shall be able to communicate at 100 kbps and 400 kbps rates	Functional testing		I ² C bus operates at 100 kbps & 400 kbps rates	
TM & TC-006	The EPS shall have dead-man's switch reset functionality	Design check, functional testing		EPS turns PCMs off and on, if heartbeat signal is not sent from OBC for 4 to 10 minutes	
TM & TC-007	The EPS shall have reset functionality for voltage buses through I ² C	Functional testing			
DEL-001	The supplier shall provide failure detection, isolation and recovery (FDIR) information	Verification		Documentation delivered	
DEL-002	The supplier shall provide failure mode, effects and criticality analysis (FMECA) results (TBD)	Verification		Documentation delivered	
DEL-003	The supplier, the EPS or any of its components shall not be under any regulations (e.g. ITAR) which would affect the participation of foreign students in the project or co-operation with international parties.	Verification from supplier		Assurance delivered	
DEL-004	The supplier shall deliver CAD-models of the systems before April 2013 (TBD)			CAD-model supplied on time	
DEL-005	An engineering model shall be delivered before May 2013 (TBD)			EM supplied on time	
DEL-006	A flight model shall be delivered before November 2013 (TBD)			FM supplied on time	
DEL-007	The supplier shall provide at least the following documentation:			Documents delivered	

	<p>Operating manual</p> <p>Test specification and test reports</p> <p>Functional test report including a procedure to reproduce functional tests at Aalto University</p> <p>Copy of statement of origin</p> <p>Copy of relevant export papers</p>				
--	---	--	--	--	--

Appendix C

Requirements for Aalto-2

ID	Requirement	Procedure	Result	Model	Success Criteria	Compliance (pass / fail)	Notes
QB50-SYS-1.1.5	The EPS shall use materials which fulfils NASA outgassing requirements of TML < 1.0%, CVCM < 0.1%	Choosing materials using NASA/ESA outgassing tables. Creating and checking materials list. Outgassing tests if materials used, where TML or CVCM unknown		EM	Materials in materials list fulfil the requirement of TML < 1.0%, CVCM < 0.1%		QB50-SYS-1.1.5 Singarayar et al. 2013
QB50-SYS-1.3.1	The CubeSat shall provide sufficient power at the appropriate voltage, either by solar array generation or battery, to meet the power requirements of all satellite subsystems in all modes of operation.	Simulation of power production and consumption in different operation modes with margins. Power conversion efficiency measurements. Voltage outputs of 3.3 V and 5 V buses stable	Outputs stable. Efficiency from SA inputs to output regulators needs improvements	Prototype	Power budget positive. Power conversion efficiencies matches the estimations in the budget. Voltage range for the buses shall be within $\pm 1\%$ of stated value on full load range (TBD)		QB50-SYS-1.3.1 Singarayar et al. 2013
QB50-SYS-1.3.2	The CubeSat shall be able to be commissioned in orbit following the last powered-down state without battery charging, inspection or functional testing for a period of up to 4 months (TBC before CDR).	Design check. Battery charged before satellite is handed over to QB50 consortium		EM/PFM	Design check		QB50-SYS-1.3.2 Singarayar et al. 2013
QB50-SYS-1.3.3	The CubeSat shall be powered OFF during the entire launch and until it is ejected from the deployment system.	Separation switch design. Ground testing	Interfaces operational	Prototype /EM	Power off, when separation switch is pressed down. Ground testing successful	PASS	QB50-SYS-1.3.3 Singarayar et al. 2013
QB50-SYS-1.6.1	The CubeSat shall maintain all its electronic components within its operating temperature range while in operation and within survival temperature range at all other times.	The EPS-board electronics shall be able to withstand an operating temperature of -40 to +85 °C, except batteries between -10 to 50 °C. Batteries shall have heater (see ELEC-011 & ELEC-012). Design check, components list, thermal-cycling		Prototype /EM	Battery heater keeps the temperature of batteries over 0°C. Components on components list fulfil the requirement. EM passes thermal-cycling		QB50-SYS-1.3.3 Singarayar et al. 2013
QB50-SYS-1.7.1.	The CubeSat shall be designed to have an in-orbit lifetime of at least 3 months.	Proper design, ensuring sufficient battery capacity		Prototype /EM/ PFM	Design check, calculation of battery capacity		QB50-SYS-1.7.1 Singarayar et al. 2013
QB50-SYS-1.7.2.	The CubeSat shall not use any materials that have the potential to degrade during the 2 years storage duration after assembly.	Design check, battery charging		EM	Design check		QB50-SYS-1.7.2 Singarayar et al. 2013
QB50-SYS-1.7.3.	Deployment switches shall be non-latching (electrically or	Choosing reliable mechanical switches with flight heritage		EM	Ground testing		QB50-SYS-1.7.3 Singarayar

	mechanically).						et al. 2013
MEC-001	The EPS mass shall be no more than 500 g (Batteries, control board, solar panels)	Weight measurement		EM	Mass ≤ 500 g		Aalto-2 mass budget
MEC-002	Mechanical interface of the EPS shall be CubeSat Kit compatible, except height shall be no more than twice the height determined in PC/104 specification	Measurement of dimensions	Prototype dimensions ok	Prototype /EM	Connectors fit, drill holes positioned right, dimensions ok. Height less than 22.10 mm	PASS	
MEC-003	All dimensional tolerances shall be within ± 0.1 mm	Measurement of dimensions	Offset < 0.1 mm	Prototype /EM	Dimension offset < 0.1 mm	PASS	
MEC-004	The EPS shall be able to withstand the launch environment	Vibration test, Shock test		PFM	Passes vibrational tests based on GSFC-STD-7000 or levels provided by QB50 consortium		
MEC-005	The EPS shall be verified to present the EPS meet the following requirements: – Functional tests – EMC tests – Thermal-vacuum cycling with acceptance levels – Mechanical tests with acceptance levels – Vibration – Shock	Functional tests, verification		PFM	Tests passed		
ELEC-001	The EPS pinout shall be compatible with COTS EPSs	Verification	Compatible with COTS system	Prototype /EM	Pins match with COTS-systems	PASS	
ELEC-002 (TBD)	The EPS shall be able to provide at least 0.8 A of current for 3.3 V and 5 V buses	Functional testing	Able to deliver > 0.8 A current for 3.3 V and 5 V buses	Prototype /EM	Test maximum current available. Current for 3.3 V and 5 V buses shall be > 0.8 A	PASS	
ELEC-003	The EPS shall be able to operate on V_{in} supply range of 8.8 to 14.5 V (TBD)	Functional testing		Prototype /EM	EPS charges batteries on input voltages of 8.8 to 14.5 V		
ELEC-004 (TBD)	The EPS shall provide an unregulated voltage line which floats following the battery voltage	Functional testing	Battery bus present	Prototype	Battery bus present	PASS	
ELEC-005	The regulated voltage range shall be within ± 1 % of stated value across the full load range	Functional testing (QB50-SYS.1.3.1)		EM	Voltages are ± 1 % range of nominal		

ELEC-006	All voltage buses shall have overcurrent protection	Functional testing	Overcurrent protection operates, but is inefficient	Prototype	Voltage line stops supplying power if $I > 0.8$ (TBD) is exceeded		
ELEC-007	The EPS shall utilize Maximum Power Point Tracking or similar technology	Design check, functional testing	Battery charging efficiency 75-80 %. Prototype is not tested in different temperatures	Prototype / EM	Efficiency testing by using Solar Simulator or manufactured panels in different temperatures		
ELEC-008	The solar panels shall produce at least 3 Watts of energy as an orbit average	Design check, functional tests, simulation results		Proto/EM	Simulation shows that chosen solar panel configuration produces orbit average of > 3 W		
ELEC-009	The Batteries shall have BOL capacity of 10Wh	Design check, measuring the capacity EM model's battery pack		EM	Measured capacity > 10 Wh		
ELEC-010	The battery shall have a heater circuit which activates when battery temperature is low	Design check, functional tests		EM	Battery heater activates if $T_{battery} < 0$ °C		
ELEC-011	Battery heater shall be deactivated when $T_{battery} > 50$ °C	Functional tests		EM	Deactivates when $T_{battery} > 5$ °C		
ELEC-012	Battery shall have undervoltage and overvoltage protection	Functional tests		EM	Charging ends when $V_{BAT} > 4.15$ V and battery stops supplying current when $V_{BAT} < 3.5$ V (TBD)		
ELEC-013	After undervoltage protection has activated, battery shall not reactivate until the battery voltage has risen to 3.7 V (TBD)	Functional tests		EM	After undervoltage lockout situation battery activates when $V_{bat} \approx 3.6$ V		
ELEC-014	The EPS shall not cause any significant interference to other systems	Functional tests		EM	Connect systems and test the operation		
ELEC-015	The EPS-system shall have blocking diode to ensure that non-illuminated solarpanel does not act as load	Design check, functional tests	Blocking diodes operational, but ideal diodes or MOSFET configuration suggested for the next version	Proto/EM	Zero current flowing to non-illuminated solarpanel	PASS	
ELEC-016	The EPS shall have interface for remove before flight and separation switch	Design check, functional tests	Interfaces present and operational	Prototype	Kill switch and separation switch interfaces operational	PASS	
ELEC-017	The EPS shall be able to deliver power in possible microcontroller failure situation	Design check, functional tests	Design check passed	Prototype /EM	Provides power to 3.3 V and 5 V buses when microcontroller output is grounded or floating	PASS	
ELEC-018	The EPS shall be able to deliver power even if one BCR or switching regulator fails	Design check, functional tests	Design check passed	Prototype /EM	Redundant BCRs and DC/DC converters in design. BCRs and converters able to operate	PASS	Depends on failure mode

					individually		
ELEC-019	The EPS shall have voltage buses protected against latch-ups	Design check, functional tests	Digital interface with current telemetry needed	Prototype /EM	DC/DC converters shuts down momentarily, when latch-up is noticed		Based on current monitoring
TM & TC-001	The EPS shall send at least the following telemetry on request: – Solar panel currents – Solar panel voltages – Solar panel temperatures – Individual battery cell voltage levels – Individual battery cell currents – Battery temperature – Battery charge/discharge status for each battery – Output voltage levels – Output currents	Design check, functional tests		Prototype /EM	Telemetry values available and precise (accuracy TBD)		
TM & TC-002	The EPS shall provide instant solar array currents to have possibility to use values as a rough attitude indicator	Design check, functional tests		EM	Telemetry values provided on demand and without significant delay		
TM & TC-003	Telemetry and telecommand shall use I ² C or Can BUS (TBD)	Design check, functional tests		EM	Sends telemetry and responds to commands through I ² C or Can BUS		
TM & TC-004	The EPS shall have reset functionality for voltage buses through I ² C or Can BUS (TBD)	Functional tests	Reset funtionality available, digital interface needs to be implemented	Prototype /EM	Powering and shutting down DC/DC converters operational		
DEL-001	Any of the EPS components shall not be under any regulations (e.g. ITAR) which would affect the participation of foreign students in the project or co-operation with international parties.	Components and materials list verification	No components or materials under ITAR regulations used	Prototype /EM/PFM	Components or materials list does not have components which are under ITAR regulations	PASS	
DEL-002	An engineering model shall be delivered before December 2013 (TBD)	Verification		EM	EM ready on time		
DEL-003	A proto flight or flight model shall be delivered before November 2014 (TBD)	Verification		PFM/FM	PFM or FM ready on time		
DEL-004	At least the following documentation shall be provided: – Operating manual – Test specification and test reports – Functional test report	Producing required test reports and manual for operating the EPS		PFM	Documents delivered and accepted		

	<p>including a procedure to reproduce functional tests</p> <p>- Failure mode, effects and criticality analysis (FMECA) results</p>					
--	--	--	--	--	--	--

Appendix D

STK MDL model of Aalto-2 nanosatellite using 4 solar cells on each long side.

Aalto-2 body

Component Aalto_2_body

 SolarPanelGroup Z_minus 29.5
 SolarPanelGroup Z_plus 29.5
 SolarPanelGroup Y_plus 29.5
 SolarPanelGroup Y_minus 29.5

Component Body

 Rotate 45 0 0
 Translate 0 0.05 0.05

Cylinder

 FaceColor white
 Numsides 4
 Face1Radius 0.07
 Face1Normal -1 0 0
 Face2Radius 0.07
 Face2Normal 1 0 0
 Length 0.227

EndCylinder

EndComponent

Aalto-2 Cell

Component 3G30C

 SolarPanel Cell

Polygon
 FaceColor yellow
 Shininess 64
 Specularity 0.4
 Numverts 6
 Data
 0 0 0
 0 0.08 0
 0 0.08 0.0265
 0 0.0665 0.04
 0 0.0135 0.04
 0 0 0.0265

EndPolygon

EndComponent

```
### Aalto-2 Panel substrate
```

```
Component panel
```

```
Rotate 0 0 0
```

```
Polygon
```

```
FaceColor green
```

```
NumVerts 4
```

```
Data
```

```
0 0 0
```

```
0 0 0.2
```

```
0 0.09 0.2
```

```
0 0.09 0
```

```
EndPolygon
```

```
EndComponent
```

```
##### Attaches the cells to panel
```

```
Component Z_minus_sp
```

```
SolarPanel Z_minus
```

```
# adds the panel
```

```
Refer
```

```
Translate 0 0 0
```

```
Component panel
```

```
EndRefer
```

```
# adds the first cell
```

```
Refer
```

```
Rotate 0 0 0
```

```
Translate 0.001 0.004 0.001
```

```
Component 3G30C
```

```
EndRefer
```

```
# adds the second cell
```

```
Refer
```

```
Rotate 0 0 0
```

```
Translate 0.001 0.004 0.044
```

```
Component 3G30C
```

```
EndRefer
```

```
# adds the third cell
```

```
Refer
```

```
Rotate 0 0 0
```

```
Translate 0.001 0.004 0.087
```

```
Component 3G30C
```

```
EndRefer
```

```
# adds the fourth cell
```

```
Refer
```

```
    Rotate 0 0 0
    Translate 0.001 0.004 0.130
    Component 3G30C
EndRefer

# adds the fifth cell - uncomment if only 4 cells used
# Refer
#     Rotate 0 0 0
#     Translate 0.001 0.004 0.173
#     Component 3G30C
# EndRefer

EndComponent
```

```
Component Z_plus_sp
# adds the panel
    SolarPanel Z_plus
    Refer
        Translate 0 0 0
            Component panel
    EndRefer
```

```
# adds the first cell
    Refer
        Rotate 0 0 0
        Translate 0.001 0.004 0.001
        Component 3G30C
    EndRefer
```

```
# adds the second cell
    Refer
        Rotate 0 0 0
        Translate 0.001 0.004 0.044
        Component 3G30C
    EndRefer
```

```
# adds the third cell
    Refer
        Rotate 0 0 0
        Translate 0.001 0.004 0.087
        Component 3G30C
    EndRefer
```

```
# adds the fourth cell
    Refer
        Rotate 0 0 0
```

```

Translate 0.001 0.004 0.130
Component 3G30C
EndRefer

# adds the fifth cell - uncomment if only 4 cells used
#   Refer
#     Rotate 0 0 0
#     Translate 0.001 0.004 0.173
#     Component 3G30C
#   EndRefer

EndComponent

Component Y_plus_sp
# adds the panel
  SolarPanel Y_plus
    Refer
    Translate 0 0 0
      Component panel
    EndRefer

# adds the first cell
  Refer
    Rotate 0 0 0
    Translate 0.001 0.004 0.001
    Component 3G30C
  EndRefer

# adds the second cell
  Refer
    Rotate 0 0 0
    Translate 0.001 0.004 0.044
    Component 3G30C
  EndRefer

# adds the third cell
  Refer
    Rotate 0 0 0
    Translate 0.001 0.004 0.087
    Component 3G30C
  EndRefer

# adds the fourth cell
  Refer
    Rotate 0 0 0
    Translate 0.001 0.004 0.130
    Component 3G30C

```

EndRefer

```
# adds the fifth cell - uncomment if only 4 cells used
#   Refer
#     Rotate 0 0 0
#     Translate 0.001 0.004 0.173
#     Component 3G30C
#   EndRefer
```

EndComponent

Component Y_minus_sp

```
# adds the panel
  SolarPanel Y_minus
    Refer
      Translate 0 0 0
        Component panel
    EndRefer
```

adds the first cell

```
  Refer
    Rotate 0 0 0
    Translate 0.001 0.004 0.001
    Component 3G30C
  EndRefer
```

adds the second cell

```
  Refer
    Rotate 0 0 0
    Translate 0.001 0.004 0.044
    Component 3G30C
  EndRefer
```

adds the third cell

```
  Refer
    Rotate 0 0 0
    Translate 0.001 0.004 0.087
    Component 3G30C
  EndRefer
```

adds the fourth cell

```
  Refer
    Rotate 0 0 0
    Translate 0.001 0.004 0.130
    Component 3G30C
  EndRefer
```

```
# adds the fifth cell - uncomment if only 4 cells used
# Refer
#     Rotate 0 0 0
#     Translate 0.001 0.004 0.173
#     Component 3G30C
# EndRefer
```

```
EndComponent
```

```
### Add everything together
```

```
Component Aalto_2
    Rotate 0 0 0
    Translate 0.05 -0.05 -0.05
    Root
    Refer
        Component Body
    EndRefer
```

```
# Add the +Z panel
```

```
    Refer
        Rotate 0 90 0
        Translate 0.02 0.01 0.0
        Component Z_minus_sp
    EndRefer
```

```
# Add the -Z panel
```

```
    Refer
        Rotate 0 -90 180
        Translate 0.02 0.095 0.1
        Component Z_plus_sp
    EndRefer
```

```
# Add the +Y panel
```

```
    Refer
        Rotate 90 180 90
        Translate 0.02 0 0.1
        Component Y_plus_sp
    EndRefer
```

```
# Add the -Y panel
```

```
    Refer
        Rotate 90 0 90
        Translate 0.02 0.1 0.01
        Component Y_minus_sp
    EndRefer
```

```
EndComponent
```